UNIVERSIDAD YACHAY TECH

UNIVERSIDAD DE INVESTIGACIÓN DE TECNOLOGÍA EXPERIMENTAL YACHAY

Escuela de Ciencias de la Tierra, Energía y Ambiente

TÍTULO: DESCRIPTION AND CHARACTERIZATION OF SECONDARY SALT MINERALS IN THE CHOTA BASIN, ECUADOR.

Trabajo de integración curricular presentado como requisito para la obtención
del título de Geóloga.

Autor:

Zapata Paredes Karen Melina

Tutor:
Ph.D.Vazquez Taset Yaniel Misael

Co-Tutor:
Ph.D. Ávila Sosa Edward Ebner

Urcuquí, agosto 2022

SECRETARÍA GENERAL
ESCUELA DE CIENCIAS DE LA TIERRA, ENERGÍA Y AMBIENTE
CARRERA DE GEOLOGÍA
ACTA DE DEFENSA No. UITEY-GEO-2022-00006-AD

En la ciudad de San Miguel de Urcuquí. Provincia de Imbabura. a los 10 días del mes de agosto de 2022. a las 10:00 horas. en el Aula S_CAN de la Universidad de Investigación de Tecnología Experimental Yachay y ante el Tribunal Calificador, integrado por los docentes:

Presidente Tribunal de Defensa	Dr. TORO ALAVA. JORGE EDUARDO . Ph.D.
Miembro No Tutor	MSC CARLOSAMA MOREJON. FELIPE JAVIER
Tutor	Dr. VAZQUEZ TASET, YANIEL MISAEL , Ph.D.

Se presenta el(la) señor(ita) estudiante **ZAPATA PAREDES, KAREN MELINA**. con cédula de identidad No. **0504280660**. de la **ESCUELA DE CIENCIAS DE LA TIERRA, ENERGÍA Y AMBIENTE**. de la Carrera de **GEOLOGÍA**. aprobada por el Consejo de Educación Superior (CES). mediante Resolución **RPC-SE-10-No.031-2016**, con el objeto de rendir la sustentación de su trabajo de titulación denominado: **Description and characterization of secondary salt minerals the chota basin, Ecuador** , previa a la obtención del título de **GEÓLOGO/A**.

El citado trabajo de titulación. fue debidamente aprobado por el(los) docente(s):

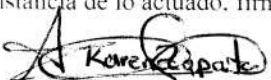|	
Tutor	Dr. VAZQUEZ TASET. YANIEL MISAEL , Ph.D.
Co - Tutor	Dr. AVILA SOSA, EDWARD EBNER , Ph.D.

Y recibió las observaciones de los otros miembros del Tribunal Calificador, las mismas que han sido incorporadas por el(la) estudiante.

Previamente cumplidos los requisitos legales y reglamentarios. el trabajo de titulación fue sustentado por el(la) estudiante y examinado por los miembros del Tribunal Calificador. Escuchada la sustentación del trabajo de titulación, que integró la exposición de el(la) estudiante sobre el contenido de la misma y las preguntas formuladas por los miembros del Tribunal, se califica la sustentación del trabajo de titulación con las siguientes calificaciones:
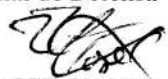
Tipo	Docente	Calificación
Miembro Tribunal De Defensa	MSC CARLOSAMA MOREJON, FELIPE JAVIER	9,1
Tutor	Dr. VAZQUEZ TASET. YANIEL MISAEL , Ph.D.	9,9
Presidente Tribunal De Defensa	Dr. TORO ALAVA. JORGE EDUARDO , Ph.D.	8,7

Lo que da un promedio de: **9.2 (Nueve punto Dos)**. sobre 10 (diez). equivalente a: **APROBADO**

Para constancia de lo actuado. firman los miembros del Tribunal Calificador, el/la estudiante y el/la secretario ad-hoc.

ZAPATA PAREDES. KAREN MELINA
Estudiante

Dr. TORO ALAVA. JORGE EDUARDO , Ph.D.
Presidente Tribunal de Defensa

Dr. VAZQUEZ TASET. YANIEL MISAEL . Ph.D.
Tutor

MSC CARLOSAMA MOREJON. FELIPE JAVIER
Miembro No Tutor

TERÁN ROSALES, ANDREA YOLANDA
Secretario Ad-hoc

AUTORÍA

Yo, **Karen Melina Zapata Paredes**, con cédula de identidad 0504280660, declaro que las ideas, juicios, valoraciones, interpretaciones, consultas bibliográficas, definiciones y conceptualizaciones expuestas en el presente trabajo; así cómo, los procedimientos y herramientas utilizadas en la investigación, son de absoluta responsabilidad de la autora del trabajo de integración curricular. Así mismo, me acojo a los reglamentos internos de la Universidad de Investigación de Tecnología Experimental Yachay.

Urcuquí, agosto 2022.

Firmado electrónicamente por:
KAREN MELINA ZAPATA PAREDES

_____
Karen Melina Zapata Paredes
CI: 0504280660

AUTORIZACIÓN DE PUBLICACIÓN

Yo, **Karen Melina Zapata Paredes,** con cédula de identidad 0504280660, cedo a la Universidad de Investigación de Tecnología Experimental Yachay, los derechos de publicación de la presente obra, sin que deba haber un reconocimiento económico por este concepto. Declaro además que el texto del presente trabajo de titulación no podrá ser cedido a ninguna empresa editorial para su publicación u otros fines, sin contar previamente con la autorización escrita de la Universidad.

Asimismo, autorizo a la Universidad que realice la digitalización y publicación de este trabajo de integración curricular en el repositorio virtual, de conformidad a lo dispuesto en el Art. 144 de la Ley Orgánica de Educación Superior

Urcuquí, agosto 2022.

Firmado electrónicamente por:
**KAREN MELINA
ZAPATA
PAREDES**

Karen Melina Zapata Paredes
CI: 0504280660

Dedicatory

I dedicate this work to my lovely family Zapata and Paredes, specially to Marcos, Margoth, Marjorie. N, Marjorie. J, and Hilda, (M&M †).

On the other hand, I dedicate this work to all those people who have been lonely. To those of you who are reading this work, you are here, you have survived adversity, pandemic, economy, traumas, and you are here. So I want to tell you to keep going, you are amazing.

Karen Melina Zapata Paredes

Acknowledgement

I want to express my gratitude to the Universe, God and Tree Lord that allowed me to be here.

A special thanks to my family, Marcos, Margoth, Marjorie. N, Marjorie. J and Maribel. P and Ruben. P that supports me during each moment.

I would like to give a very special thanks to Yaniel Vázquez and Edward Ávila, who have guided me throughout the development of this project.

To Hortencia Rodríguez and Karla Moya who support me as a person, student and woman.

My thanks to the geofamily that allowed me to be a better geogirl, well just if we exclude the part of the fear of heights behind.

Last but not least, to my dear Apatito for his unconditional support during my academic life.

Karen Melina Zapata Paredes

Resumen

Esta investigación estudia las sales secundarias en la cuenca sedimentaria del Chota y su clasificación teniendo en cuenta las concentraciones químicas funcionales. En esta área de estudio, se encuentran costras blancas similares a la sal en los suelos, muros de construcciones, drenajes y afloramientos. Estas estructuras se encuentran distribuidas a lo largo de la estratigrafía del área de interés. Por ello, como primer paso, esta investigación trabaja conceptos como la ocurrencia de las ventas, los efectos y los tipos de ventas más comunes. Además, para llevar a cabo el trabajo de campo se consideran estudios recientes de caracterización estratigráfica del material que conforma el área de estudio y un posterior muestreo aleatorio en el cual existen muestras difíciles de identificar manualmente. Por lo tanto, la metodología para esta caracterización mineralógica se basa en el análisis de fases minerales a partir de datos de difracción de rayos DRX, este análisis proporciona una evaluación mineralógica y un análisis semicuantitativo de los compuestos tomados en campo. Finalmente, las ventas reconocidas fueron Sulfatos, Carbonatos, Boratos y Nitratos, lo cual concuerda con la literatura, de estos grupos el más abundante es Sulfatos con un 37% y de acuerdo con el arreglo estratigráfico la mayor cantidad de minerales blancos se hallan en los depósitos del Cuaternario. Además, también hay Arseniatos, Fosfatos, Silicatos, Óxidos de Hidratos e Hidróxidos detectados con la técnica de difracción de rayos X.

Palabras clave: Cuenca sedimentaria del Chota, sales secundarias, costras salinas, cristales de sal, ambientes áridos, Sulfatos, Carbonatos, Boratos y Nitratos.

Abstract

This research studies the secondary sales in the Chota sedimentary basin and its classification taking into account the functional chemical concentrations. In this study area there are white salt like crusts are found in soils, walls of constructions, drainages, and outcrops. These structures are distributed throughout the stratigraphy of the area of interest. Therefore, as a first step, this research works on concepts such as the occurrence of sales, effects and the most common types of sales. In addition, to carry out the field work, recent studies of stratigraphic characterization of the material that makes up the study area are considered to develop the subsequent random sampling that corresponds to samples that are difficult to identify by hand. Therefore, the methodology for this mineralogical characterization is based on the analysis of mineral phases from X-ray diffraction (XRD) data, this analysis provides a mineralogical evaluation and a semi-quantitative analysis of the compounds taken in the field. Finally, the recognized sales were Sulfates, Carbonates, Borates and Nitrates, which is consistent with the literature, of these groups the most abundant is Sulfates with 37% and according to the stratigraphic arrangement the largest amount of white minerals are found in the Quaternary deposits. In addition, there are also Arsenates, Phosphates, Silicates, Oxides of Hydrates and Hydroxides detected with the X-ray diffraction technique.

Key words: Chota sedimentary basin, secondary salts, saline crusts, salt crystallization, arid environments, Sulfate, Carbonate, Borate, Nitrate.

List of Figures

Universidad
YACHAY
TECH

SCHOOL OF
EARTH SCIENCES,
ENERGY AND ENVIRONMENT

List of tables

List of Annexes

1 INTRODUCTION

X-ray diffraction analysis allows recognition of the type of salt crystallization that occurs at the surface level in outcrops, soils and constructions in the Chota Basin. In addition, in order to develop a recognition is important to know that the most common primary minerals in the environment are residuals of physical and chemical weathering processes, most commonly occurring in coarser particles (of sand- and silt-size). However, the phyllosilicates and volcanic glass can also be found in reasonable proportions in the clay-size factions of some soils. Alteration of primary minerals to give secondary products involves either transformation within the solid-state, with either partial or complete dissolution of solutes, then their re-precipitation as new secondary phases.

The modern mineral classification system, rooted in the chemical corresponds to James Dwight Dana (Hazen, 2019). Therefore, considering this classification there are eight groups of categories that are based on dominant anionic or anionic groups and in a similar way in the geological setting (Mishra & Deshmukh, 2019). The groups are described below.

Native Elements: This category of the pure metals, like the Copper (Cu), is found in a naturally pure form. Although the occurrence of gold (Au), argentum (Ag), and platinum (Pt) in native state are rare, but most carbon (C), sulfur (S), and copper (Cu) are commonly found.

Silicates are made from metals that combine with silicon and oxygen atoms. This group is more abundant in the Earth's Crust than the sum of all the mineral groups. Some minerals are feldspar, quartz, olivine, pyroxene, amphibole, garnet, and mica.

Oxides: These groups result from the combination of a metal with oxygen. The oxide class includes the oxide and the hydroxide minerals. Oxide minerals commonly occur either as precipitates at or near the Earth's surface, or as oxidation products, or accessory minerals in igneous

rocks found in the crust and mantle. Some of the common oxides are hematite (iron oxide), magnetite (iron oxide), chromite (iron chromium oxide), rutile (titanium dioxide), and ice (hydrogen oxide).

Sulfides: Sulfides are made up of sulfur compounds, usually with a metal. Some common minerals are pyrite (iron sulfide), chalcopyrite (copper-iron sulfide), pentlandite (nickel iron sulfide), and galena (lead sulfide).

Sulfates: Sulfates contain the sulfate anion $(SO_4)^{2-}$. They are a large group of minerals made up of compounds of sulfur combined with metals and oxygen. They commonly form in evaporitic settings, in hydrothermal veins as gangue minerals and the sulfide ores, and as secondary oxidation products of the original sulfide minerals. Some of the common examples of sulfate minerals are anhydrite (calcium sulfate), barite (barium sulfate), gypsum (hydrated calcium sulfate), and celestine (strontium sulfate). In addition, this class includes chromate, molybdate, selenate, sulfite, tellurate, and tungstate minerals.

Halide: Correspond to halogen elements like chlorine, bromine, fluorine, and iodine combined with metallic elements. Halide minerals form natural salts and include fluoride, chloride, bromide, and iodide minerals such as fluorite (calcium fluoride), sylvite (potassium chloride), and salt ammoniac (ammonium chloride). This group is also commonly found in evaporitic settings such as playa lakes and landlocked seas such as the Dead Sea and the Great Salt Lake or artificial salt pans.

Carbonate: Refers to a group of minerals that is made up of carbon, oxygen, and a metallic element. In addition, they contain $(CO_3)^{2-}$ anions. The common minerals are calcite and aragonite (both calcium carbonate), dolomite (magnesium/calcium carbonate), and siderite (iron carbonate).

Carbonates minerals are commonly formed in marine settings. It also includes nitrates and borates minerals.

Phosphate: Represent the group of minerals made up of minerals with PO_4 complex ions acting as a non-metal with a metallic element. The most common example is apatite found in the teeth and bones of many animals. This class includes phosphate, arsenate, vanadate, and antimonate minerals.

1.1 General information about salt crystallization

In general, minerals form under certain conditions of temperature, pressure, and chemical environment. There are minerals behave as stable species these are the primary species. Based on Churchman and Lowe (2012) the most common primary minerals are phyllosilicates and volcanic glass can also be found in reasonable proportions in the clay-size factions of some soils. Alteration of primary minerals to give secondary products involves either transformation within the solid-state, with either partial or complete dissolution of solutes, then their precipitation as new secondary phases. These secondary phases are associated with salts, halides, sulfates, and some carbonates, which often occur in saline soils and arid environments such as Antarctica. Then other groups work as indicators of its extreme aridity that nitrate, borate, chromate, and perchlorate salts have been found in the Atacama Desert in Chile.

However, Kashif et al. (2020), related with salts there is a recirculation in the groundwater and root zone results in the accumulation of salts at the soil surface and is known as primary salinization. However, this recirculation is not the only cause of salinization as this can result from processes driven by factors outside nature, secondary salinization, such as artificial irrigation and removal of native vegetation by human activities (Gavrichkova et al., 2020). So, in accordance with Montoroi (2018) salts exist in two states: a crystallized state that is readily observable in solid

systems such as rocks and soils; and a dissolved state that is not perceptible in water systems such as continental, marine, meteoric, and geothermal waters. In addition, magmatic systems such as fluid, viscous lava; and colloidal systems such as clay minerals, organic matter.

As a result of secondary salinization, the soil deteriorates with the annual accumulation of salt (Liu et al., 2020). Consequently, as stated by Metternicht and Zinck (2002), eutrophication of river estuaries and damage to infrastructure impact on the agricultural sector represent the main effects of salinization which are directly associated with economic losses.

Salts define all minerals that can be formed by the concentration and combination of major ions (chloride, sulfate and carbonate for anions; calcium, magnesium, sodium and potassium for cations; Montoroi, 2018). The leaching is one of the processes that is influenced by increasing temperature. (González et al., 2013). However, the presence of salts occurs in sub-humid, arid and semi-arid regions, as well as in humid coastal regions, where depressions are enriched with salts at a rate greater than that of their leaching.(Álava & Haz, 2017). Then, air humidity is an important control of the effectiveness of salt crystallization, for a salt can crystallize only when the ambient relative humidity is lower than the equilibrium relative humidity of the saturated salt solution (Goudie, 2004).

1.2   Problem statement

The accumulation of salt on the surface and the salinization of the soil is a problem that affects some regions affected by salt degradation as Amu-Darya and Syr-Darya river basins in Central Asia, the Indo-Gangetic basin in India, the Indus basin in Pakistan, the Yellow River basin in China, the Euphrates Basin in Syria and Iraq, the Murray-Darling Basin in Australia, and the San Joaquin Valley in the United States (Shahid et al., 2018).

Due to geology and the heterogeneity of climates, Ecuador represents an excellent place to evaluate the incidence of salt crystallization. However, salinization is generally more pronounced in arid and semi-arid environments (Chesworth, 2008). According to Pérez et al. (2002), arid zones are found in mid-latitudes, generally between the Tropics of Cancer and Capricorn in the South American continent.

Consequently, the Chota River and the sedimentary basin are relevant for the elaborate characterization of secondary salts due to climatological, geographical and geological features. In this place, the occurrence of salts on the surface is very frequent, and affects both crops and constructions in the area. The crystallization of salts is produced by the saturation of a saline solution by evaporation or temperature changes made in the environment. Subsequently, as Doornkamp and Ibrahim (1990) mentioned, weathering es produced by salt crystallization in the soils and constructions. Therefore, to understand these phenomena, this study seeks to characterize the secondary salts growing in the Chota sedimentary basin.

1.3 Objectives

1.3.1 General Objective

This project aims to characterize the secondary salts found in the different stratigraphic members of the Chota sedimentary basin. X-ray diffraction is a helpful method that gives detailed information about the crystallographic structure of salt samples. In addition, X-ray diffraction makes it possible to identify the phases present in a sample that generally results difficult to determine by methods such as observation of hand samples, optical microscopy, and the scanning electron microscope SEM.

1.3.2 Specific Objectives

- To identify the main groups of secondary salts in the Chota Sedimentary Basin.

- To describe the stratigraphic member's features that present the accumulation of salts crystals.

- To stablish the structures with the highest content of white minerals.

1.4 Introduction to the study area

The study area is located in the north part of Ecuador in Imbabura province (Figure 1). This area is important because is one of the most relevant for studying the evolution of the Neogene geology (Reinoso, 2021)
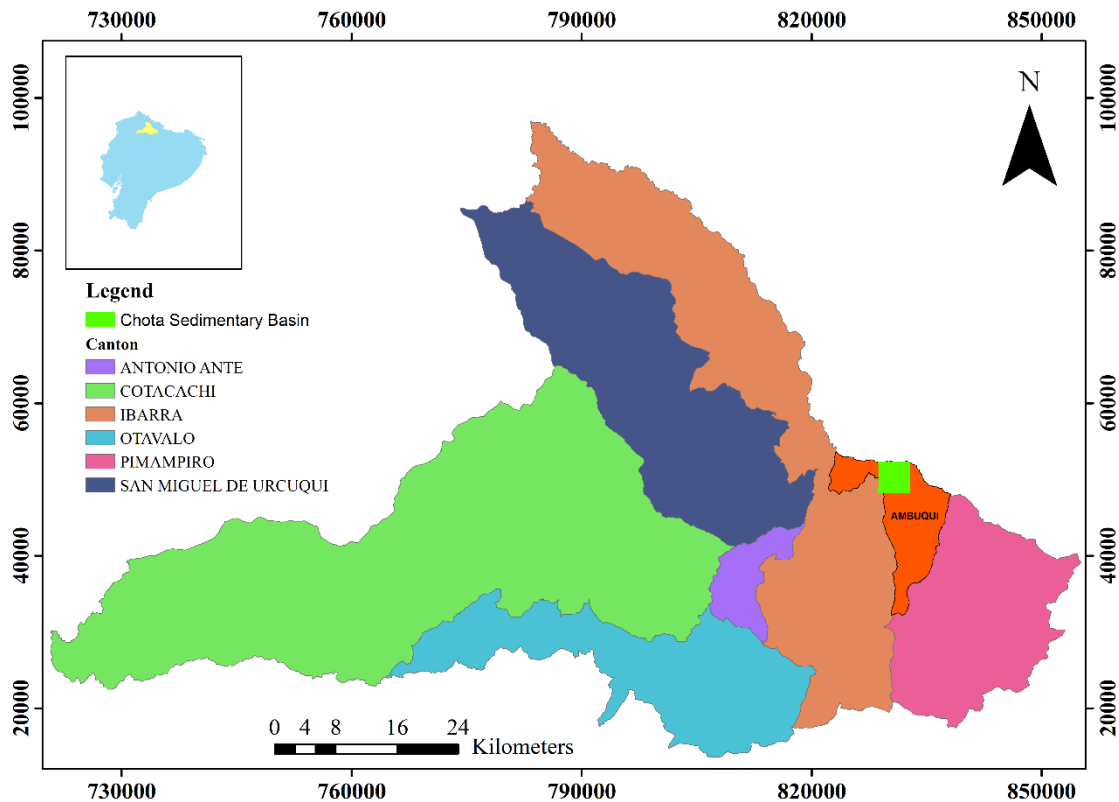
Figure 1.Imbabura province cantons consider the study area (Ambuquí parish). Modified from (INAMHI) data.

Based on González et al. (2013), in Ecuador, four main categories of arid zones are classified according to registered temperatures and precipitation regimes: Hyper-arid regions that present precipitation values below 100 mm/year. The same ones are characterized by periods of drought greater than one year. Arid regions with precipitation values not exceeding 200 mm / year. Semi-arid regions with rainfall values ranging between 200 to 400 mm/year in summer and 500 to 800 mm/year in winter. Finally, dry sub-humid areas with a rainy regime have a solid seasonal character. Guachamín et al. (2015) explain that the inter-Andean zone has significant climatic variations. There are cold and humid areas with low but persistent rainfall on the mountain peaks. On the other hand, the Chota region has exceptional characteristics, with arid valleys, annual rainfall of less than 300 mm, and deficient rainfall (Figure 2).
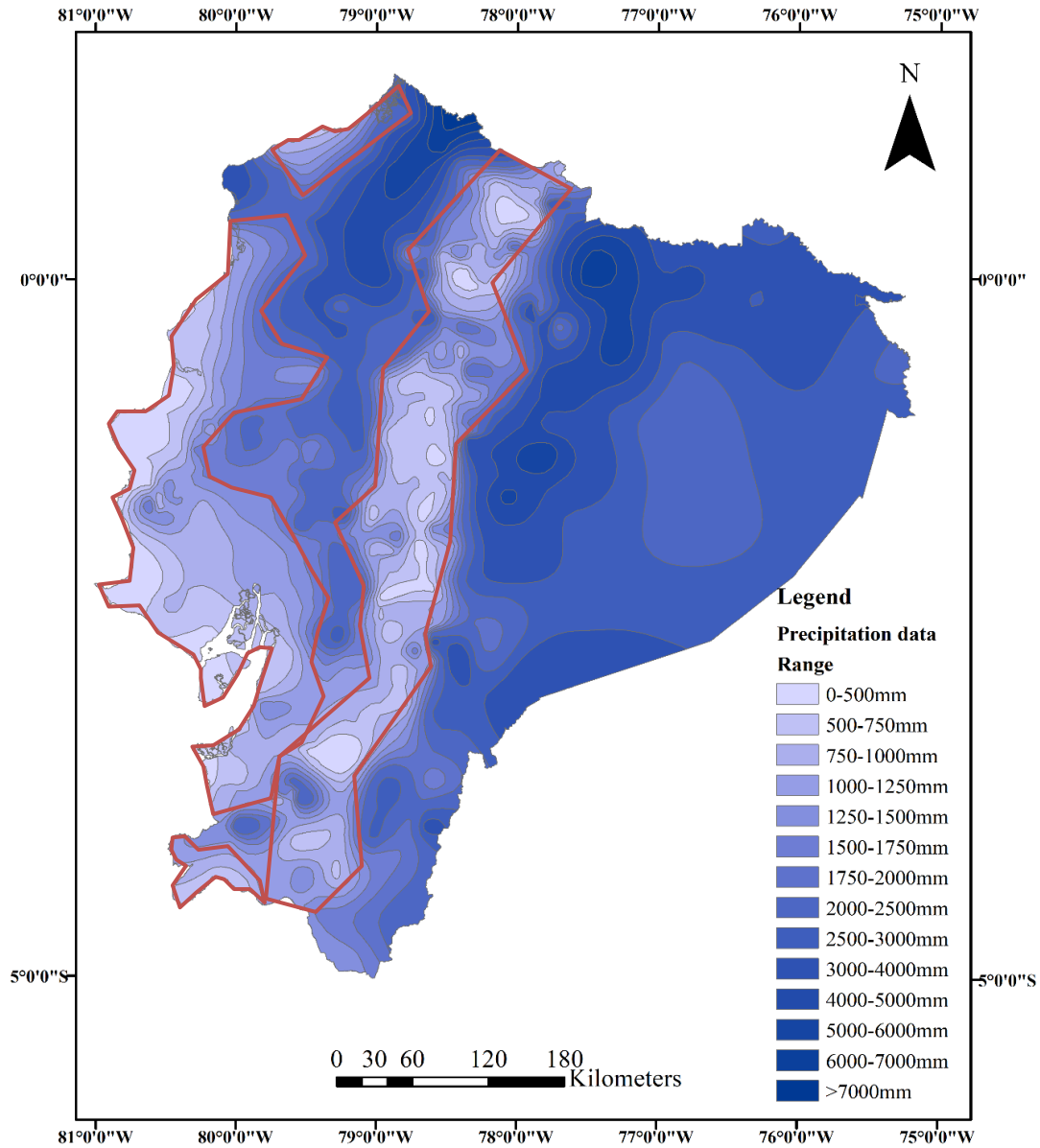
Figure 2. Map of precipitation values in Ecuador, where the lowest values are in the center and west coast which is marked with red polygon, while the highest are in the east. Modified from (INAMHI) data.

Based on the data base from the Instituto Nacional de Meteorología e Hidrología (INAMHI), and focusing in the study area isotherm range values go from 18 °C to 20°C (Figure 3 A), precipitation values less than 500mm for the parish of the study area (Figure 3 B). Then, the type of climate that is dated in the area is consistent with that of an arid climate with a mesothermal

weather (Figure 3 C). In addition, due to this features, one relevant feature in the study area there are cultivation, here there are ditches and a furrow irrigation system is also used for the crops used.
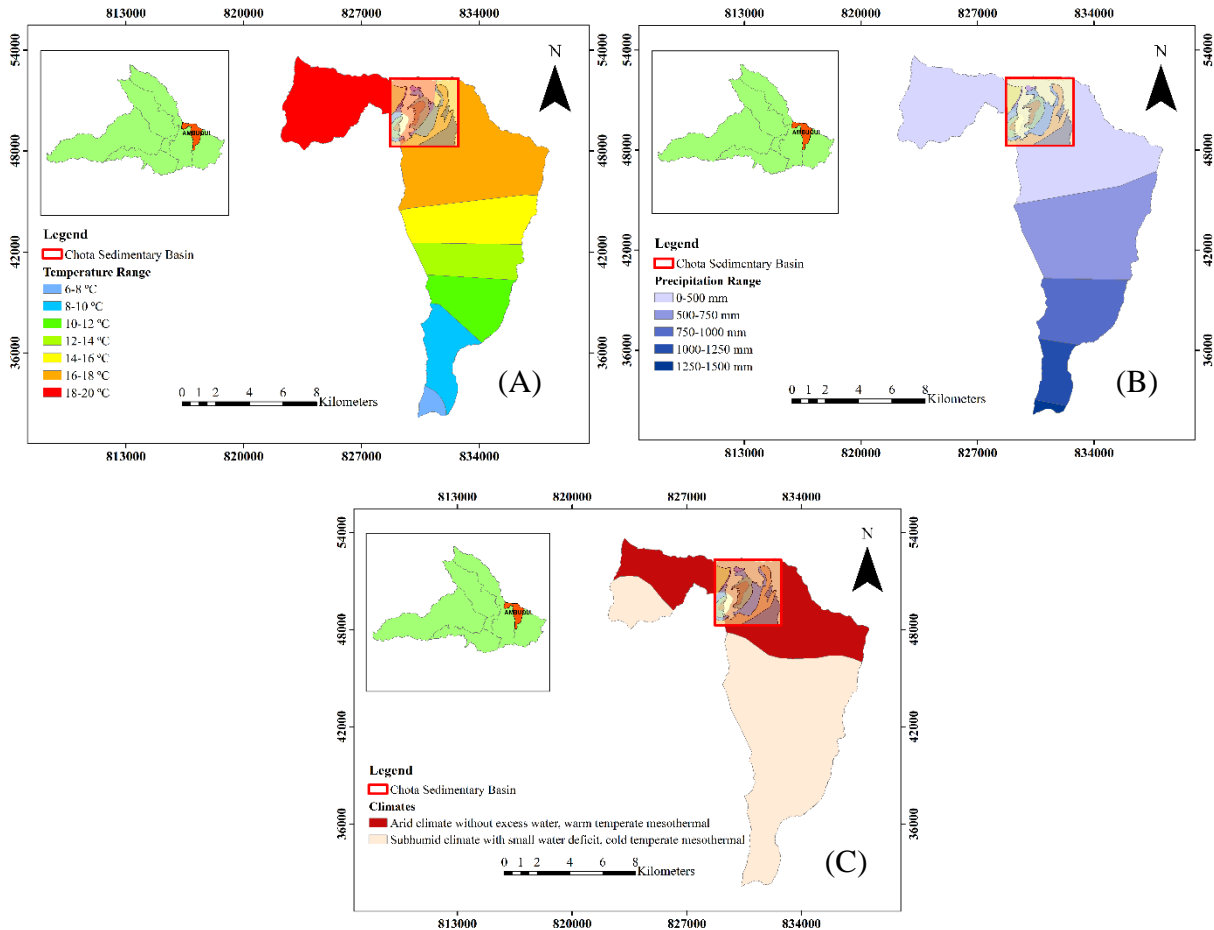
Figure 3. Climatic features in the parish that contains the Chota basin A) Temperature range, 2008. B) Precipitation range, 2008. C) Types of climates. Modified from (INAMHI) data.

2   THEORETICAL BACKGROUND

This depression is known as the inter-Andean valley, a descriptive term indicating its parallelism and location between the two main mountain ranges of the Cordillera Occidental and Cordillera Real (Tibaldi & Ferrari, 1992), which comprises several distinct basins filled with volcano-sedimentary sequences deposited (Siravo et al., 2021). These sediments could be mainly

because, as Coltorti & Ollier (2000) described, active volcanoes are found along the edge of the inter-Andean depression. These volcanoes are aligned with the edges of tectonic depressions and some of the main active faults in the country. However, in this area also are thick continental alluvial, lacustrine, and volcanoclastic sediments (Barragán et al., 1996)

2.1 Stratigraphy of the study area

The stratigraphic analysis details a subdivision of the sedimentary sequence in four central units. The first sequence, Chota Unit, shows a transition from alluvial braided to lacustrine facies. The second sequence, represented by the Santa Rosa Unit to the west and the Peñas Coloradas and Carpuela Units to the east, shows a thickening-widening evolution related to the basin filling and the development of progressive alluvial fan deposits (Barragán et al., 1996).

Previous studies in the Chota Basin suggest that it is composed by Peñas Coloradas Formation, Chota Formation, Santa Rosa Formation, Gavilanes Breccia and metamorphic rocks (Barragán et al., 1996; Winkler et al., 2002). However recent studies as Reinoso (2021) and Fonseca (2021) reported would be described starting with the metamorphic basement as a constituent of the Chota basin. This is composed of folded rocks of gray quartzite and graphitic schist. This basement shows both depositional and fault contact with the Peñas Coloradas Formation, the material is highly fractured, folded and foliated, locally presents a chemical alteration, showing a red coloration. Then Chota formation consists of sandstone and mudstone intercalation, including shale layers. Here the material is folded on a broad scale, including small folds controlled by local faults. The following is Peñas Coloradas formation, composed of four Members: the Canales Colorados Member, Brillosas Member, Tabulares Member, Volcanicas and Sub Volcanicas Member (Figure 4).

Canales Colorados Member is formed by different breccia layers, conglomerate, and sandstone. Following the Brillosas, Member is characterized by a high content of micas and pumice. This Member at the base begins with very fine to fine sandstone that goes to sandstone. The upper part is composed of fine to medium sandstone and claystone intercalations and occasional tuff layers.

Furthermore, Tabulares Member is mainly composed of sandstone layers. In this part, the first layer represents a conglomerate with metamorphic and sedimentary clasts. The second layer is mainly clay to silt grain size material; the third layer goes from fine to medium sandstone. The fourth layer is formed by breccia deposits with metamorphic, sedimentary, and volcanic clasts. Then, the last part of the section goes from very fine to massive fine-grained sandstone.

Finally, Volcanicas Member at the base is defined by massive coarse sand, angular clasts with high pumice content. The next part comprises intercalation of medium to coarse sand, very angular clast, massive, also breccias of cobble to boulder grain size. And at the last part, the subvolcanic and volcanic deposits are intrusions like sills and dykes located in the Canales Colorados and Brillosas Member.
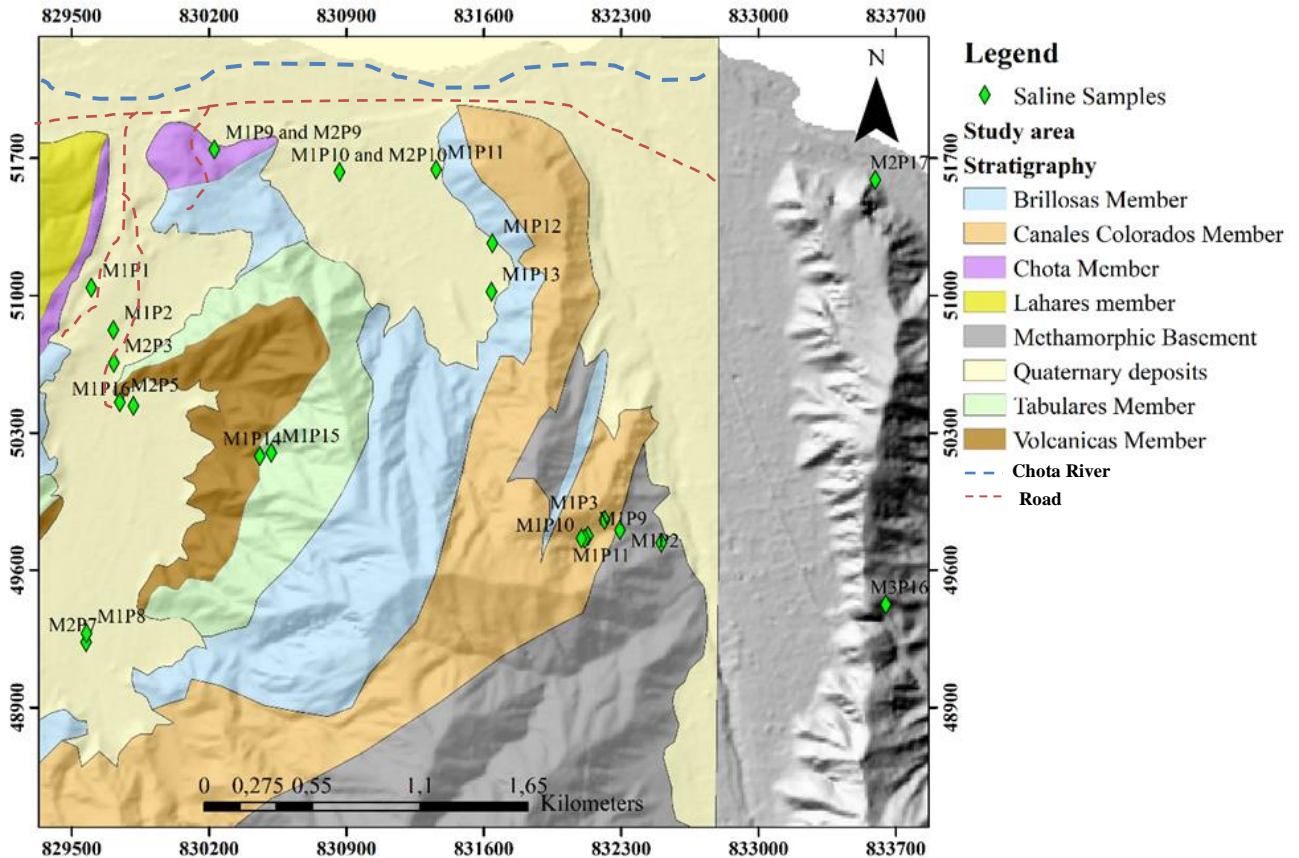
Figure 4. Distribution of salt crystallization in Chota Sedimentary basin. Modified from (Fonseca, 2021 and Reinoso 2021)

Then, based on Barragán et al. (1996) in the study area there are a thick sequence of volcanic, volcanoclastic, alluvial, and colluvial sub horizontal. Also, its composed of debris flow deposits, volcanic breccias and epiclastic sediments all this material associated with quaternary deposits. In addition, from these stratigraphic material, based on (Winkler et al., 2002) Peñas Coloradas Fm., which yields a zircon fission track analyses an age of 5.4±0.4 Ma and is cut by a dyke that yields an apatite fission track with an age of 3.7±1.7 Ma, is the same age or partly pre-dating the Chota Fm. Finally in general terms these material record a period in the evolution of the basin covering at least from the Miocene to the early Pliocene (Barragán et al., 1996).

2.2 Salt crystallization occurrence

The depression areas constitutes the local base level and its intermountain arrangement is the natural receptacle for the products of erosion and evaporation, generating an evaporite plain with different salt crusts (Martínez et al., 2020). Based on Warren (2006), evaporites are produced by precipitation. These salty rocks originally precipitate from a near-surface saturated surface in hydrologies driven by solar evaporation. When there is precipitation by solar energy and other surface and groundwater loss mechanisms, bodies and beds of mineral salts can form.

This type of rock can be differentiated according to its texture which can be "primary" a fully formed rock. However, when an evaporite is found in the subsurface, it exhibits "secondary" textures that precipitate as growths and replacements of intrasediment, these crystals that formed from primary or pre-existing evaporite sediments. When they occur as remnants lifted back to the surface, they show "tertiary" overprints.

There is white saline crust in the structures in Chota Basin and the general description is described below:

2.2.1 *Natural environment occurrence of salts*

The salts accumulations result from precipitation plus high evapotranspiration rates that typify arid and semi-arid regions resulting in the persistence of soluble salts (such as efflorescent salts; Hayes et al., 2012). In this process, salts are formed from reactions between acids and bases.

According to Salama et al. (1999), the accumulation of salts could result from sources such as: the ocean through rainfall, weathering of soil, rock materials, also marine deposition in previous geological periods.

Moreover, Álava and Haz (2017) describes that the natural causes proceed directly from the original material, such as sedimentary rocks, in which salts are constituent minerals or can be produced in the soil by changes in the original minerals of the parent rock. Another factor for salts accumulation is that the dissolved salts in the runoff water accumulate in the depressions, and when the solution evaporates, salt accumulations are formed.

2.2.2   *Occurrence of salts on construction*

As claimed by Herrera (2016), the crystallization of salts in the construction, represents a pathology (Figure 5) characterized by the rise of humidity through capillary ducts and pores from the subsoil. Usually, the salts in constructions are sulfates, carbonates, chlorides, also nitrates; the salt crystallization occurs due to the porosity of materials, constant humidity, and defects.

Besides, salts in construction were mainly produced: by leached ions from falling rocks, mortars, bricks and other construction materials; soil ions; deposition of atmospheric products or generated by the metabolism of organisms (Grossi & Esbert, 1994).
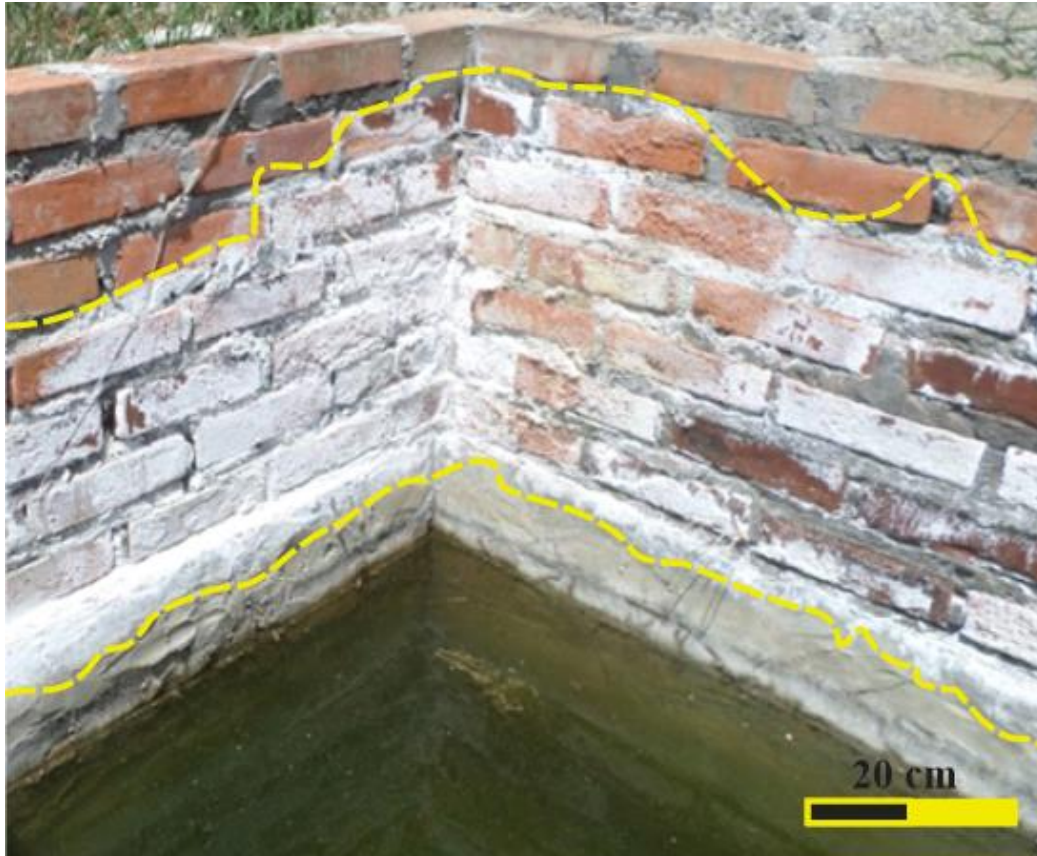
Figure 5. Water reservoir located in the Chota basin where the salt crystallization is affecting the construction.

As determined by Agila (2017) that in constructions, salt crystallization (efflorescence) is mainly composed of soluble potassium, chloride, or sodium salts. These salts are expelled by the pressure of the water that eliminates all the crystals by the direct action of the sun. As a result, white spots are produced on the outside, which represent the expulsion of the salts that pass through the brick due to the action of pressure.

2.2.3 *Weathering by growing of salts on rocks*

The effects that salt crystallization show based on Warke (2013) involve physical mechanisms in which there are crystallization pressures, volumetric increase arising from phase change related to hydration and dehydration events, and thermal expansion followed by contraction (Figure 5 and Figure 6). On the other hand, there are chemical factors were the creation

of alkaline conditions in the presence of salts, under which typically durable elements such as silica can destabilize and submit to the chemical solution, explaining that salt efflorescence (Figure 6 A) is the growth of salt crystals deposited by saline solution.
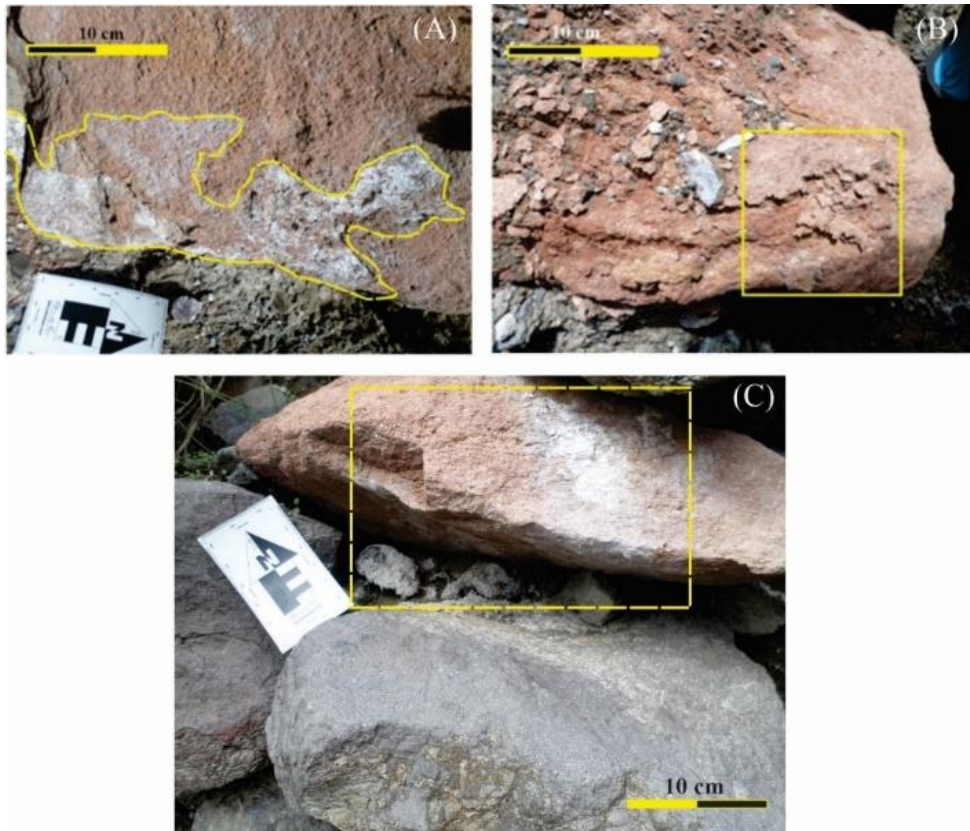
Figure 6. Effects of secondary salts in a volcanic clast (A) Salt crystallization on the rock surface (B) Breaking rock, (C) Effloresce, and traces of haloclasty.

Soil salinity is one of the main forms of soil degradation (Figure 7) in arid and semi-arid regions where precipitation is too low to maintain regular percolation of salts from the root zone of crops (Molina, 2018).

Moreover, the crystallization of a saline solution at a decrease in temperature affects a much larger volume of salt per unit of time than the crystallization induced by evaporation, which is more gradual. However, evaporation helps create saturated solutions from which crystallization can occur; also, highly soluble salts produce large volumes of crystals. It is

essential to note that of the common salts, gypsum is much less soluble than many of the others and that there will be less crystalline material available in a given volume of solution to cause the rock to break down (Parsons & Abrahams, 1994; Figure 7).
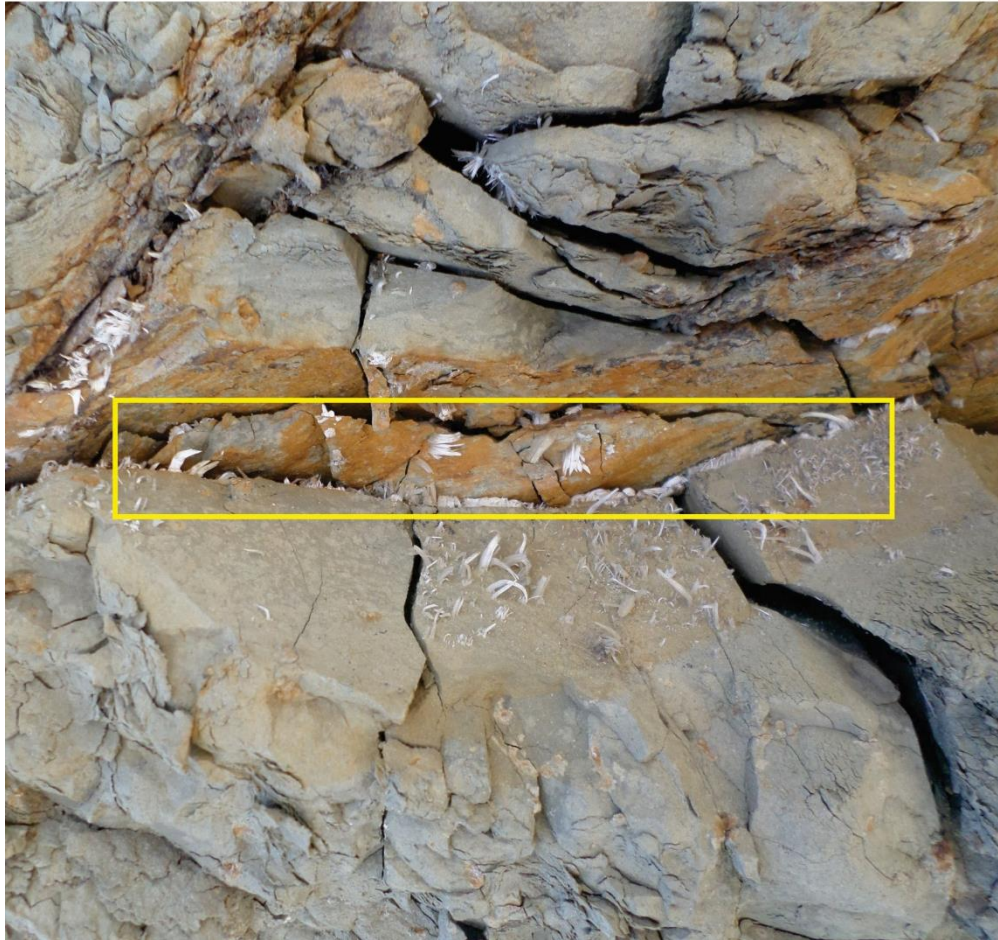
Figure 7. Gypsum crystals grown in local fractures of Chota member

According to Morales Tassinai et al. (2017), soluble salts can cause considerable damage when salts crystallize inside pores and capillaries. In addition, the crystallization of soluble salts affects materials used in construction, from: rocks, mortars, plasters, and bricks, to polychrome sculptures, mural paintings, and many other materials traditionally used in construction or as decorative elements.

According to Irassar et al. (2010) in the porous body, the crystallization of salts can occur on the surface, causing the typical efflorescence, or inside its mass, causing sub-efflorescence that can cause significant deterioration (Figure 8).
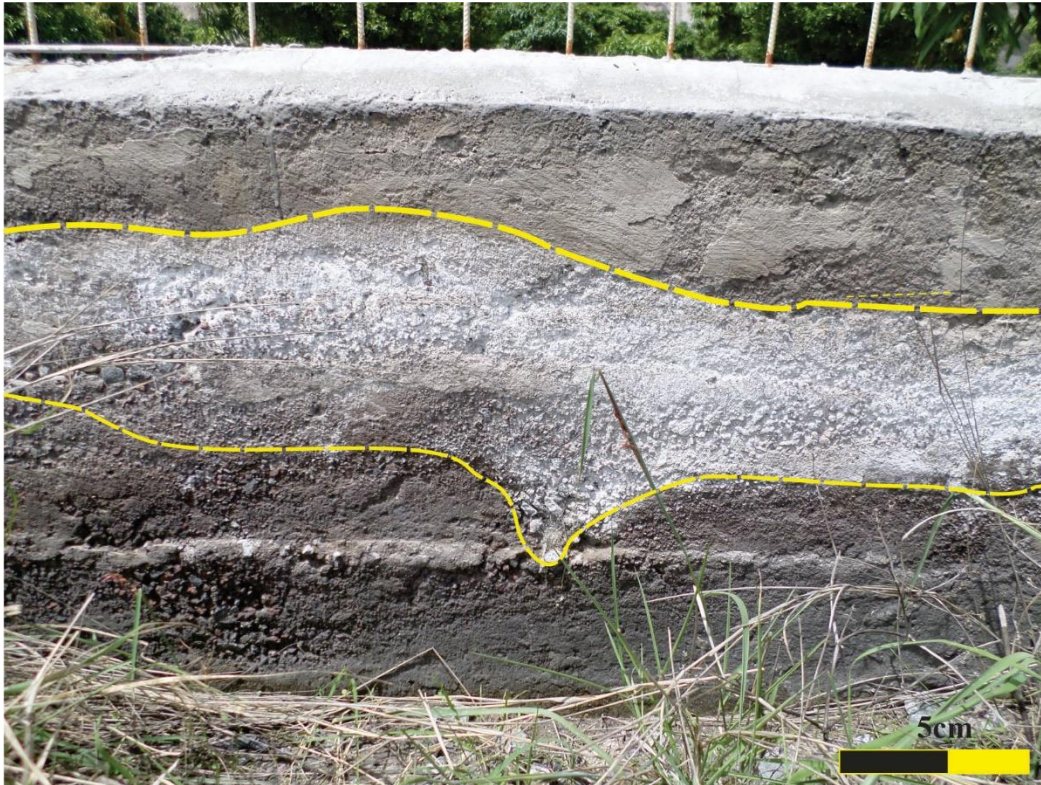
Figure 8. Salt crystals penetrating the concrete in Chota Basin

2.3   Salt crystallization effects

2.3.1   *Natural environment effects*

The most common model considers a saline solution circulating inside the pore network, where salt precipitation begins when water starts to evaporate or temperature raises (Scrivano & Gaggero, 2020). In the natural environment hen solution concentration reaches to the solubility and excess saturation point of the compounds, precipitation or crystallization will occur. The

pressure caused by the crystallization becomes higher than the rock strength, especially tensile strength, the rock will destroy (Oguchi & Yu, 2021).

So, according to Kamh (2005), landslides and salt weathering are two influential factors affecting rocks in the natural environment. These factors depend on the stability of the bedrock for the former and the source of salt. In another case, as reported by Maček et al. (2015), the Slano blato detachment is located in Slovenia (salty mud) detachment gets its name from the high concentration of sulfide and sulfate salts in the bedrock of the flysch, as well as in some of the spring waters. Water from the carbonate aquifer percolates through the fissured flysch bedrock and sandstones and maintains a high pore pressure within the flysch even during dry periods. When monthly precipitation exceeded 200 mm, the flysch behaved as an overland flow.

2.3.2 Construction effects

According to Özşen et al. (2017), the rocks were exposed to salt over time by rain and salts deposited in the pores at the construction level. Here, the crystallization of salts in porous materials can generate pressures within the pores high enough to exceed the elasticity of the material. Scrivano and Gaggero (2020) suggest that salt crystallization significantly affects exposed ornamental and construction rock weather. Furthermore, crystallization is common to all salt species, inducing weathering in the host rock. Therefore, the most common model considers a salt solution circulating within the pore network, where salt precipitation begins when water evaporates or the temperature increases.

Moreover, for construction magnesium sulphate is considered as one of the most aggressive salts and its damage can be caused by direct precipitation of a crystal from an oversaturated pore solution, as well as by a volume increase of a salt (Martínez-Martínez et al., 2021) Therefore, porosity and the amount of salt solution absorbed by the rock are directly related. It has, for

example, been identified as a major cause of construction decay in these areas and being instrumental in the formation of many natural salt-weathering phenomena (Parsons & Abrahams, 1994).

2.3.3 *Agronomical effects*

Soil salinization reduces productivity of agricultural and pasture lands, leading to a reduction in food availability. The reduction in biotic production potential is due not only to ecotoxicological effects of salts on crops but also to soil physical degradation (Payen et al., 2016). Then, boron, chloride, sodium, and carbonate are toxic for many plants, resulting in drying leaves, damaging fruit, and affecting root growth (Uri, 2018).

2.4 Common salts in the environment

The concentration of soluble salts would be mainly controlled by cations of sodium (Na), calcium (Ca), and magnesium (Mg; Álava & Haz, 2017; Allen & Hajek, 1989).

Therefore, the common saline minerals are calcite ($CaCO_3$), gypsum ($CaSO_4 \cdot 2 H_2O$), kieserite, hexahydrite, and epsomite ($MgSO_4H_2O$, $MgSO_4 \cdot 6 H_2O$, $MgSO_4 \cdot 7 H_2O$, respectively), thenardite (Na_2SO_4), mirabilite and halite (NaCl; Chesworth, 2008). For this study is essential to remember that the Chota Sedimentary basin is a semi-arid zone and corresponds to a natural environment analysis. The secondary phases are associated with salts, halides, sulfates, and some carbonates, which often occur in saline soils and arid environments such as Antarctica. Then other groups work as indicators of its extreme aridity that nitrate, borate, chromate, and perchlorate salts have been found in the Atacama Desert in Chile (Churchman & Lowe, 2012).

Based on this information some functional chemical concentrations are described below:

2.4.1 Sulfates

Doner and Lynn (1989) describes gypsum ($CaSO_4$) as the most common sulfate mineral in soils due to its low solubility compared to mirabilite (Na_2SO_4) or Epsomite ($MgSO_4$). Furthermore, Thomas (2011) explains that the natural environment occurs like a sulfate crust composed of the superposition of sulfates (e.g., barite, gypsum) on rocks.

2.4.2 Carbonates

According to Okrusch and Frimmel (2019), carbonates are salts composed of carbonic acid, H_2CO_3, and cations, such as Mg^{2+}, Zn^{2+}, Fe^{2+}, or Mn^{2+}. These salts as claimed by Ibáñez (2003) are characterized due to very slowly and weakly soluble features, commonly forming part of crusts in archaeological structures. In addition, carbonate minerals are present in some sedimentary rocks in the natural environment. Their metamorphic equivalents in the scarce igneous rock carbonatite and soil are found in arid and semi-arid environments (Chesworth, 2008).

Moreover, sodium carbonate like trona $Na_3H(CO_3)_2 *2(H_2O)$ is alternated with fine-grained, organic-rich tuff or tuffaceous hydrocarbon source rocks (Yu et al., 2019).

2.4.3 Chlorides

Rain is the source of the high chloride content of groundwater and salt lakes in coastal regions (Oguchi & Yu, 2021). The chlorides, as Thomas (2011) describes is that it infiltrates at a shallow depth. Then there is a displacement of substances which causes the accumulation of high concentrations of chloride and nitrate. Furthermore, vegetation is mainly absent on smooth surfaces due to the saline nature of the soil and low infiltration capacity.

2.4.4 Nitrates

Chesworth (2008) explains that nitrogen appears in the soil as nitrate ions; these are easily lost from the soil by the displacement of soluble substances. In addition, Okrusch and Frimmel (2019) describes that nitric acid is the component of salts nitrates, and part of the composition is isolated anionic complexes $[NO_3]^-$. Furthermore, the essential nitrate mineral, nitratine, is analogous to calcite, whereas niter displays an aragonite structure. It has long been known that chloride impurities in nitrate salts will accelerate corrosion (Kruizenga, 2012). Besides, nitrates ($NO_3 -$) and nitrates ($NO_2 -$) are some of the first oxyanion salts to melt and decompose to oxides in the molten salt layer (Nienhuis & McCloy, 2020).

Finally, nitrates rarely appear as efflorescence. These salts have resulted from the decomposition of organic matter, the action of nitrifying bacteria, human or animal activity, and nitrogenous fertilizers (Ibáñez, 2003).

2.4.5 Borates

Considering this type of functional chemical concentration it appears in different concentrations in all the Andean salt flats, however, due to their volume of reserves, accessibility and exploitation costs, only some are exploitable (Chong Díaz et al., 2020).

3 METHODOLOGY

This section shows the methodology applied in the work, the materials, methods and steps to characterizing secondary salts in the Chota Basin.

3.1 Field observations and sampling

The study area is composed by different sediments for this reason previous studies classify the material in Brillosas Member, Canales Colorados Member, Chota Member, Lahares Deposits

Metamorphic Basement, Quaternary Deposits, Tabulares Member, and Volcanicas Member. Furthermore, the accumulation of light-colored minerals is in soils, walls building, drainages and outcrops. However, these concentrations are as visible crust in the Quaternary Deposits, Metamorphic Basement, Canales Colorados, Chota Member, and Tabulares Member.

In order to collect the light-colored minerals sample during the fieldwork randomly points were considered based in the accessibility, location, concentration of light- colored minerals salts evidenced (Figure 7 and Figure 8) and the concentration of salt at the macroscopic level. Moreover, the main feature of the samples is white color, fine material with different shapes, like pellets, crust, crystals.

These samples were collected during two days in November 2021 under humid weather and traces of rain in the previous days, however the sun would be a factor that would favor the growth of minerals on the surfaces.

In addition, one feature and pattern to found saline points is considering the detachment, and exfoliation of the rock surface, mainly in nearby areas of cultivation, drainage and buildings. Finally, the amount of material goes from 1kg of saline sample to small portions of salt crusts-based appearance of material in the field. The point and the material collected is illustrated in (Table 1) that show the coordinates for saline samples and the sample name.

Table 1. *Sample points taken in the Chota basin according to the coordinates*

X	Y	Elevation (m)	Sample	Place of sample
829600	51039	1614	M1P1	Outcrop
829713	50823	1617	M1P2	Soil
829715	50657	1619	M2P3	Outcrop
829746	50455	1627	M2P5	Soil
829573	49233	1694	M2P7	Wall building
829576	49279	1686	M1P8	Wall building
830701	51760	1580	M1P9 and M2P9	Outcrop
830865	51628	1594	M1P10 and M2P10	Soil
831358	51641	1585	M1P11	Wall building
831644	51265	1617	M1P12	Soil
831639	51019	1628	M1P13	Soil
833649	49425	1733	M3P16	Outcrop
833595	51588	1701	M2P17	Outcrop
832505	49740	1700	M1P1 M5P1 and M6P1	Outcrop
832294	49804	1739	M1P2	Outcrop
832232	49793	1754	M1P3	Drainage base
832130	49775	1776	M1P9	Drainage base
832115	49760	1781	M1P10	Drainage base
832098	49761	1788	M1P11	Drainage wall
830459	50181	1699	M1P14	Drainage base
830517	50198	1692	M1P15	Drainage wall
829815	50437	1631	M1P16	Drainage base

3.2 Laboratory work

To develop a characterization of the secondary salts of the study area is necessary to prepare the taken samples in the laboratory. For instance, is difficult to establish which sample represent a salt. In consequence from the bags taken in the field is important to do a collection of the light-colored minerals.

3.2.1 *Saline crystals separation*

The main criterion applied was the selection of light-colored minerals there are some sample that easily could be separated by hand from the principal bag (Figure 9 A). The amount of sample considered in this process varies, however we can establish that from the 1kg bags that correspond to 100% of the sample, around 10g to 20g have been separated, corresponding to 10% and 20%, respectively. Instead, for samples that are not pure, such as crusts and salts in soils sediments, to develop the characterization it is important to select the light-colored minerals crystals from the collected samples by hand or using the spatula (Figure 9 B). The aim of these selection is to determine the type of secondary salinization that is occurring in the study area. The objective of this white material separation process is to carry out the subsequent analysis by X-ray diffraction, and to make observations under the stereomicroscope. Finally, although the samples were taken under a humid environment, the white crystals collected were not wet, so no extra processes were required for subsequent drying.

Figure 9. Sample preparation sequence (A) Manual selection of saline structures (B) Separation and scraping of salts. (C) Saline samples collected (D) Samples for X-RAY DIFFRACTION (XRD) analysis.

3.2.2 Crushing process

Since mostly clear or white pure minerals were collected, it is not necessary to subject the samples to a sieving process. Therefore, in this process it is necessary to grind light-colored minerals, for which white crusts and white samples are placed in the agate mortar. During this stage, the samples are subjected to a friction process that, as a result, gives us a homogeneous,

pulverized mixture of the desired size. Once the powder is obtained, it is not necessary to subject the sample to any sieving process. Grinding the samples helps to achieve a talc-like texture to reduce the roughness on the surface of the mounted sample (Betancourth et al., 2010). So, the size of particle would be less than ~10 microns (Figure 10).

Figure 10. Crushing process (A) Saline samples for X-RAY DIFFRACTION (XRD) analysis (B) Crushing samples in an agate mortar. (C)Samples for X-RAY DIFFRACTION (XRD) analysis.

3.2.3 X-RAY DIFFRACTION (XRD) analysis

X-ray diffraction is an important technique in the field of materials characterization to obtain information on an atomic scale from both crystalline and noncrystalline (amorphous) materials (Suryanarayana & Grant Norton, 1999). The diffraction is a consequence of the interaction between electromagnetic radiation and electrons. The electromagnetic radiation enters the material with a certain frequency and the electrons in the material oscillating in the direction of the polarization of the incident light (Lavina et al., 2014). This type of analysis is used for materials with a crystallographic structure where a set of atoms can be seen in an ordered arrangement (Betancourth et al., 2010).

It also allows us to determine the preferential orientations of the crystals and identify and quantify the phases that compose the material, whether of natural or mineral origin, information that allows us to study the material (Quiroga, 2021). Achieving success in qualitative analysis by employing any search-match utility becomes more and more challenging as the complexity of the powder diffraction pattern increases, especially when a material is a mixture of several phases (Pecharsky & Zavalij, 2005). Then to identify the secondary, the Powder Diffraction File (PDF), 2011 helped us establish the majority phases in each sample. The diffraction pattern is made up of a number of contributions, including the diffraction of wanted and unwanted wavelengths. So, to develop this analysis process, according to Jenkins and Snyder (1996).

These analyses were performed on twenty-six salt crust samples. To carry out this analysis the process is illustrated (Figure 11). Furthermore, the amount of material recommended to put in the holder would be more than 1g.

Figure 11. Process before X-RAY DIFFRACTION (XRD) analysis. (A) crushed samples. (B) Preparation in the aluminum sample holder. (C) Samples before X-RAY DIFFRACTION (XRD) analysis

These samples were analyzed in the materials characterization laboratory of the School of Chemical Sciences and Engineering of Yachay Tech University. First, salt crust samples with a minor amount of the material.
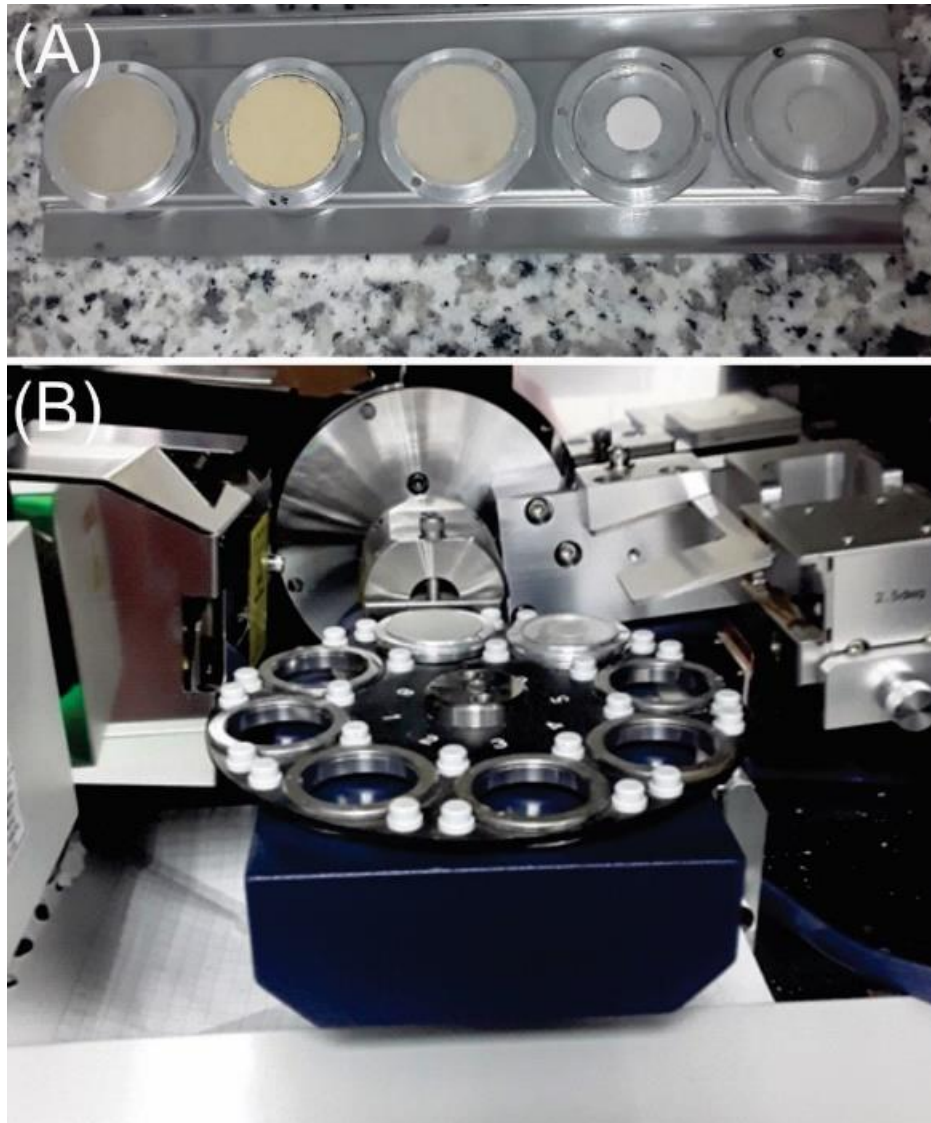
X-RAY DIFFRACTION (XRD) analysis is the primary technique used to identify and quantify the minerals present in a sample. Each mineral or compound has a characteristic X-ray diffraction pattern that functions as a "fingerprint" that is subsequently compared to a database. (Sánchez et al., 2017). It is used for those materials that meet the condition of having a

crystallographic structure where a set of atoms can be seen in an ordered arrangement. (Betancourth et al., 2010). X-RAY DIFFRACTION (XRD) analysis was used to determine the geo-mineral composition of the rock salt along with the qualitative analysis. (Chander et al., 2020). Based on Singh & Agrawal (2012), a Qualitative phase analysis of salt crystals found in the soil of the Chota Sedimentary Basin is necessary to understand and identify areas that are more prone to salt crystallization. On the other hand, X-ray diffraction (XRD) results are complex due to chemical compositions and various defects in the soil that can cause significant differences in X-RAY DIFFRACTION (XRD) reflection intensities between different species of the same mineral.

X-RAY DIFFRACTION (XRD) occurs when radiation is scattered through the atoms found in the periodic positions of the unit cells that form the crystal. The results obtained with X-RAY DIFFRACTION (XRD) are reflected in a diffraction profile. The profile can extract information about the diffraction peaks (fingerprints), their 2θ positions, peak intensities, areas, and the width of the diffraction peaks representing interference maxima. This information is used to understand the microstructural properties such as crystal size and micro deformations. It also allows us to determine the preferential orientations of the crystals and identify and quantify the phases that compose the material, whether of natural or mineral origin, information that allows us to study the material. (Quiroga, 2021)

The analysis was carried out with a Rigaku Mini-flex-600 powder diffractometer with a D/tex Ultra2 detector that is controlled by a computer able to provide qualitative and quantitative analysis for unknown powder crystalline materials. (Figure 12 B). The peaks obtained from this analysis were compared with all possible crystalline components in the database. Furthermore, Match! is software for phase analysis using powder diffraction data. This software compares the

diffraction pattern of sample the Chota Sedimentary sample to a database containing reference patterns to identify the present phases. Additional knowledge about the sample, like known phases, elements, or density, can be applied easily.

Figure 12. X-RAY DIFFRACTION (XRD) analysis (A) Prepared samples before analysis;(B) Samples at the Rigaku diffractometer.

X-ray diffraction (XRD) analysis was used to determine the geo-mineral composition of the rock salt along with the qualitative analysis (Chander et al., 2020). This analysis is the primary technique used to identify and quantify the minerals present in a sample. Each mineral or

compound has a characteristic pattern that works as a "fingerprint" that is subsequently compared to a database (Sánchez et al., 2017).

The steps to determine the phases in samples based on Jenkins and Snyder, 1996 are:

1.-Collection of the digitized data, the raw digitized pattern is stored along with the appropriate experimental parameters (Figure 13A).

2.- Smoothed data to reduce counting statistical fluctuations (Figure 13B).

3.- The background may subtract depending on the average peak/ background ratio across the pattern (Figure 13C).

4.- Alfa 2 striping as diffraction work is carried out using the Cu Ka, Ka. Here some peak distortion may occur due to partial separation of the Cu Ka, Ka, doublet over some parts of the 20 range because the angular dispersion of the diffractometer increases with increasing 20 (Figure 13D).

5.- The peaks are located according to the manual peak location or computer location that the most common procedure here we fit profiles to the raw pattern using all points in the peak (Figure 13E).

6.- Based on the internal standard or an external calibration curve, we will correct the whole pattern for the sensitivity of the particular instrument employed (Figure 13F).

7.- In the evaluation of data quality, here we consider the figures of merit (FOM) that provide us a useful guide to considering the salts according tools to analysis.

UNIVERSIDAD
YACHAY
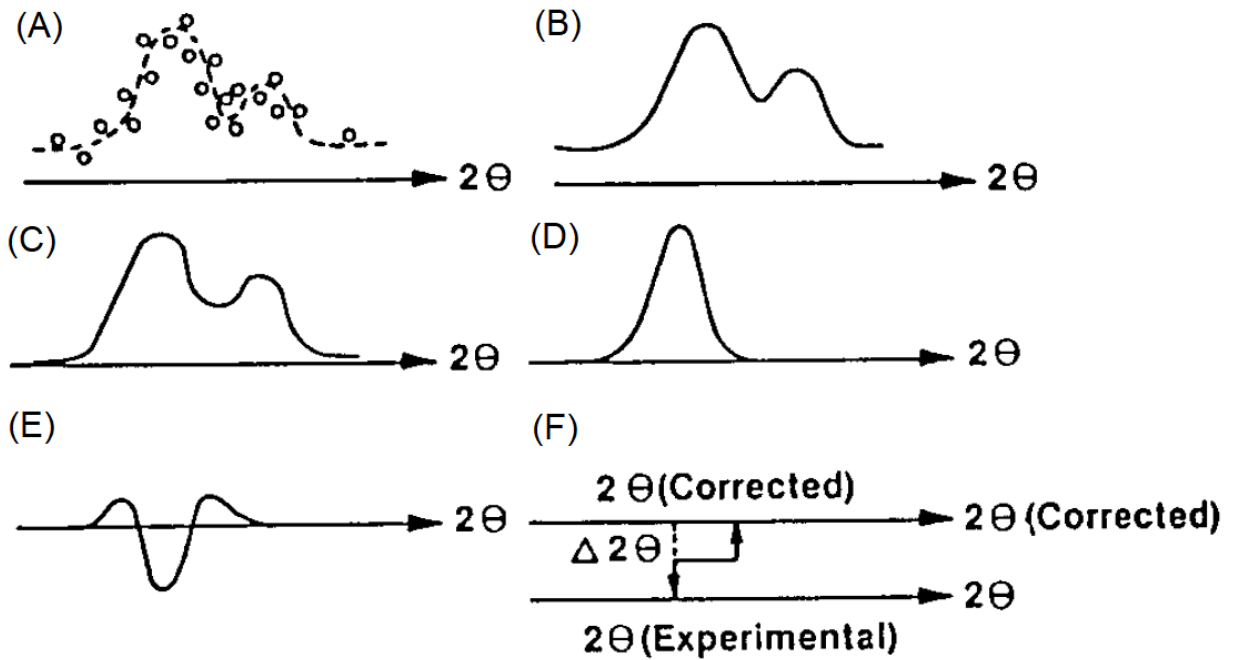TECH

SCHOOL OF
EARTH SCIENCES,
ENERGY AND ENVIRONMENT

Figure 13. Steps to determine the mineral phases. A) Collection step, B) Smooth data step, C) Background subtraction step, D) Alfa 2 striping, E) Peaks location, F) Pattern correction, taken from (Jenkins & Snyder, 1996).

3.2.4   Stereomicroscopic observations.

Through the use of the stereo microscope, the physical characteristics of the samples, such as transparency, luster and color, can be identified. However, conclusive data cannot be obtained from the samples because some samples have similar characteristics, so in this study applying the X-ray diffraction technique allows determining what types of minerals are found in the Chota basin and which they are saline. Finally, under stereomicroscopy observations there is the possibility of correlations between features and X-RAY DIFFRACTION (XRD) phases.

4 RESULTS AND DISCUSSION

Table 2. *Detailed mineral phases detected based in the samples*

Sample	Place of sample	Mineral Phase	Semiquantitative value
M1P1	Outcrop	Trona	82.8%
		Thenardite	17.2%
M1P2	Soil	Ezcurrite	87.4%
		Richelsdorfite	12.6%
M2P3	Outcrop	Bavenite	100%
M2P5	Soil	Cordierite	52.2%
		Muscovite 2\ITM\RG#1	36.6%
		Becquerelite	11.2%
M2P7	Wall building	Gowerite	81.2%
		Bavenite	18.8%
M1P8	Wall building	Thenardite, syn	100%
M1P9	Outcrop	Gypsum (deuterated)	100%
M2P9	Outcrop	Hydrotalcite, syn	63%
		Gypsum, syn	37%
M1P10	Soil	Thenardite, syn	43.2%
		Gowerite	41%
		Gordonite	15.8%
M2P10	Soil	Anorthite sodian	65.3%
		Thenardite, syn	34.7%
M1P11	Wall building	Thenardite, syn	100%
M1P12	Soil	Sericite	100%
M1P13	Soil	Dolomite	52.7%
		Gypsum	47.3%
M3P16	Outcrop	Epsomite, syn	86.5%
		Serpierite	13.5%
M2P17	Outcrop	Thenardite, syn	74.5%
		Saleeite	25.5%
M1P1	Outcrop	Berlinite, syn	44.4%
		Todorokite	41%
		Sidwillite	14.5%
M5P1	Outcrop	Gypsum	100%
M6P1	Outcrop	Potassium Cobalt Tungsten Oxide Hydrate	100%
M1P2	Outcrop	Thenardite, syn	100%
M1P3	Drainage base	Thenardite, syn	100%
M1P9	Drainage base	Labradorite	77.9%
		Thenardite, syn	22.1%
M1P10	Drainage base	Laumontite	62.4%
		Potassium Nitrate	37.6%
M1P11	Drainage wall	Calcite magnesian	100%
M1P14	Drainage base	Sassolite, syn	91.8%
		Haiweeite	8.2%
M1P15	Drainage wall	Bloedite	83.8%
		Bearsite, syn	16.2%
M1P16	Drainage base	Berlinite, syn	58.1%
		Thenardite, syn	32%
		Chudobaite	10%

Twenty-six samples were collected each one shows a semiquantitative value identification using X-RAY DIFFRACTION (XRD) technique that is in (Table 2). The material that shows the saline concentration or white minerals from soils, walls building, outcrops, drainage base and walls that are located in the different stratigraphic members of Chota basin. Consequently, the samples were analyzed under the X-RAY DIFFRACTION (XRD) approach so that the mineralogical composition of the components of the raw material and the qualitative analysis of the phases of the mixtures were determined. To determine the secondary salt of the samples according to Putz (2003), we use the semi-quantitative analysis Reference Intensity Ratio (RIR) method to compare the intensity scale factors of the identified phases with reference to a standard, where reference standard is corundum, RIR is known as I/Ic (Hubbard & Snyder, 1988; Putz, 2003). This factor is considered for all the phases, relating to the intensity of the highest peak of a standard peak phase.

The samples studied with the established procedure belong to the wall building, soils, outcrops, base and walls of drainages that are located in the stratigraphic members of the Chota basin. Twenty-six samples of secondary salts were analyzed and subjected to a crushing process, and finally, all were subjected to X-ray diffraction. According to the obtained diffractograms, the groups of secondary salts were recorded. Therefore, of the 26 samples of salt crystals samples taking into account the majority phases of the highest intensity peaks, there are 46 mineral phases identified (Annexes from 1 to 26). The results based in the mineral groups are presented with the percentage according to the number of samples (Figure 13).
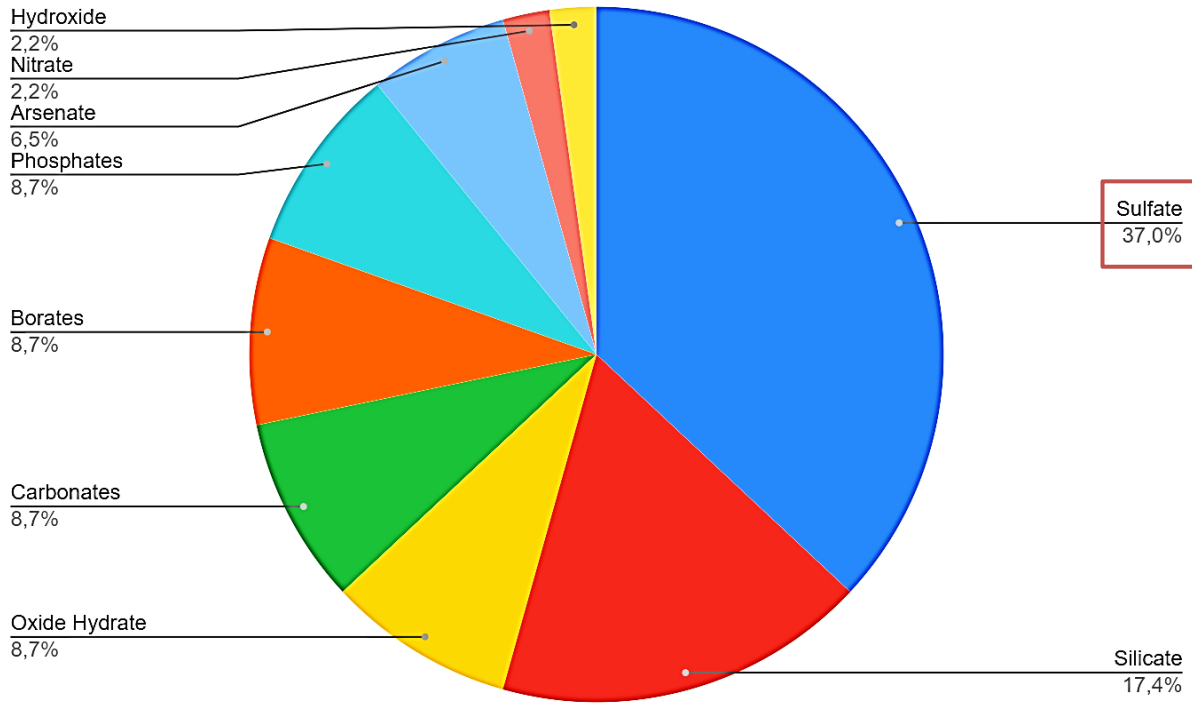
Figure 14. Percentage of functional chemical concentrations from 26 saline samples in which the red is marked the main functional group.

The results based in the identified phases are presented with the percentage according to the number of total phases (Figure 14). Considering the 46 phases detected in the diffractograms (Annexes from 1 to 26). The most common salt is thenardite that represent 21.7%. Then there is gypsum with 8.6% of the total samples. However, the 56.5 % correspond to others minerals.
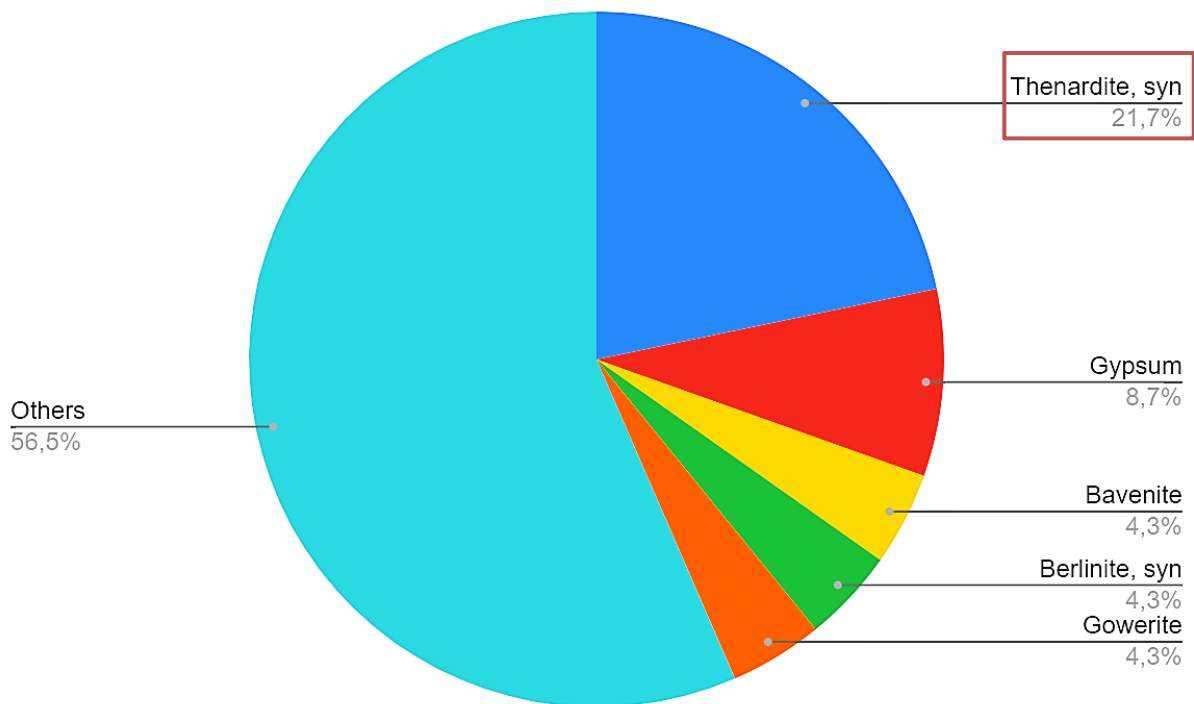
Figure 15. Percentage of minerals dominance in the samples collected based in the identified phases using X-RAY DIFFRACTION (XRD) technique, the red is marked the main phase.

Ultimately X-RAY DIFFRACTION (XRD) analyzes show salts belonging to the groups of sulfates, borates, carbonates, nitrates, arsenates, and other groups of minerals composed of cations such as Na^+, K^+, Ca^{2+}, Mg^{2+}, were detected. To illustrate the functional chemical and mineralogical features of detected minerals concentrations, we based the description in the X- ray diffraction patterns (Annexes from 1 to 26). Then we propose a table that consider the parameters like sample, mineral name, chemical name, chemical formula, crystal system, and powder diffraction file (PDF) code. Each of these detected functional chemical concentrations are described below:

4.1 Sulfates

From the total samples (Table 1), the Table 2 report sixteen mineral species whose chemical concentrations are associated with the sulfates in these samples, one M3P16 reports two

different sulfate minerals. In this group we can see that sodium sulphate predominates compared to hydrated calcium sulphate, hydrated magnesium sulphate and hydrated calcium copper-zinc sulphate hydroxide. In addition, considering the minerals, thenardite predominates over gypsum, bloedite, epsomite and serpierite. These data were obtained from the diffractogram and represents the qualitative information of the analysis (Annexes.1, 3, 4, 12, 5, 13, 6, 8, 14, 15).

Table 3. *Minerals with functional chemical concentrations associated to sulfates based in semiquantitative value of diffractogram.*

Sample	Mineral name	Name	Formula	PDF Code	Mineral Composition
M1P1	Thenardite	Sodium Sulfate	Na_2SO_4	00-074-2036	17.2%
M5P1	Gypsum	Calcium Sulfate Hydrate	$CaSO_4*2H_2O$	00-074-2036	100%
M1P2	Thenardite, syn	Sodium Sulfate	Na_2SO_4	00-074-2036	100%
M1P3	Thenardite, syn	Sodium Sulfate	Na_2SO_4	00-074-2036	100%
M1P8	Thenardite, syn	Sodium Sulfate	Na_2SO_4	00-074-2036	100%
M1P9	Thenardite, syn	Sodium Sulfate	Na_2SO_4	00-074-2036	22.1%
M1P9	Gypsum	Calcium Sulfate Hydrate	$CaSO_4(H_2O)_2$	00-076-1746	100%
M2P9	Gypsum, syn	Calcium Sulfate Hydrate	$CaSO_4*2H_2O$	00-076-1746	37%
M1P10	Thenardite, syn	Sodium Sulfate	Na_2SO_4	00-074-2036	43.2%
M2P10	Thenardite, syn	Sodium Sulfate	Na_2SO_4	00-074-2036	34.7%
M1P11	Thenardite, syn	Sodium Sulfate	Na_2SO_4	00-074-2036	100%
M1P13	Gypsum	Calcium Sulfate Hydrate	$CaSO_4(H_2O)_2$	00-076-1746	47.3%
M1P15	Bloedite	Sodium Magnesium Sulfate Hydrate	$Na_2Mg(SO_4)_2(H_2O)_4$	00-088-1789	83.8%
M1P16	Thenardite, syn	Sodium Sulfate	Na_2SO_4	00-074-2036	32%
M3P16	Epsomite, syn	Magnesium Sulfate Hydrate	$MgSO_4(H_2O)_7$	00-072-0696	86.5%
	Serpierite	Calcium Copper Zinc Hydroxide Sulfate Hydrate	$Ca(Cu_{0.66}Zn_{0.34})_4(OH)_6(SO_4)_2(H_2O)_3$	00-076-1675	13.5%
M2P17	Thenardite, syn	Sodium Sulfate	Na_2SO_4	00-074-2036	74.5%

Thenardite tends to be colorless and light brown in color with a glassy, luster, and transparency ranging from translucent to transparent (Figure 15). Then the second group of minerals is gypsum here it is colorless with a vitreous luster and ranges from transparent to translucent (Figure 16). Finally, in this sample it is not very clear to identify but in there is bloedite in (Figure 17 A) and epsomite or serpierite (Figure 17 B) the stereomicroscopic view the material is white to gray and probably has a silky or earthy sheen and shows a translucent transparency.
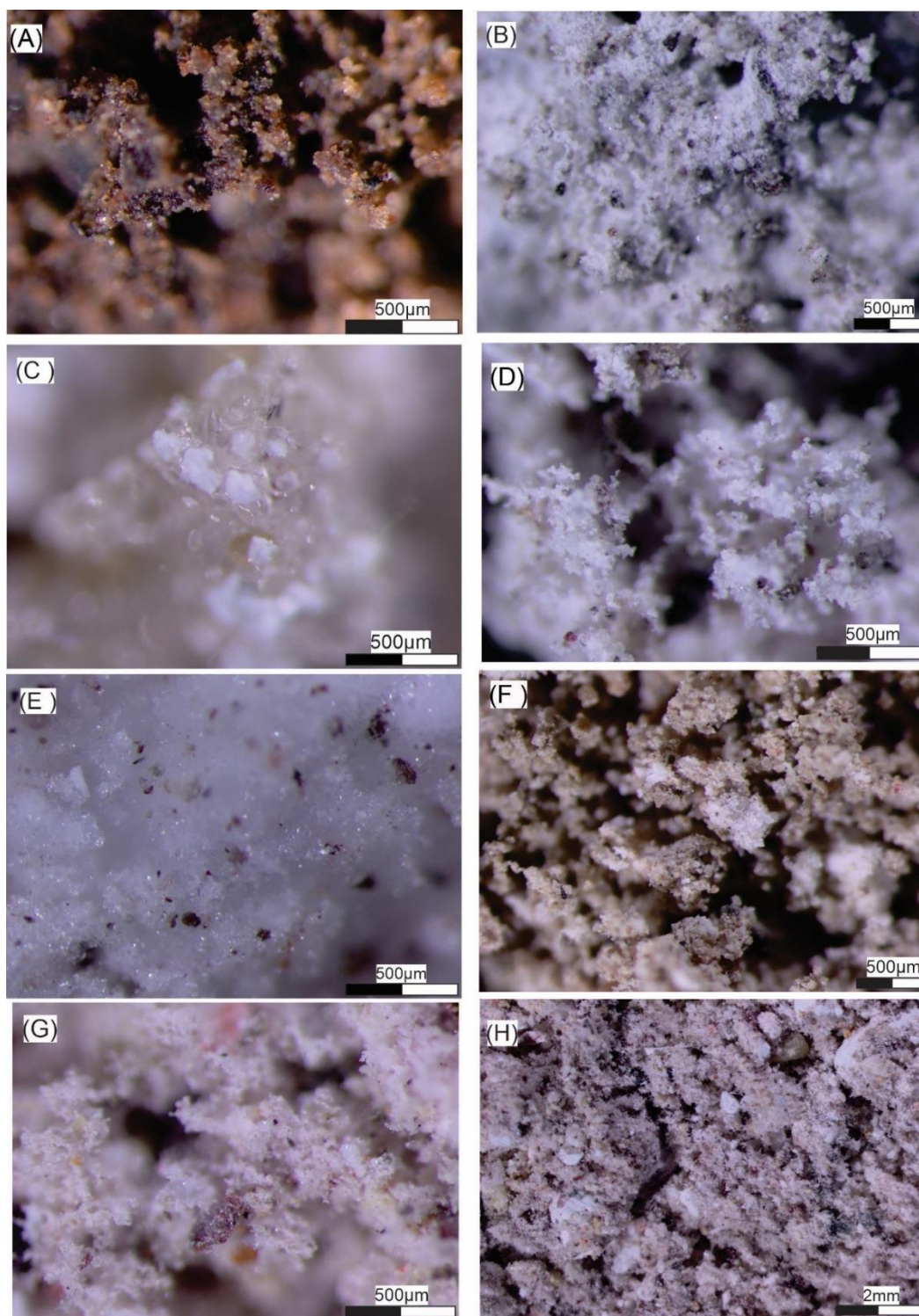
Figure 16. Thenardite samples. A) M1P1. B) M1P2. C) M1P3. D) M1P8. E) M1P9. F) M1P10. G) M1P11. H) M2P17
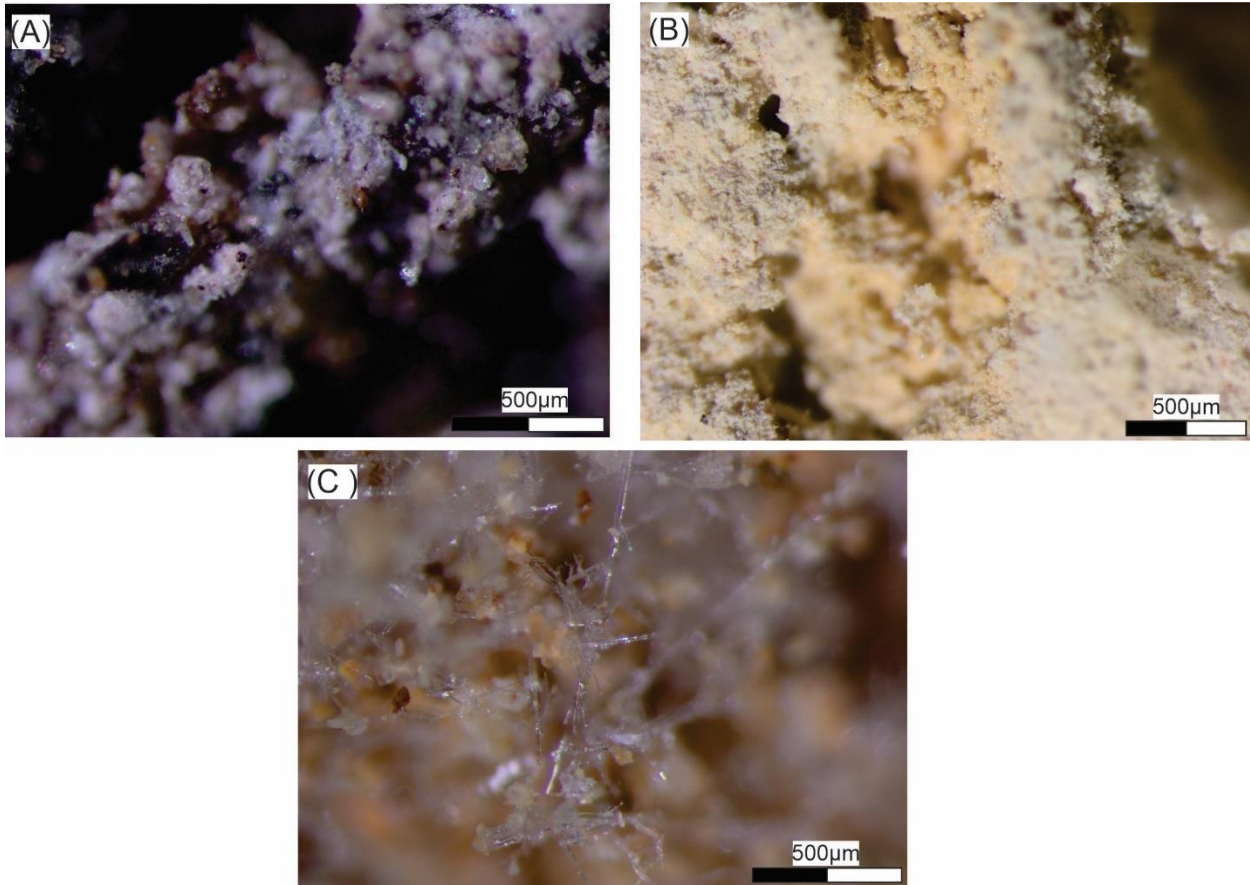
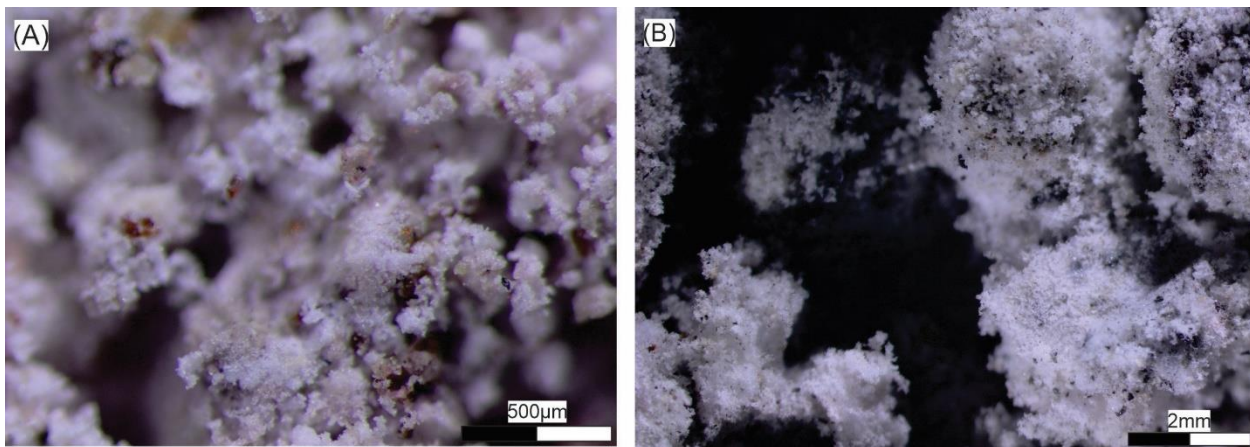Figure 17. Gypsum samples. A) M5P1. B) M1P9. C) M1P13

Figure 18. Sulfates minerals. A) Sample associate with bloedite M1P15. B) Sample associate with epsomite and serpierite M3P16.

4.2 Borates

Based on Table 2 of the total samples (Table 1), four are associated with borates. From these samples we can see that Calcium Hydroxide Borate Hydrate predominates over Sodium Borate Hydroxide Hydrates and Hydrogen Borate. On the other hand, considering the minerals, it is gowerite that predominates over ezcurrite, sassolite syn. These data were obtained from the diffractogram and represents the qualitative information of the analysis reported in Annexes. 2, 11, 5, 22.

Table 4. *Minerals with functional chemical concentrations associated to borates based in semiquantitative value of diffractogram.*

Sample	Mineral Name	Name	Formula	PDF Code	Mineral Composition
M1P2	Ezcurrite	Sodium Borate Hydroxide Hydrate	$Na_4(B_5O_7(OH)_3)_2(H_2O)_4$	00-071-1548	87.4%
M2P7	Gowerite	Calcium Hydroxide Borate Hydrate	$CaB_5O_8(OH)B(OH)_3(H_2O)_3$	00-073-0283	18.8%
M1P10	Gowerite	Calcium Hydroxide Borate Hydrate	$CaB_5O_8(OH)B(OH)_3(H_2O)_3$	00-073-0283	41%
M1P14	Sassolite, syn	Hydrogen Borate	H_3BO_3	00-073-2158	91.8%

Between sample M2P7 and M1P10 the white crystals accumulation looks similar with white color, and little vitreous luster (Figure 18).
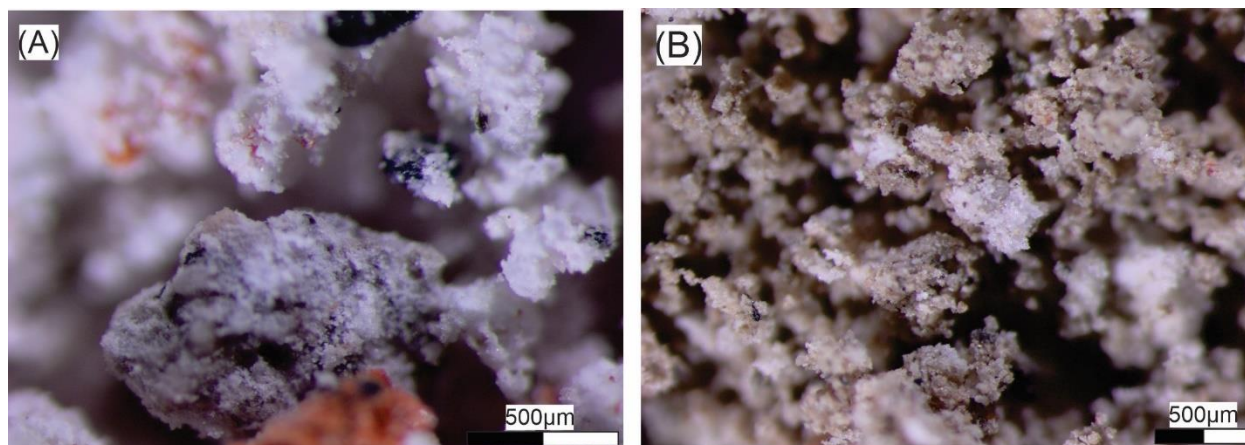

Figure 19. Samples associate with gowerite content under stereomicroscopic view. (A) M2P7. (B) M1P10

In M1P2 sample the material is colorless with vitreous, silky and transparent; while M1P4 sample shows the colorless and yellow material with pearly luster and transparent apparency (Figure 19).
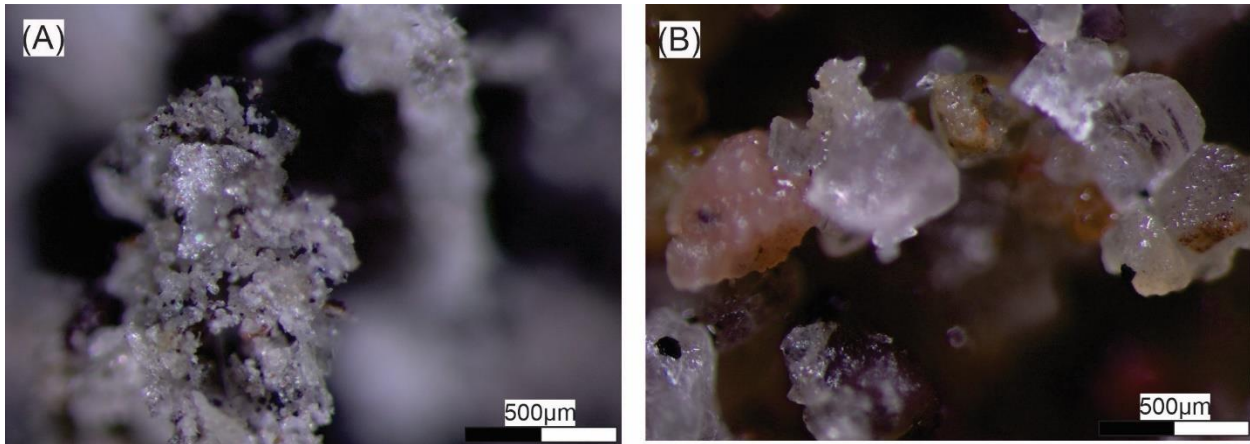

Figure 20. Samples associate with borate content under stereomicroscopic view. (A) Ezcurrite, M1P2. (B) Sassolite, M1P4.

4.3 Carbonates

Based in Table 4 from the total samples there are four carbonates this are trona, hydrotalcite, dolomite, and calcium magnesian. These data were obtained from the diffractogram and represents the qualitative information of the analysis reported in Annexes. 1, 12, 8, 21.

Table 5 . *Minerals with functional chemical concentrations associated to carbonates* based in semiquantitative value of diffractogram.

Sample	Mineral name	Name	Formula	PDF Code	Mineral Composition
M1P1	Trona	Sodium Hydrogen Carbonate Hydrate	$Na_3H(CO_3)_2*2H_2O$	00-029-1447	82.8%
M2P9	Hydrotalcite, syn	Magnesium Aluminum Hydroxide Carbonate Hydrate	$(Mg_{0.667}Al_{0.333})(OH)_2(CO_3)_{0.167}(H_2O)_{0.5}$	00-089-0460	63%
M1P13	Dolomite	Calcium Magnesium Carbonate	$CaMg(CO_3)_2$	00-073-2324	52.7%
M1P11	Calcite magnesian	Magnesium Calcium Carbonate	$(Mg_{.064}Ca_{.936})(CO_3)$	00-086-2335	100%

Carbonates content at the four samples is not completely clear to identify. But in M1P1 the sample there are colorless crystals with vitreous luster and translucent apparency. In M2P9 the material is yellowish with pearly luster and transparent apparency is not clear in this sample. In

M1P13 there are yellow material with pearly luster and translucent apparency crystals. In M1P11

the material is gray and brownish-white with pearly luster and translucent apparency. (Figure 20).
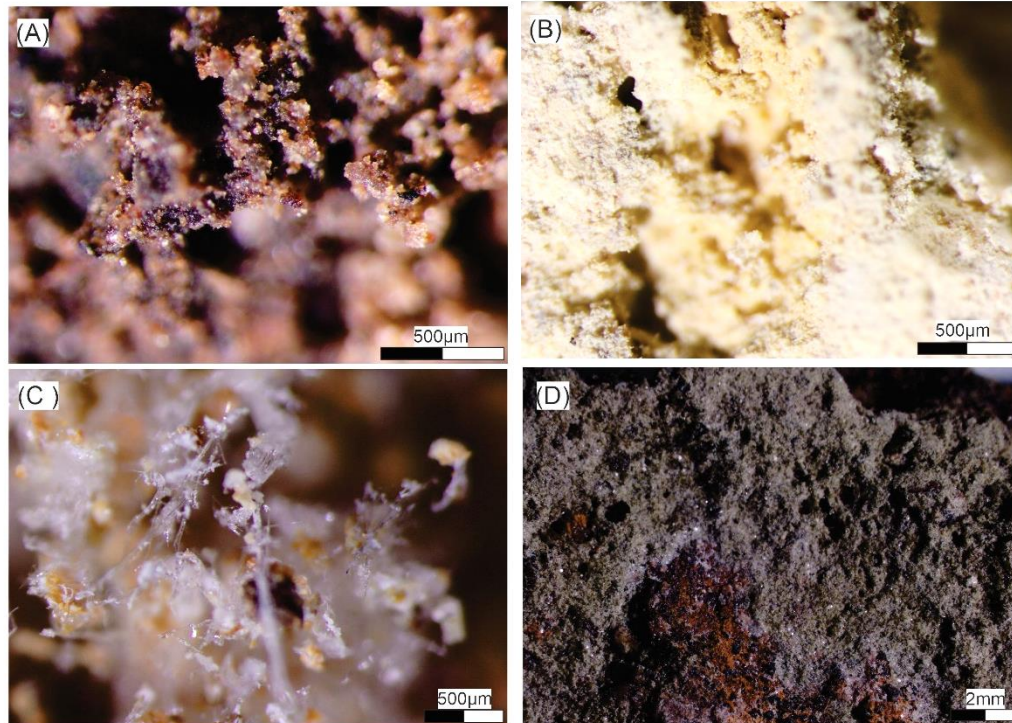

Figure 21. Samples associate with carbonate content under stereomicroscopic view. (A) Trona, M1P1. (B) Hydrotalcite, syn, M2P9. (C) Dolomite, M1P13. (D) Calcite magnesian, M1P11.

4.4 Nitrates

In the Table 5 there is one sample of a nitrate associate with potassium nitrate compound

in the chemical description. But there is not any mineral name reported in the diffraction pattern

Annexes. 20.

Table 6. *Minerals with functional chemical concentrations associated to nitrates based in semiquantitative value of diffractogram.*

Sample	Mineral name	Name	Formula	PDF Code	Mineral Composition
M1P10	-	Potassium Nitrate	KNO_3	00-070-0205	37.6%

Potassium nitrate in this sample could be represented by crystals in this samples, so here the color crystals are white, luster is milky and there is no transparency (Figure 21).
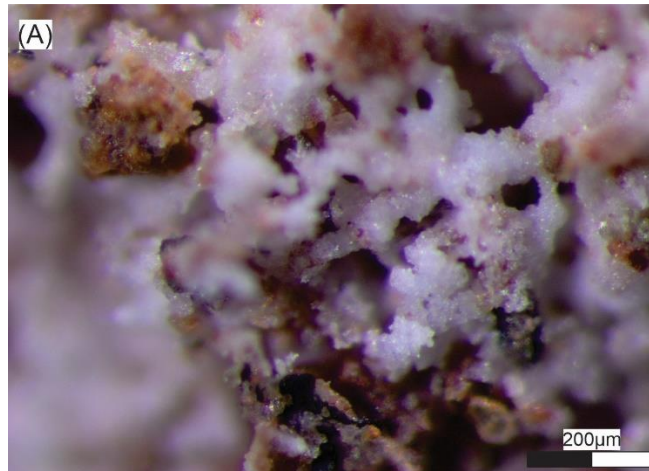

Figure 22. Sample associate with nitrate content under stereomicroscopic view. (A) Potassium Nitrate, M1P10

4.5 Phosphates

Based in the information of the Table 6, aluminum phosphate predominates in the chemical description compared to magnesium aluminum aqua phosphate hydroxide hydrates and magnesium uranium oxide phosphate hydrate. Moreover, bernalite, syn predominates in the mineralogical description compared to gordonite and saleeite are respectively. These data were obtained from the diffractogram and represents the qualitative information of the analysis that is reported in Annexes. 16, 5, 24, 14.

Table 7. *Minerals with functional chemical concentrations associated to phosphates based in semiquantitative value of diffractogram.*

Sample	Mineral name	Name	Formula	PDF Code	Mineral Composition
M1P1	Berlinite, syn	Aluminum Phosphate	$AlPO_4$	00-076-0228	44.4%
M1P10	Gordonite	Magnesium Aluminum Aqua Phosphate Hydroxide Hydrate	$MgAl_2((PO_4)_2(OH)_2(H_2O)_6)(H_2O)_2$	00-078-2047	15.8%
M1P16	Berlinite, syn	Aluminum Phosphate	$AlPO_4$	00-076-0228	58.1%
M2P17	Saleeite	Magnesium Uranium Oxide Phosphate Hydrate	$Mg(UO_2)_2(PO_4)_2(H_2O)_{10}$	00-071-0531	25.5%

In M1P1 and M1P10 there are small white crystals accumulation looks similar with white color. Besides, in M1P10 are smoky white to colorless with pearly luster (Figure 22).
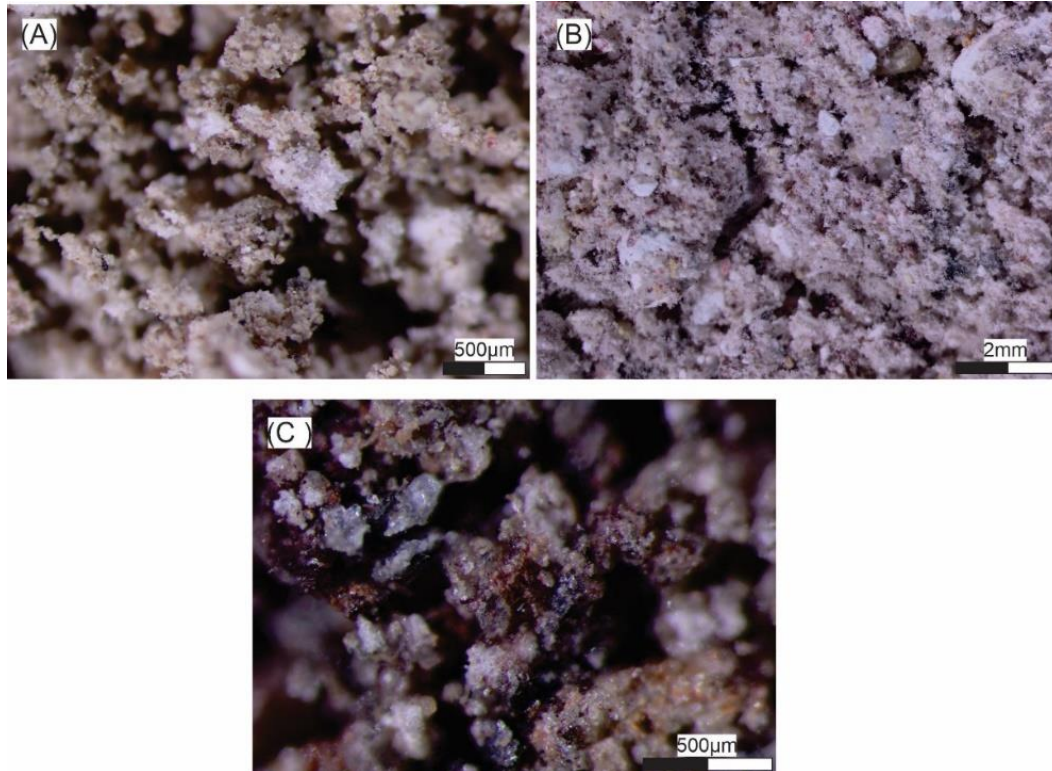

Figure 23. Samples associate with phosphate content under stereomicroscopic view. (A) Berlinite M1P1 (B) Gordonite M1P10. (C) Saleeite, M2P17.

4.6 Arsenates

There are three samples associated with arsenates the compounds are calcium copper antimony chloride arsenate hydroxide hydrates, beryllium arsenate hydroxide hydrates, magnesium zinc arsenate hydrate. The minerals respectively are richelsdorfite; bearsite, syn. These data were obtained from the diffractogram and represents the qualitative information of the analysis that is reported in Annexes. 2, 23, 24.

Table 8. *Minerals with functional chemical concentrations associated to arsenates based in semiquantitative value of diffractogram.*

Sample	Mineral name	Name	Formula	PDF Code	Mineral Composition
M1P2	Richelsdorfite	Calcium Copper Antimony Chloride Arsenate Hydroxide Hydrate	$Ca_2Cu_5Sb(Cl(OH)_6(AsO_4)_4)(H_2O)_6$	00-078-1248	12.6%
M1P15	Bearsite, syn	Beryllium Arsenate Hydroxide Hydrate	$Be_2(AsO_4)(OH)(H_2O)_4$	00-082-0067	16.2%
M1P16	Chudobaite	Magnesium Zinc Arsenate Hydrate	$(Mg_{0.7}Zn_{0.3})_5H_2(AsO_4)_4(H_2O)_{10}$	00-070-0136	10%

In the samples with arsenate content for the sample M1P2 is green to gray color with vitreous luster (Figure 23. A). Whiles the M1P15 show white crystals accumulation with a little vitreous luster (Figure 23. B)
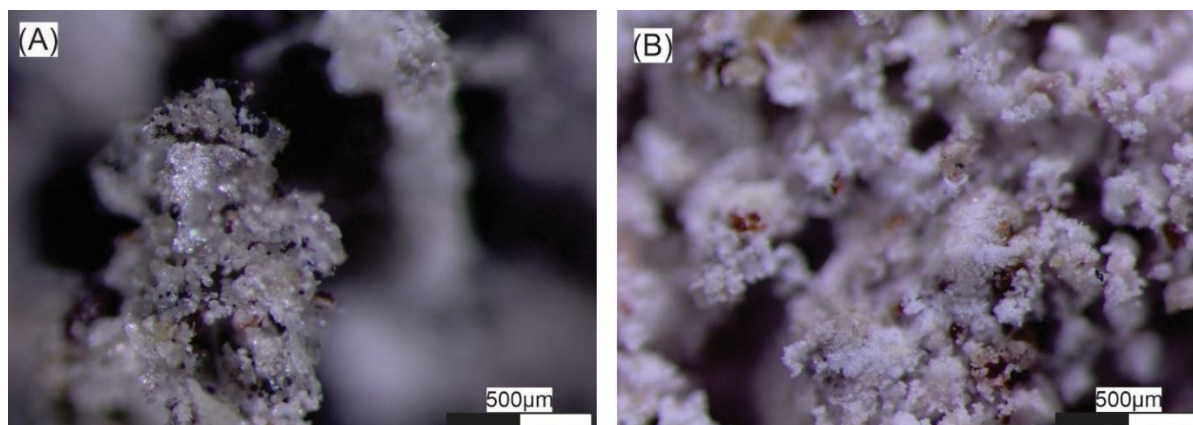
Figure 24. Samples associate with arsenate content under stereomicroscopic view. (A) Richelsdorfite M1P2. (B) Bearsite, syn M1P15

4.7 Oxide Hydrates

In the Table 8 there are four samples associated to oxide hydrates that was taken from the diffractogram, represents the qualitative information of the analysis and are reported in the Annexes. 16, 26, 10, 22.

Table 9. *Minerals with functional chemical concentrations associated to oxide hydrates based in semiquantitative value of diffractogram.*

Sample	Mineral name	Name	Formula	PDF Code	Mineral Composition
M1P1	Todorokite	Calcium Manganese Oxide Hydrate	$Ca_{0.8}(Mn_4O_8)(H_2O)_2$	00-087-0389	41%
	Sidwillite	Molybdenum Oxide Hydrate	$MoO_3(H_2O)_2$	00-088-1799	14.5%
M6P1	Potassium Cobalt Tungsten Oxide Hydrate	Potassium Cobalt Tungsten Oxide Hydrate	$K_5(CoW_{12}O_{40})(H_2O)_{20}$	00-076-1236	100%
M2P5	Becquerelite	Calcium Uranyl Oxide Hydroxide Hydrate	$Ca(UO_2)_6O_4(OH)_6(H_2O)_8$	00-084-0513	36.6%
M1P14	Haiweeite	Calcium Uranium Silicate Oxide Hydroxide Hydrate	$Ca(UO_2)_2(Si_5O_{12}(OH)_2)(H_2O)_{4.5}$	00-088-0774	8.2%

In samples with oxide hydrates content there are white to colorless crystals, with a pearly luster (Figure 24).
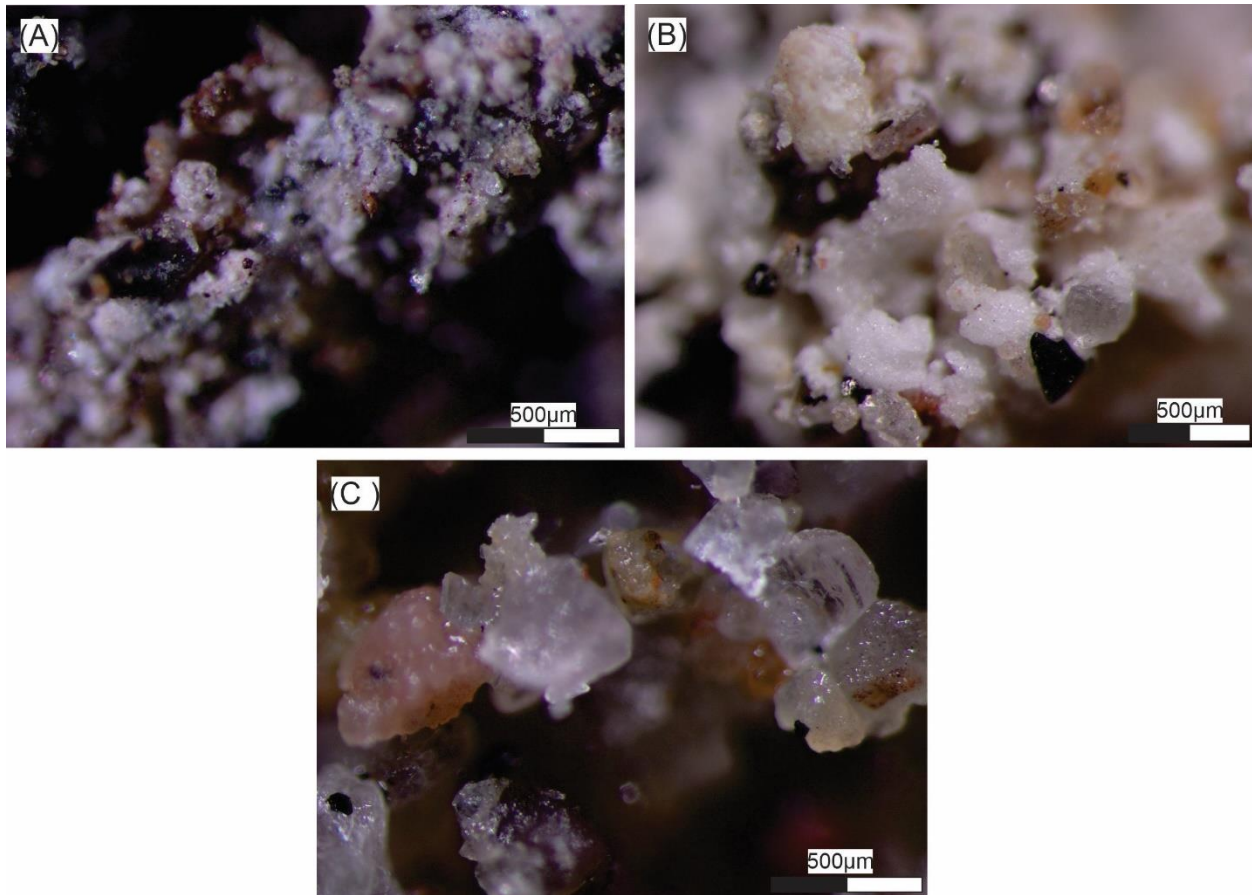

Figure 25. Samples associate with oxide hydrates content under stereomicroscopic view. (A) Becquerelite, M2P15. (B) Todorokite and Sidwillite, M1P1 (C) Potassium cobalt tugsten oxide hydrates, M6P1.

4.8 Silicates

Based in the Table 9 calcium beryllium aluminum hydrogen oxide silicate predominates, the mineral is bavenite. These data were obtained from the diffractogram, represents the qualitative information of the analysis and are reported in Annexes. 9, 10,11, 3, 4, 19, 20, 13.

Table 10. *Minerals with functional chemical concentrations associated to silicates based in semiquantitative value of diffractogram.*

| Sample	Mineral name	Name	Formula	PDF Code	Mineral Composition
M2P3	Bavenite	Calcium Beryllium Aluminum Hydrogen Oxide Silicate	Na_2SO_4	00-074-2068	100%
M2P5	Cordierite	Magnesium Aluminum Silicate	$Mg_2Al_4Si_5O_{18}$	00-076-1794	52.2%
	Muscovite	Potassium Aluminum Silicate Hydroxide	$KAl_3Si_3O_{10}(OH)_2$	00-075-0948	36.6%
M2P7	Bavenite	Calcium Beryllium Aluminum Hydrogen Oxide Silicate	Na_2SO_4	00-074-2068	81.2%
M1P9	Labradorite	Sodium Calcium Aluminum Silicate	$Na_{0.45}Ca_{0.55}Al_{1.55}Si_{2.45}O_8$	00-078-0434	77.9%
M1P10	Laumontite	Potassium Sodium Calcium Aluminum Silicate Hydrate	$K_{0.10}Na_{0.30}Ca_{3.60}(Si_{16.40}Al_{7.60}O_{48})(H_2O)_{14}$	00-080-0648	62.4%
M2P10	Anorthite sodian	Calcium Sodium Aluminum Silicate	$Ca_{.66}Na_{.34}Al_{1.66}Si_{2.34}O_8$	00-086-1650	65.3%
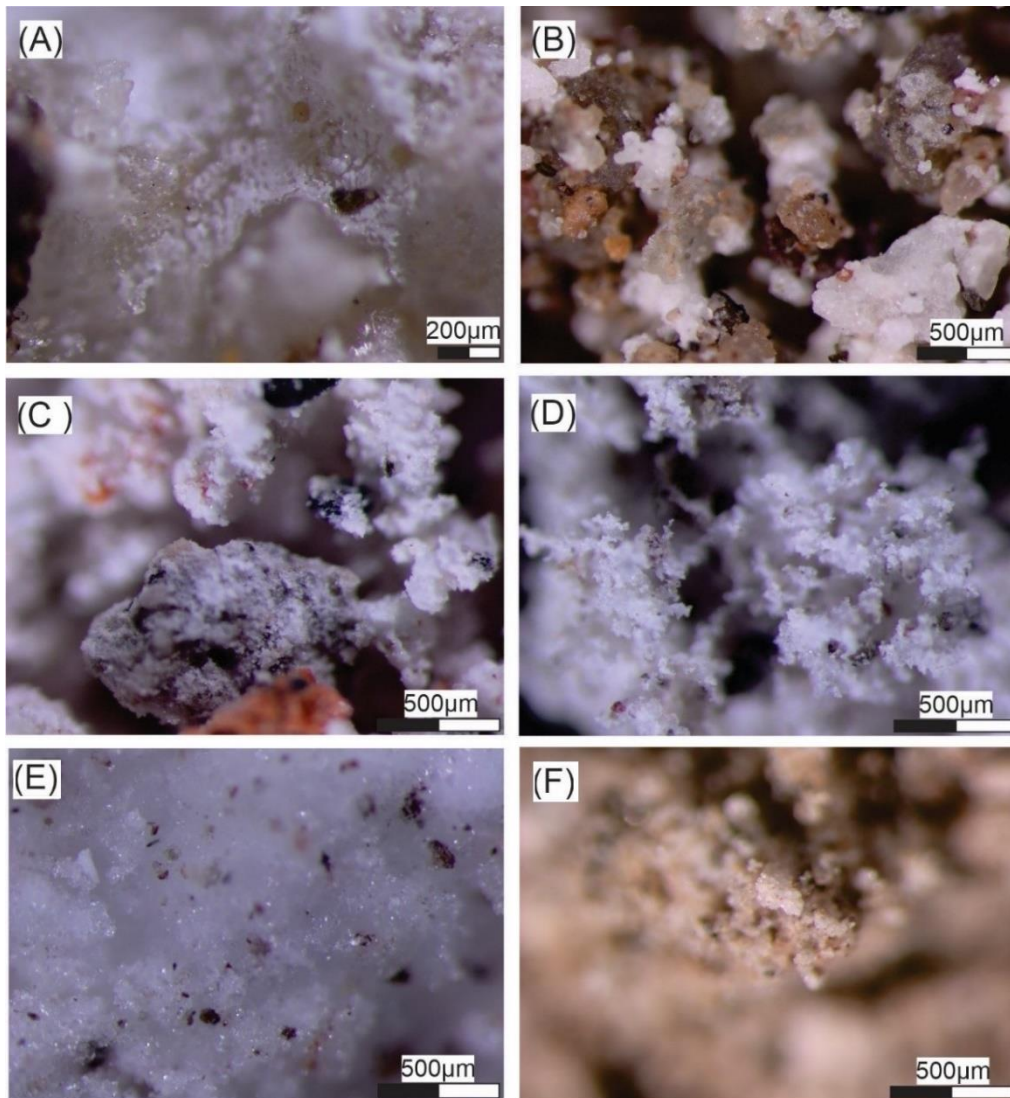
Figure 26. Samples associate with silicates content under stereomicroscopic view. (A) Bavenite, M2P3. (B) Cordierite and Muscovite, M2P5. (C) Bavenite, M2P7. (D) Labradiorite, M1P9 (E) Laumontite, M1P10 (F) Anortite Sodian, M2P10.

4.9 Hydroxides

Table 10 describes the data that correspond to one sample associate with a hydroxide and is associated with a sericite mineral from the diffractogram that represents the qualitative information of the analysis reported in Annexes. 7.

Table 11. *Minerals with functional chemical concentrations associated to hydroxides based in semiquantitative value of diffractogram.*

Sample	Mineral name	Name	Formula	PDF Code	Mineral Composition
M1P12	Sericite	Hydroxide	$(K_{0.727}Na_{0.170}Ca_{0.011})(Al_{0.933}Fe_{0.016}Mg_{0.011})_2(Si_{0.782})$	00-089-6216	100%

In the sample that show a content of sericite the material is white to colorless, and show a vitreous luster (Figure 26).
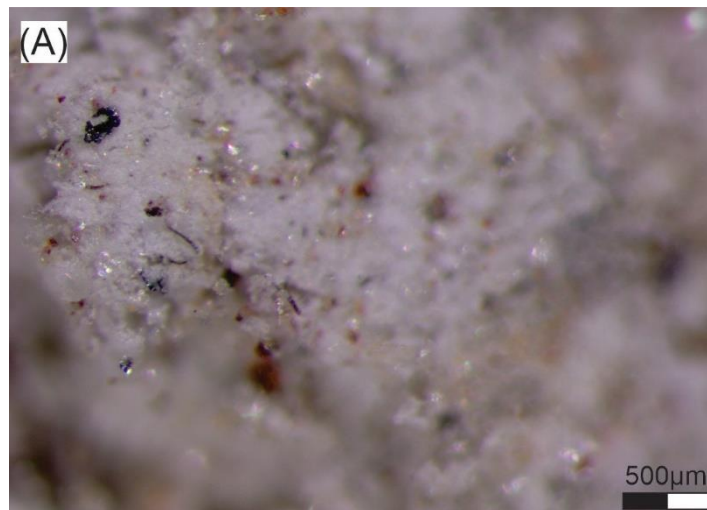
Figure 27. Sample associate with sericite M1P12

4.10 Salts accumulation based in the stratigraphic arrangement

There are different structures sampled in the study area. However, the stratigraphic arrangement that was previously described show different accumulation percentages, from the total samples, Quaternary deposits show 46.2% accumulation of salt crust, Metamorphic Basement

with 23.1%, then there is Canales Colorados member with 15.4%. Finally, Chota and Tabulares, both with 7.7% according to (Figure 27).
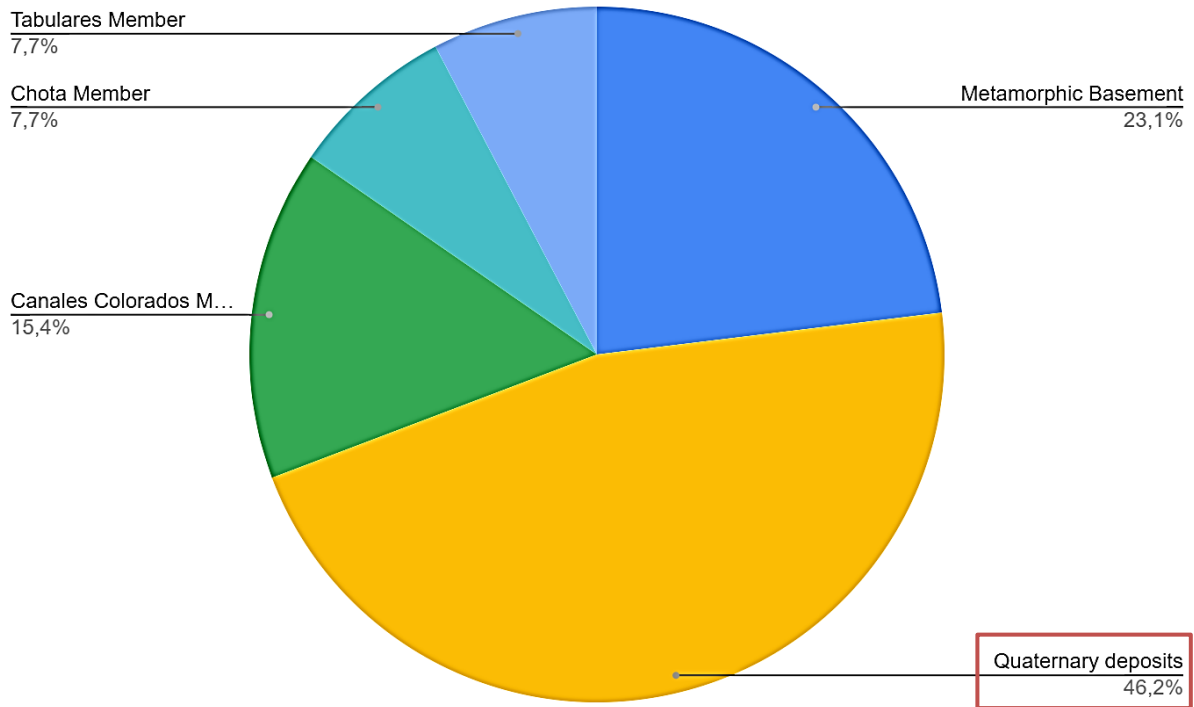

Figure 28. Percentage of salts concentration based in the stratigraphic arrangement from 26 samples in which the red square marked the main deposit.

The accumulation of salts in the study area is shown in Figure 4. Quaternary deposits, that are associated with cultivations areas, and is influenced by human activity show salt accumulation. Taking account, the rest of the stratigraphic arrangement this accumulation occurs in lower elevation (Table 1). There are twelve samples associated with white crusts, of which eight samples belong to the sulfates in this group, seven are salt samples with thenardite (M1P1, M1P2, M2P8, M1P10, M2P10, M1P1 and M1P16) content and one with gypsum content (M1P13). Also, there is a borate in M2P7.

In the Metamorphic Basement, that is composed of medium to high grade metamorphosed rocks, common quartzites, and phyllites that show high content of micas and quartz. The standard color is black and reddish. Here, from six samples, four show sulfate content (M1P2, M5P1, M2P17 and M3P16), two samples show oxide hydrates content (M1P1 and M6P1) and two phosphate content (M1P1 and M2P17).

In the Canales Colorados member, that is formed by intercalation of conglomerates, breccias, and sandstones, with gray, yellowish, and reddish colors. The clast's sizes are between coarse to boulder, which shows matrix support, and the shapes of clasts are subrounded to subangular that are poorly to medium sorted. There are three samples, two of them show the silicate content (M1P9 and M1P10), one sample shows sulfate content (M1P9), another nitrate content (M1P10) and the last sample shows carbonate content (M1P11). Then, Potassium Nitrate is not found in a crop area or area close to a crop and the source for this compound is nitrogen. Thus, we can infer that it was moved as a particle and deposited in this member.

In the Tabulares Member, there are two samples, one of them (M1P14) shows content of borates and hydroxides, the second sample (M1P15) indicates content of sulfate and hydroxide.

In the Chota Member, that is formed by intercalation of sandstones and shales that commonly shows lamination and cross-stratification and several colors like yellowish, dark grey, and dark red. Here, the collected samples show sulfate content (M1P9 and M2P9), there is also hydrotalcite content (M2P9).

Finally, the accumulation of salts accumulates in the depression zone corresponding to the Quaternary deposits, this occurs because the sulfates that make it up are soluble and move through the soil until they accumulate in depression zones. However, the study area is located between two

and the agriculture activity in the area.

5   CONCLUSIONS AND RECOMMENDATIONS

5.1   Conclusions

From the X-RAY DIFFRACTION (XRD) analysis of 26 samples, the main group chemical functional groups correspond to sulfates and the most common mineral is thenardite. Moreover, there are 46 mineral phases have been identified, of which 33 correspond to saline groups, being the predominant phase. Considering constructions from 3 shown, 2 that correspond to 66.67% of them show the thenardite content it is suggested that its formation may be associated with manufactured rock mass that has content of minerals that are expelled. For the samples whose origin was outcrops from 10 sampled, 3 of them that correspond to 30% show thenardite content, and there are 3 that correspond to 30% show gypsum content. Moreover, from 6 samples collected from the soils, 2 of them that correspond to 33.33% show content of Thenardite which could be mainly influenced by irrigation process and human activity.

In the areas corresponding to drainages from the 5 samples collected at the base of the drainage, 3 of them that correspond to 60% show a content of thenardite. Finally, two samples were taken from the drainage walls and the mineral content of this sample corresponds to calcite magnesian, bloedite, bearsite, these minerals could be associated with water transport that are produced in these areas and movements of ions.

The analytical procedure developed in this work allowed us to characterize the secondary minerals of the Chota Basin. From the results obtained with the analysis by X-ray diffraction

(XRD). From twenty-six samples, we identify forty-seven mineral phases. In which sulfate salts are predominant form being the thenardite followed by gypsum, epsomite bloedite and serpierite.

The dynamics of salt crystallization around the study area would be influenced by the geological material, temperature and humidity of the environment during the sampling days. Here the influence of this factors could be produced leaching, and movements of ions that shows saline crystals accumulation at the surfaces.

Furthermore, based on the semi-arid environment shown by Instituto Nacional de Meteorología e Hidrología (INAMHI), we can verify the saline crusts around the study area. However, there is salt accumulations under construction. In these cases, the salts crystallize on the surface of the construction, exerting pressure on the structure and damaging walls of contruction.

5.2   Recommendations

Finally, this characterization helps us to propose futures studies related to the effects of salinization in vegetation, influence of borates in the soils. Impacts of salt crystallization at construction levels and the index of weathering produced by accumulation of saline crystals. Moreover, is necessary to carry out studies of salt content at different deeps to stablish and understand the triggers.

Considering the fieldwork, the saline samples for this project were taken using plastic bags. However, we suggested that, in order to protect the qualities of the sample, do the collections in glass containers. In addition, develop studies on the crops to see what amounts of salts they contain and the possible negative effects. Also, we suggest to carry out studies to quantify the number of salts, using the conductivity of soils.

6 BIBLIOGRAPHY

Agila, R. S. (2017). Determinación y prevención de los niveles de eflorscencia primaria por uso del mortero en las paredes de ladrillo en el barrio Cuba al sur de la ciudad de Guayaquil. *Tesis*, 121.

Álava, D., & Haz, E. (2017). *Aplicación de cocteles microbiano y bovinaza- cascarilla de arroz para la recuperación de muestras de suelos salinos del sitio correagua, Manabí*. 54.

Barragán, R., Baudino, R., & Marocco, R. (1996). Geodynamic evolution of the Neogene intermontane Chota basin, Northern Andes of Ecuador. *Journal of South American Earth Sciences*, *9*(5–6), 309–319. https://doi.org/10.1016/s0895-9811(96)00016-8

Betancourth, D., Gomez, J., Mosquera, J., & Tirado, L. (2010). *Análisis por difracción de rayos X de rocas provenientes de región esmeraldífera*. *44*, 257–260.

Chander, V., Tewari, D., Negi, V., Singh, R., Upadhyaya, K., & Aleya, L. (2020). Structural characterization of Himalayan black rock salt by SEM, XRD and in-vitro antioxidant activity. *Science of the Total Environment*, *748*, 141269. https://doi.org/10.1016/j.scitotenv.2020.141269

Chesworth, W. (2008). Encyclopedia of Soil Science. In *Springer* (Vol. 33, Issue 4). https://doi.org/10.1089/jamp.2020.29028.whf

Chong Díaz, G., Demergasso, C., Urrutia Meza, J., & Vargas A., M. (2020). El Dominio Salino del norte de Chile y sus yacimientos de minerales industriales. *Boletín de La Sociedad Geológica Mexicana*, *72*(3), A020720. https://doi.org/10.18268/bsgm2020v72n3a020720

Churchman, G. J., & Lowe, D. J. (2012). Alteration, Formation, and Occurrence of Minerals in Soils Introduction: The Role of Mineralogy in Soil Science. *Handbook of Soil Sciences. 2nd Edition. Vol. 1: Properties and Processes*, *1*, 20.1-20.72.

Coltorti, M., & Ollier, C. D. (2000). Geomorphic and tectonic evolution of the Ecuadorian Andes. *Geomorphology*, *32*(1–2), 1–19. https://doi.org/10.1016/S0169-555X(99)00036-7

Doner, H. E., & Lynn, W. C. (1989). Chapter 6 Carbonate , Halide , Sulfate , and Sulfide. *Minerals in Soil Environments (2nd Edition)*, 280–330.

Doornkamp, J. C., & Ibrahim, H. (1990). *Salt weathering*. *14*(3).

Fonseca, E. (2021). *Sedimentological and paleoenvironmental study of the Peñas Coloradas Formation of the Chota basin, Ecuador*. Universidad de Investigación de Tecnología Experimental Yachay.

Gavrichkova, O., Brykova, R. A., Brugnoli, E., Calfapietra, C., Cheng, Z., Kuzyakov, Y., Liberati, D., Moscatelli, M. C., Pallozzi, E., & Vasenev, V. I. (2020). Secondary soil salinization in urban lawns: Microbial functioning, vegetation state, and implications for carbon balance. *Land Degradation and Development*, *31*(17), 2591–2604. https://doi.org/10.1002/ldr.3627

González, J., Dávila, A., & Martinez, T. E. (2013). *Ministerio del Ambiente (MAE)*.

Goudie, A. S. (2004). *Encyclopedia of Geomorphology*.

Grossi, C. M., & Esbert, R. M. (1994). Las sales solubles en el deterioro de rocas monumentales. Revisión bibliográfica. *Materiales de Construcción*, *44*(235), 15–30. https://doi.org/10.3989/mc.1994.v44.i235.579

Guachamín, W., Cadena, J., Carvajal, J., & García, F. (2015). Estudios e Investigaciones Hidrologicas. *INAMHI*. http://www.serviciometeorologico.gob.ec/Publicaciones/Hidrologia/ESTUDIO_DEL_MIRA.pdf

Hayes, S. M., Webb, S. M., Bargar, J. R., Day, P. A. O., Maier, R. M., & Chorover, J. (2012). *Geochemical Weathering Increases Lead Bioaccessibility in Semi-Arid Mine Tailings*.

Hazen, R. (2019). An evolutionary system of mineralogy: Proposal for a classification of planetary materials based on natural kind clustering k. *American Mineralogist*, *106*(1), 150–153. https://doi.org/10.2138/am-2021-7590

Herrera, J. (2016). Estudio de las patologías en elementos constructivos de albañilería estructural, aplicado en un proyecto específico y recomendaciones para controlar, regular y evitar los procesos físicos en las edificaciones que se desarrollan en la Ciudad de Guayaquil [Universidad de Guayaquil]. In *Maestría En: "Tecnologías de la edificación."* http://repositorio.ug.edu.ec/bitstream/redug/12001/1/Arq. Julieta Herrera.pdf

Hubbard, C. R., & Snyder, R. L. (1988). RIR — Measurement and Use in Quantitative XRD. *Powder Diffraction*, *3*(2), 74–77. https://doi.org/10.1017/S0885715600013257

Ibáñez, C. (2003). *Las sales y su incidencia en la conservación de la cerámica arqueológica*.

Irassar, E. F., Di Maio, A., & Batic, O. R. (2010). Deterioro del hormigón por cristalización de sales. *Cinpar*. www.cinpar2010.com.ar

Jenkins, R., & Snyder, R. (1996). *Introduction to X-ray Powder Diffractometry*.

Kamh, G. M. E. (2005). The impact of landslides and salt weathering on Roman structures at high latitudes - Conway Castle, Great Britain: A case study. *Environmental Geology*, *48*(2), 238–254. https://doi.org/10.1007/s00254-005-1294-2

Kashif, M., Arshad, M., Cheema, J. M., & Waraich, E. A. (2020). Modeling root zone salinity dynamics using integrated effect of soil, water, crop and climate for semi-arid region. *Pakistan Journal of Agricultural Sciences*, *57*(3), 849–863. https://doi.org/10.21162/PAKJAS/20.9582

Kruizenga, A. (2012). Corrosion mechanisms in chloride and carbonate salts. *... , Livermore, CA Report No. SAND2012-7594*, *September*, 34. http://energy.sandia.gov/wp-content/gallery/uploads/SAND2012-7594-Corrosion-Mechanisms-in-Chloride-and-Carbonate-Salts-Kruizenga.pdf

Lavina, B., Dera, P., & Downs, R. T. (2014). Modern X-ray diffraction methods in mineralogy and geosciences. *Spectroscopic Methods in Mineralogy and Materials Sciences*, *78*, 1–31. https://doi.org/10.2138/rmg.2014.78.1

Liu, H., Li, M., Zheng, X., Wang, Y., & Anwar, S. (2020). Surface salinization of soil under mulched drip irrigation. *Water (Switzerland)*, *12*(11), 1–11.

https://doi.org/10.3390/w12113031

Maček, M., Petkovšek, A., Arbanas, Ž., & Mikoš, M. (2015). Geotechnical aspects of landslides in flysch in Slovenian and Croatian. *Proceedings of the 2nd ReSyLAB—Regional Symposium on Landslides in the Adriatic-Balkan Region*, *May*, 25–30.

Martínez-Martínez, J., Torrero, E., Sanz, D., & Navarro, V. (2021). Salt crystallization dynamics in indoor environments: Stone weathering in the Muñoz Chapel of the Cathedral of Santa María (Cuenca, central Spain). *Journal of Cultural Heritage*, *47*(xxxx), 123–132. https://doi.org/10.1016/j.culher.2020.09.011

Martínez, V. R., Alonso, R. N., & Galli, C. I. (2020). Morfología de Las Costras Evaporíticas del Salar de Pozuelos (Puna Salteña). *Revista de La Asociación Geológica Argentina*, *77*(1), 163–173.

Metternicht, G. I., & Zinck, J. A. (2002). Remote sensing of soil salinity: Potentials and constraints. *Remote Sensing of Environment*, *85*(1), 1–20. https://doi.org/10.1016/S0034-4257(02)00188-8

Mishra, M., & Deshmukh, B. (2019). *Classification of minerals (Chemical properties of minerals)* (pp. 113–132).

Molina, J. (2018). *Evaluación de la salinidad del suelo en la hacienda calera - iancem para determinar medidas de manejo y conservación*. Pontificia Universidad Católica del Ecuador Sede Ibarra.

Montoroi, J. P. (2018). Soil salinization and management of salty soils. In *Soils as a Key Component of the Critical Zone 5: Degradation and Rehabilitation* (Vol. 5). https://doi.org/10.1002/9781119438298.ch5

Morales Tassinai, A. M., Guevara Rivera, J., Cruz Ortega, P., & Hernández Zárate, J. A. (2017). Medición de la alteración del peso en el mármol tipo Café Tabaco mediante una prueba de cristalización de sales por cloruro de sodio. *Ingeniantes*, *1*, 158–164. http://citt.itsm.edu.mx/ingeniantes/articulos/ingeniantes4no2vol1/MediciondelaAlteraciónde lPeso_Marmol.pdf

Nienhuis, E. T., & McCloy, J. S. (2020). Low Temperature Sequential Melting and Anion Retention in Simplified Low Activity Waste. *MRS Advances*, *5*(5–6), 195–206. https://doi.org/10.1557/adv.2020.52

Oguchi, C. T., & Yu, S. (2021). A review of theoretical salt weathering studies for stone heritage. *Progress in Earth and Planetary Science*, *8*(1). https://doi.org/10.1186/s40645-021-00414-x

Okrusch, M., & Frimmel, E. H. (2019). *Mineralogy An Introduction to Minerals, Rocks and Mineral Deposits* (9th ed.). 2014.

Özşen, H., Bozdağ, A., & İnce, İ. (2017). Effect of salt crystallization on weathering of pyroclastic rocks from Cappadocia, Turkey. *Arabian Journal of Geosciences*, *10*(12). https://doi.org/10.1007/s12517-017-3027-8

Parsons, A. J., & Abrahams, A. . (1994). *Geomorphology of Deserts Environments* (2nd ed., Vol.

1). 1994.

Payen, S., Basset-Mens, C., Núñez, M., Follain, S., Grünberger, O., Marlet, S., Perret, S., & Roux, P. (2016). Salinisation impacts in life cycle assessment: a review of challenges and options towards their consistent integration. *International Journal of Life Cycle Assessment*, *21*(4), 577–594. https://doi.org/10.1007/s11367-016-1040-x

Pecharsky, V., & Zavalij, P. (2005). *Fundamentals of powder diffraction and structural characterization of materials* (2nd ed.).

Pérez, F., Oliva, B., & Callejas, B. (2002). *Impacto de la contaminación de río Las Vacas sobre la calidad del agua del Río Motagua, Guatemala.* (1st ed.).

Putz, H. (2003). *MATCH! Phase Analysis using Powder Difracction Manual* (3.13).

Quiroga, M. (2021). *Evaluación del efecto térmico en arcillas por difracción de rayos X: análisis cuantitativo de fases por el método de Rietveld*.

Reinoso, M. (2021). Stratigraphic and tectonic characterization of the Peñas Coloradas Formation , and its relation with the deposits of the Chota formation in the Chota Basin of northern Ecuador Trabajo de integ. In *Repositorio Yachay Tech*. Universidad De Investigación De Tecnología Experimental Yachay.

Salama, R. B., Otto, C. J., & Fitzpatrick, R. W. (1999). Contributions of groundwater conditions to soil and water salinization. *Hydrogeology Journal*, *7*(1), 46–64. https://doi.org/10.1007/s100400050179

Sánchez, E., Mejía, F., Vizcaíno, G., & Cipriani-Ávila, I. (2017). *Análisis mineralógico y multielemental de la ceniza volcánica, producto de la erupción del cotopaxi en 2015, por difracción de rayos x (xrd) y espectrometría de masas con plasma acoplado inductivamente (icp-ms) y sus posibles aplicaciones e impactos.* 9–24.

Scrivano, S., & Gaggero, L. (2020). An experimental investigation into the salt-weathering susceptibility of building limestones. *Rock Mechanics and Rock Engineering*, *53*(12), 5329–5343. https://doi.org/10.1007/s00603-020-02208-x

Shahid, S. A., Zaman, M., & Heng, L. (2018). Soil Salinity: Historical Perspectives and a World Overview of the Problem. *Guideline for Salinity Assessment, Mitigation and Adaptation Using Nuclear and Related Techniques*, 43–53. https://doi.org/10.1007/978-3-319-96190-3_2

Singh, V., & Agrawal, H. M. (2012). Qualitative soil mineral analysis by EDXRF, XRD and AAS probes. *Radiation Physics and Chemistry*, *81*(12), 1796–1803. https://doi.org/10.1016/j.radphyschem.2012.07.002

Siravo, G., Speranza, F., Mulas, M., & Costanzo-Alvarez, V. (2021). Significance of Northern Andes Terrane Extrusion and Genesis of the Interandean Valley: Paleomagnetic Evidence From the "Ecuadorian Orocline." *Tectonics*, *40*(7), 1–25. https://doi.org/10.1029/2020TC006684

Suryanarayana, C., & Grant Norton, M. (1999). X-Ray diffraction: a practical approach. In *Choice Reviews Online* (Vol. 36, Issue 06). https://doi.org/10.5860/choice.36-3382

Thomas, D. S. G. (2011). *Geomorphology* (3rd ed.).

Tibaldi, A., & Ferrari, L. (1992). From latest miocene thrusting to Quaternary transpression and transtension in the Interandean Valley, Ecuador. *Journal of Geodynamics*, *15*(1–2), 59–83. https://doi.org/10.1016/0264-3707(92)90006-E

Uri, N. (2018). Cropland soil salinization and associated hydrology: Trends, processes and examples. *Water (Switzerland)*, *10*(8). https://doi.org/10.3390/w10081030

Warke, P. A. (2013). Weathering in Arid Regions. In *Treatise on Geomorphology* (Vol. 4). Elsevier Ltd. https://doi.org/10.1016/B978-0-12-374739-6.00060-9

Warren, J. K. (2006). Evaporites: A geological compendium. In *Springer* (2nd ed.).

Winkler, W., Spikings, R., Villagómez, D., Egüez, A., Abegglen, P., & Tobler, S. (2002). The Chota Basin and its Significance for the formation of the Inter-Andean Valley in Ecuador. *Internatonal Symposium on Andean Geodynamic (ISAG)*, *5*(1), 705–708.

Yu, K., Cao, Y., Qiu, L., & Sun, P. (2019). Depositional environments in an arid, closed basin and their implications for oil and gas exploration: The lower Permian Fengcheng Formation in the Junggar Basin, China. *AAPG Bulletin*, *103*(9), 2073–2115. https://doi.org/10.1306/01301917414

7 ANNEXES

Diffraction pattern of saline samples
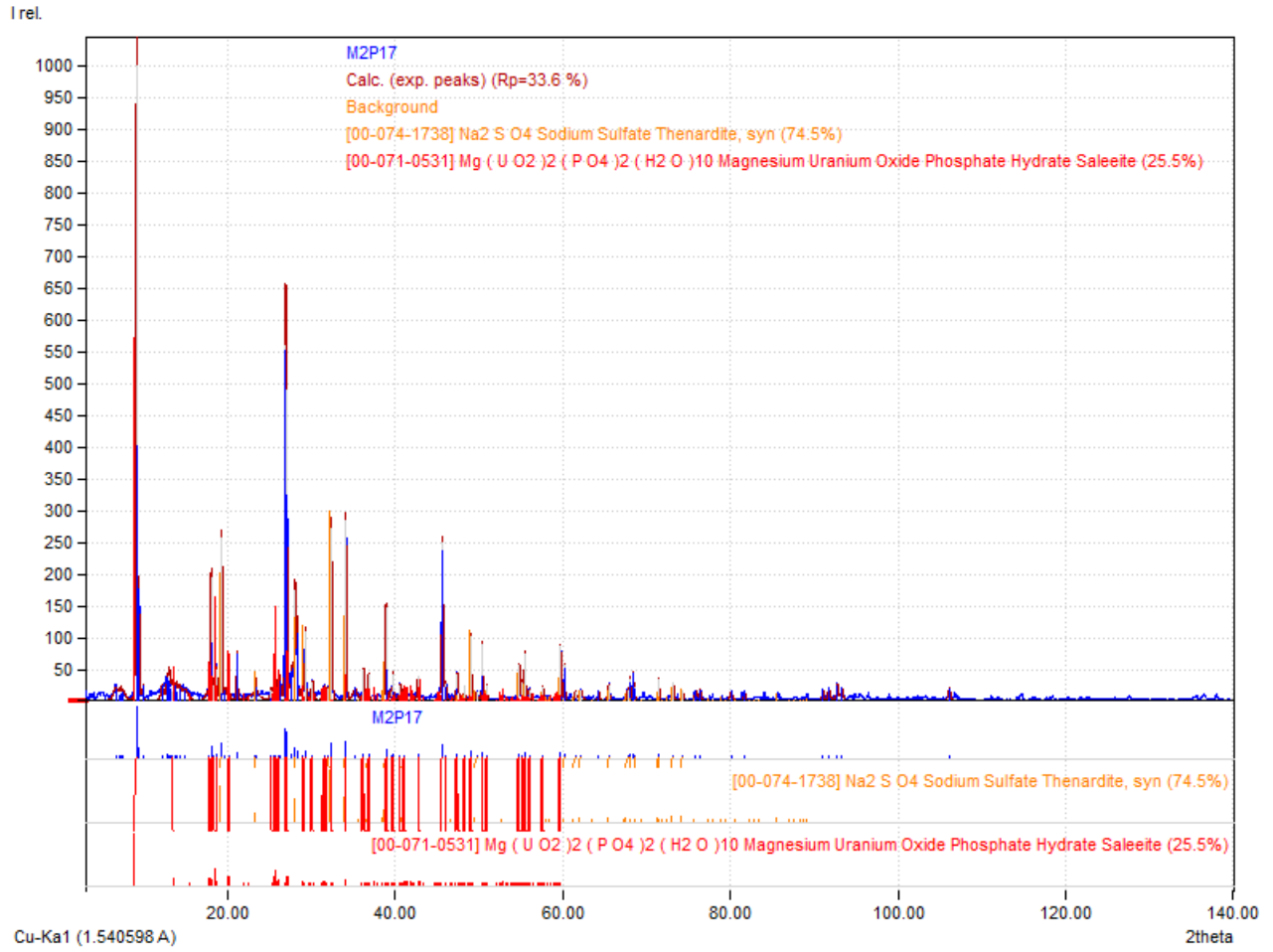
November 12, 2021
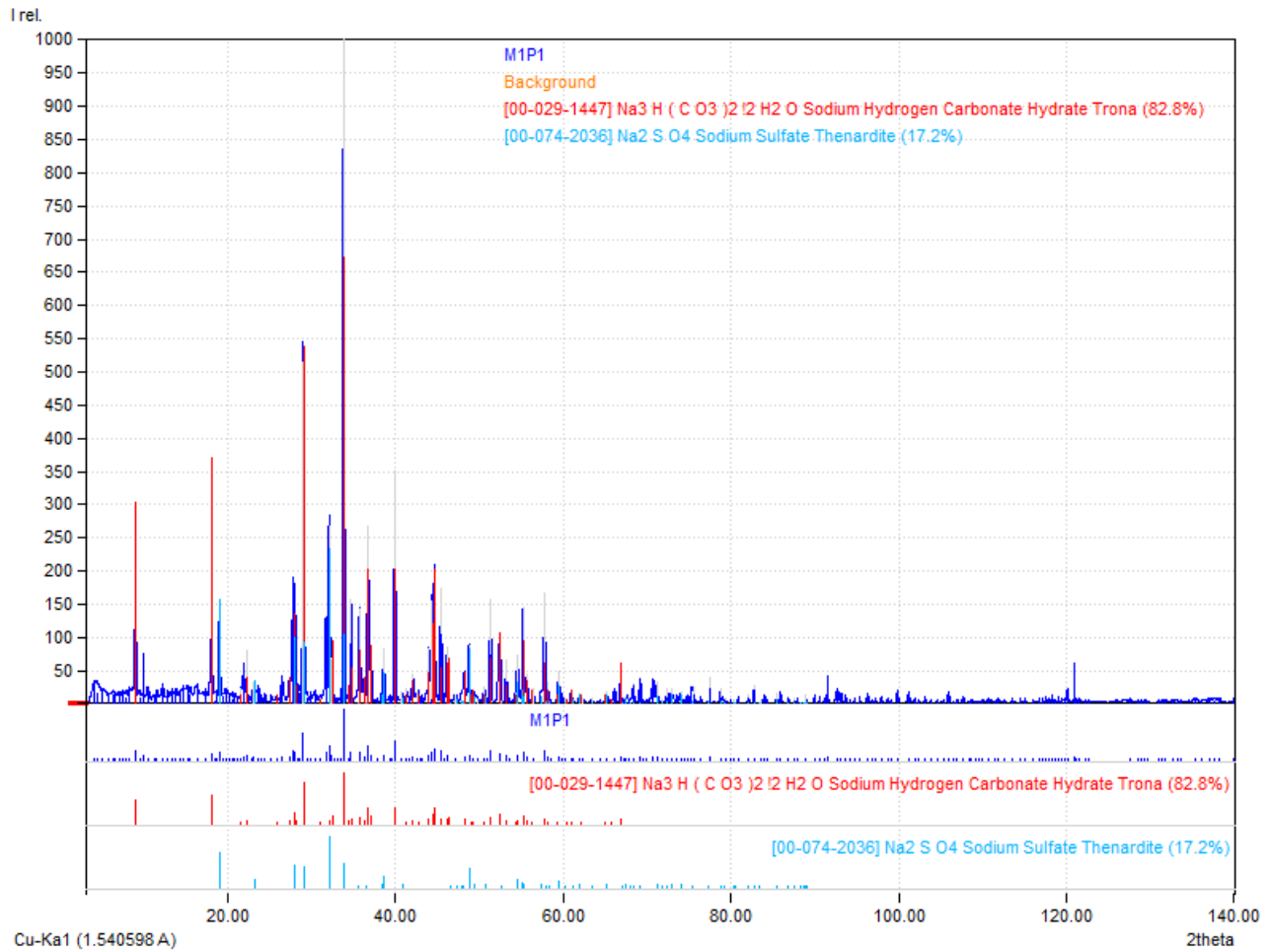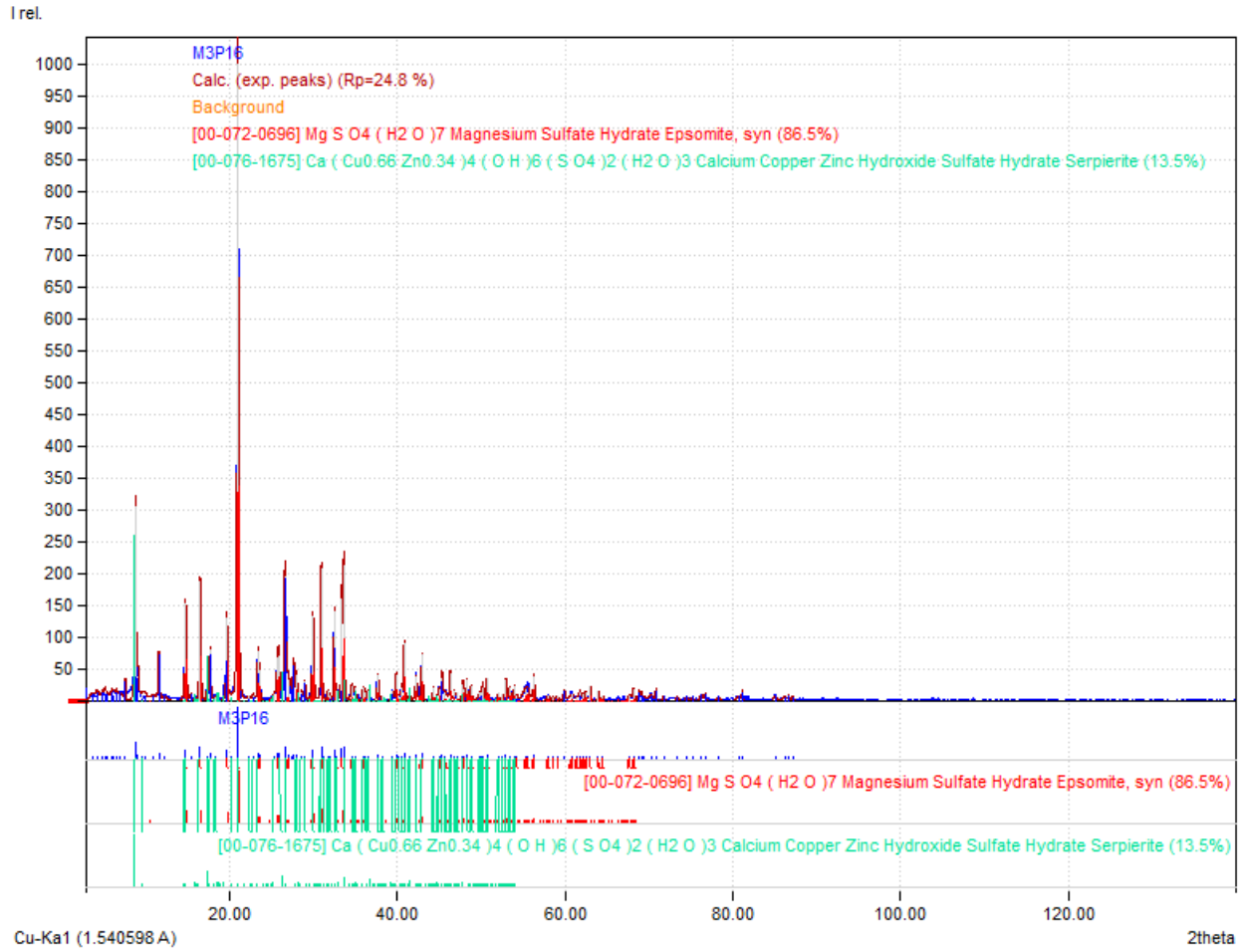

1. X-ray diffraction pattern of sample M1P1
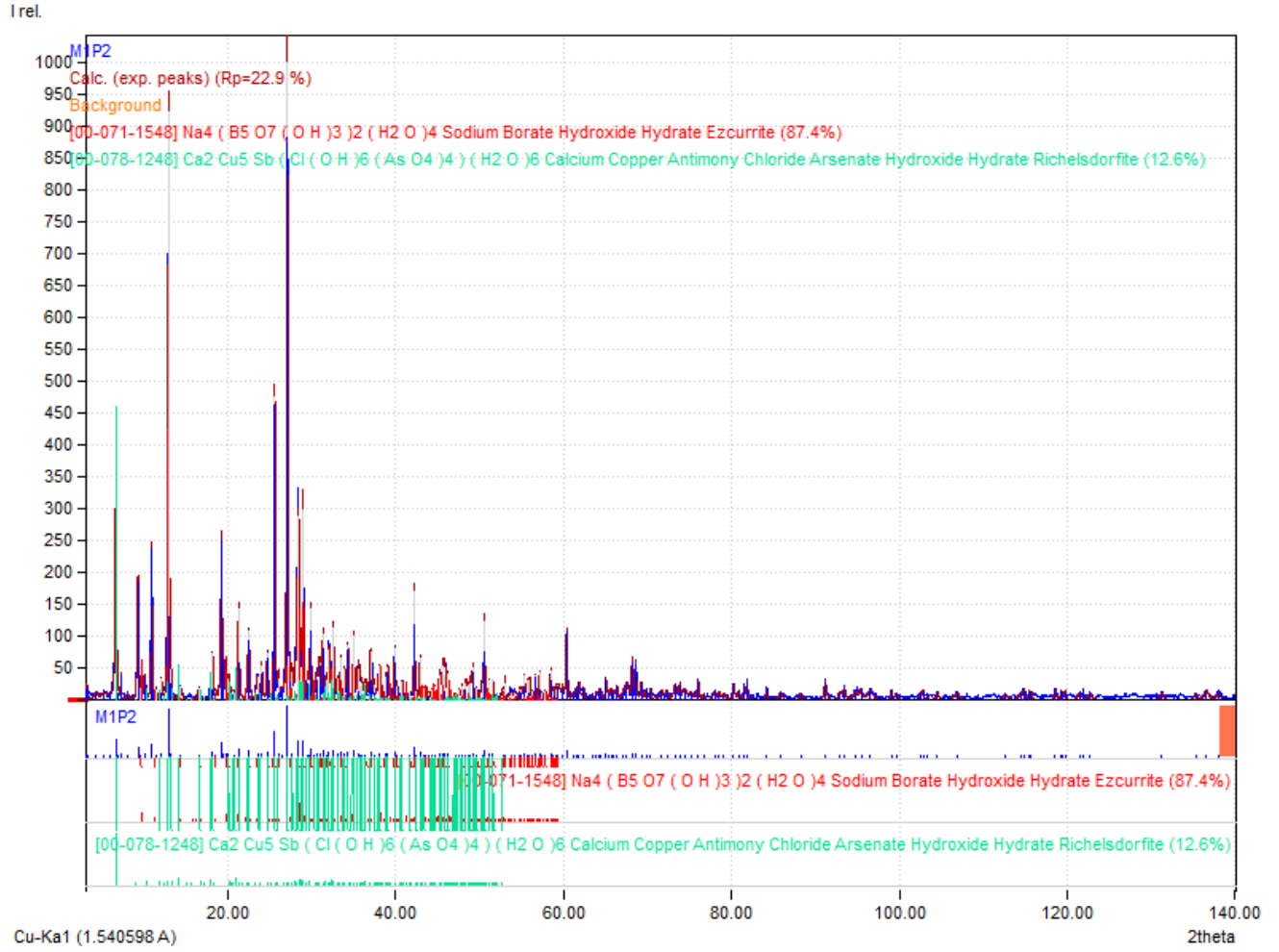
2. X-ray diffraction pattern of sample M1P2
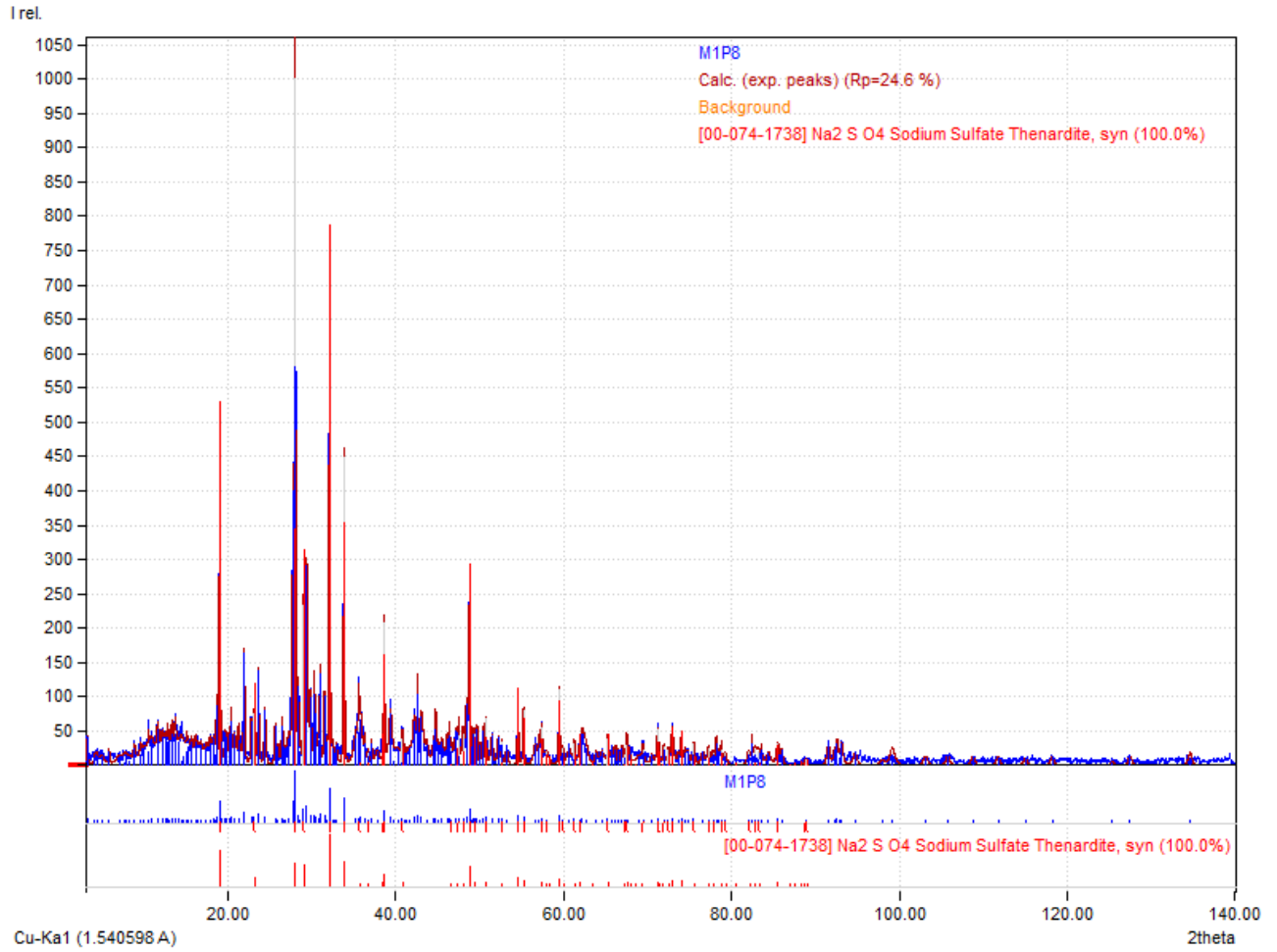
3. X-ray diffraction pattern of sample M1P8
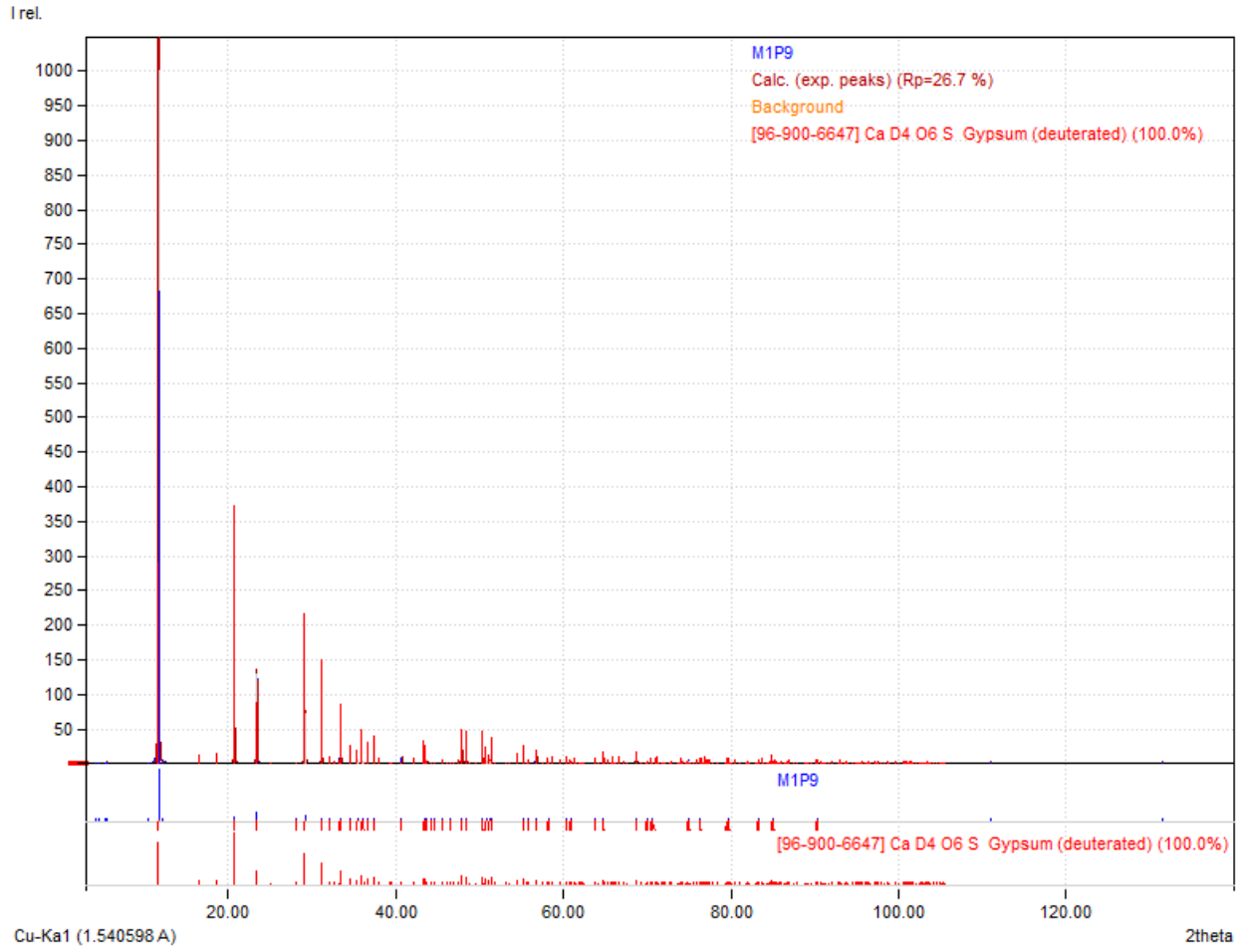
4. X-ray diffraction pattern of sample M1P9
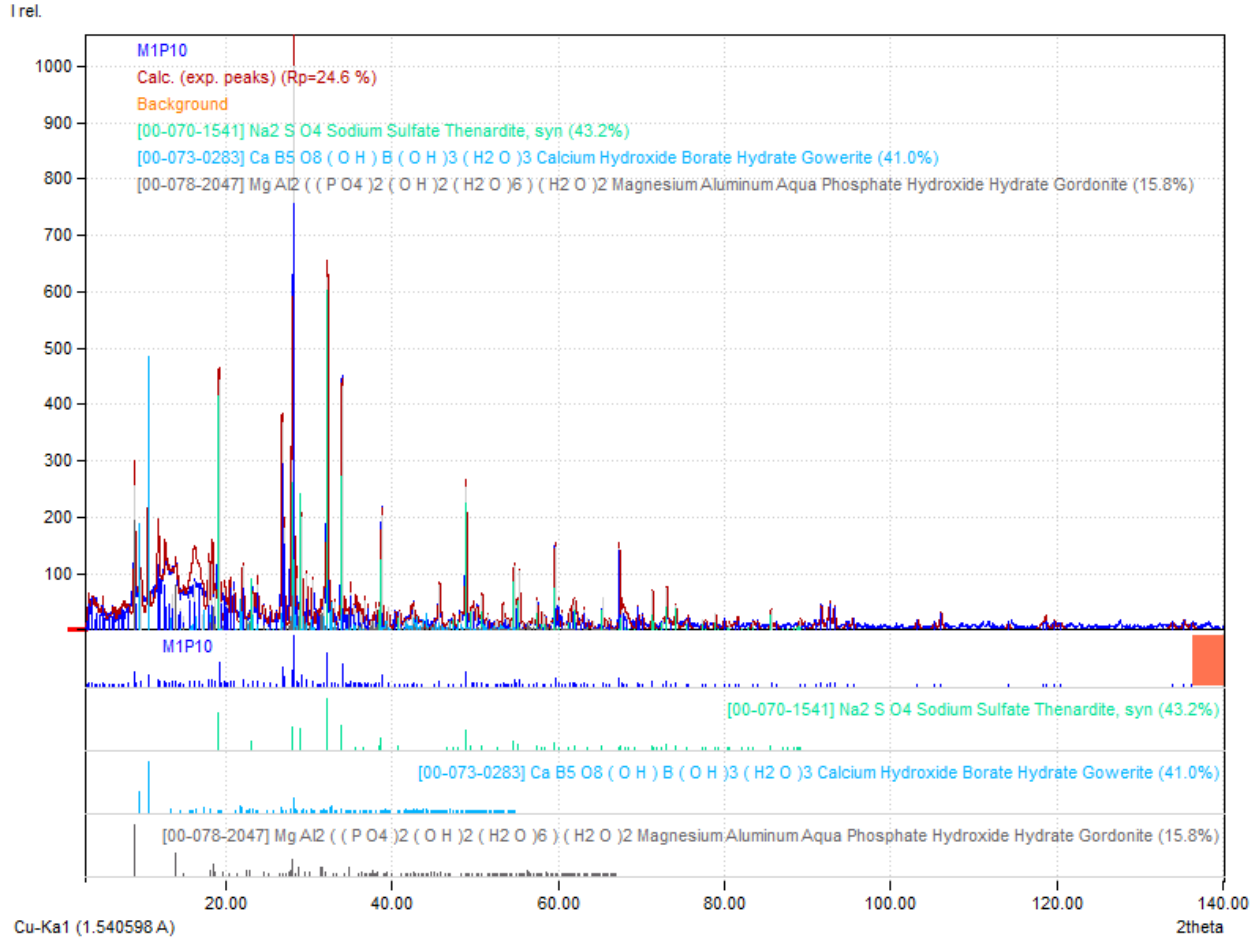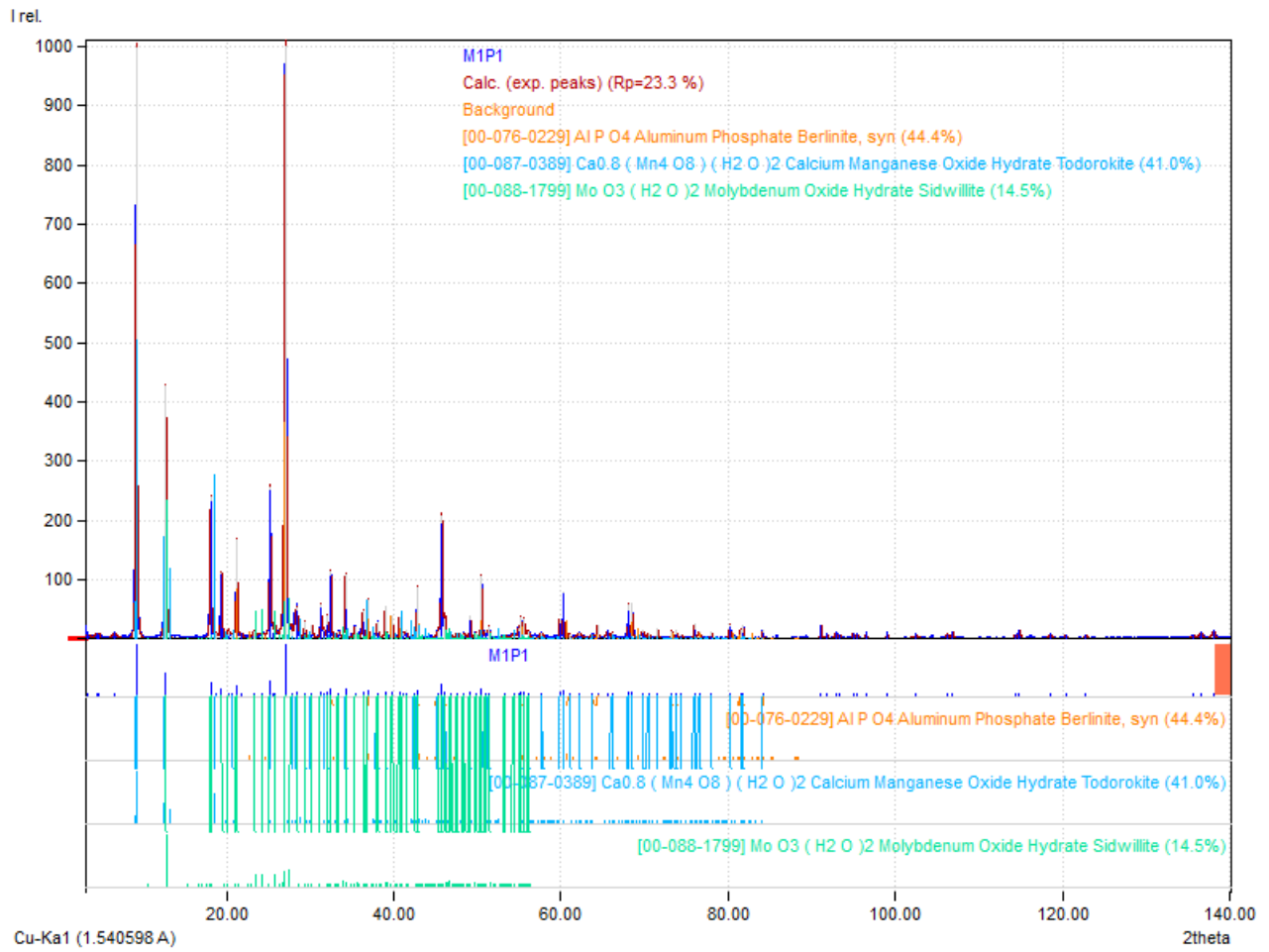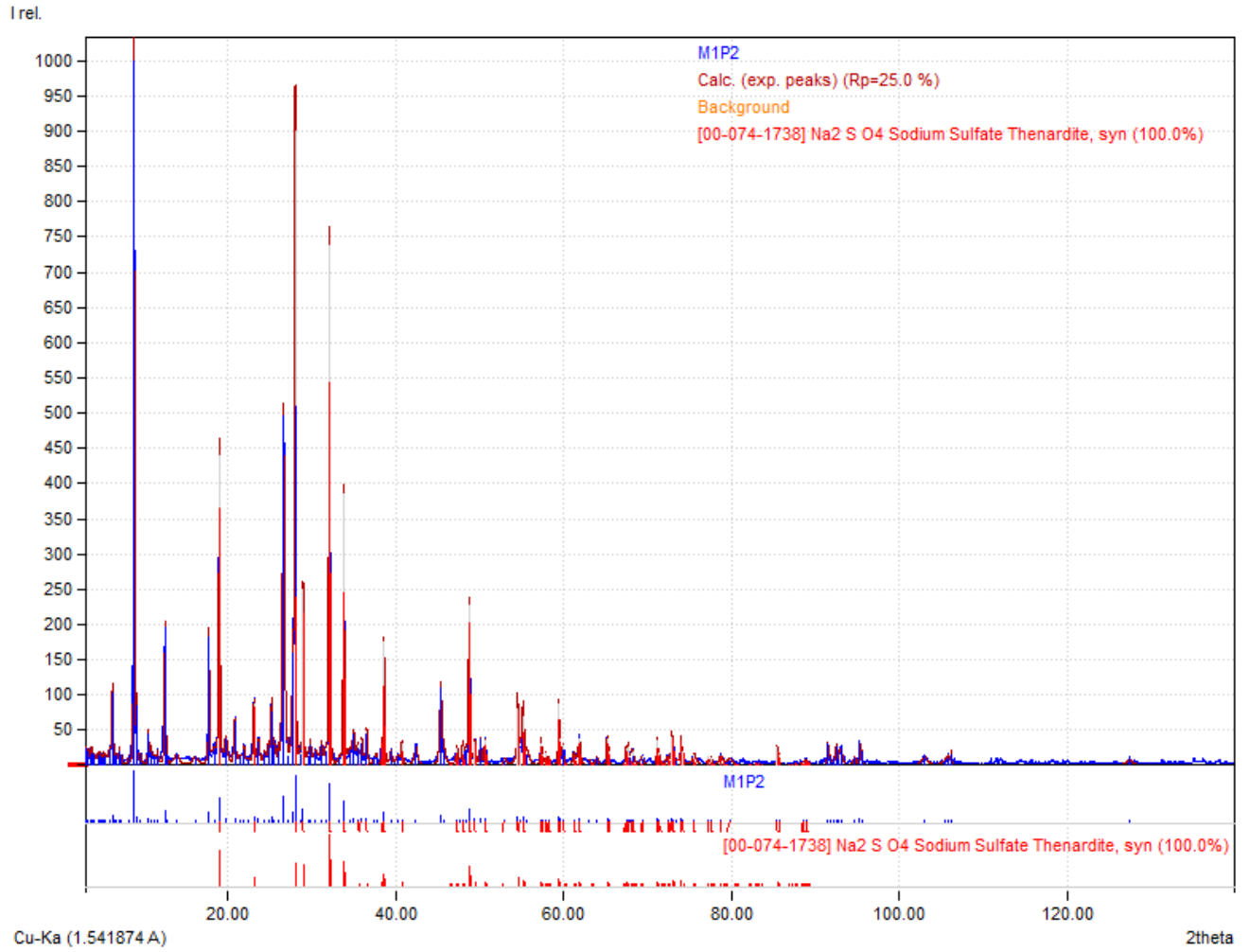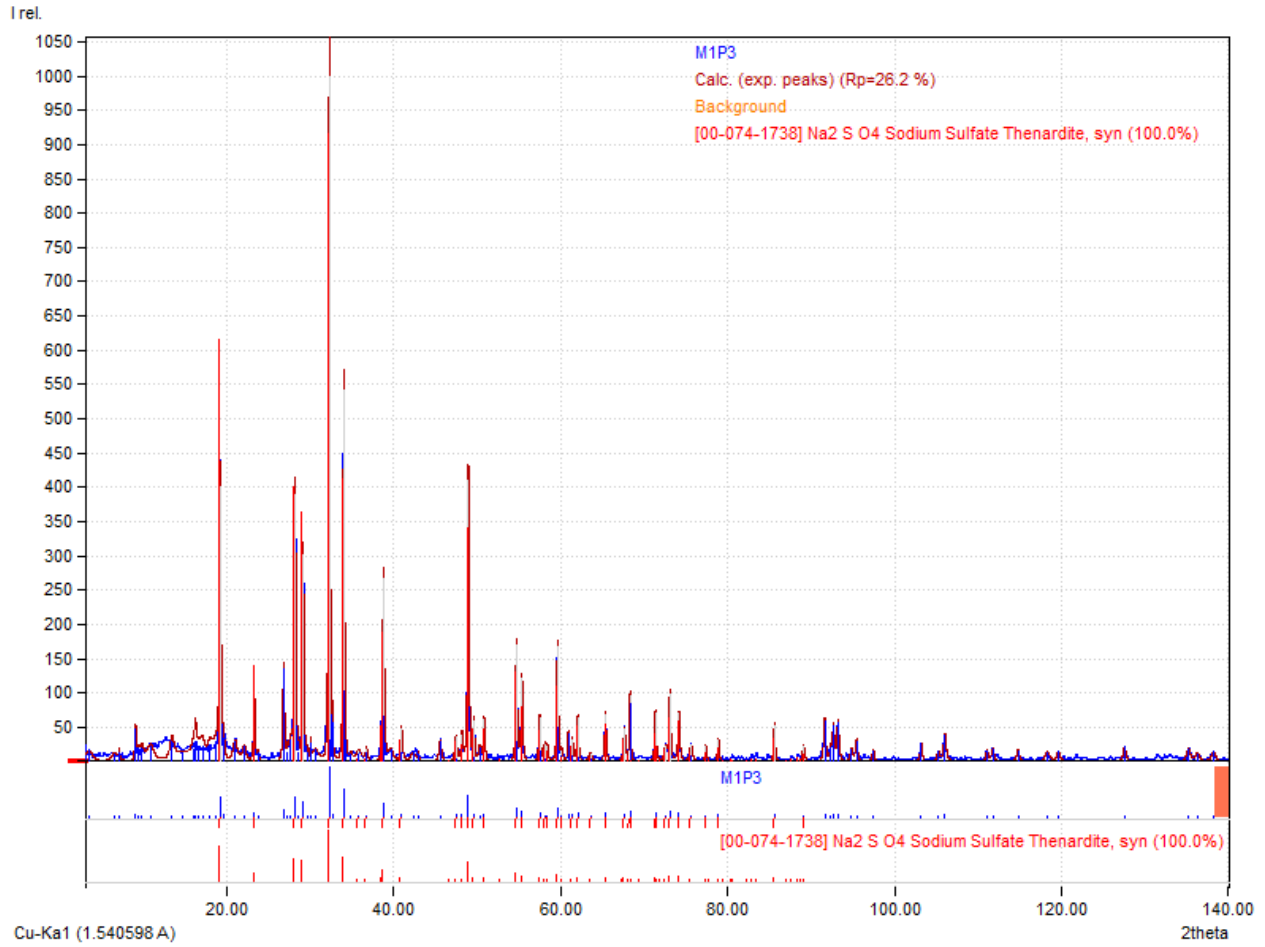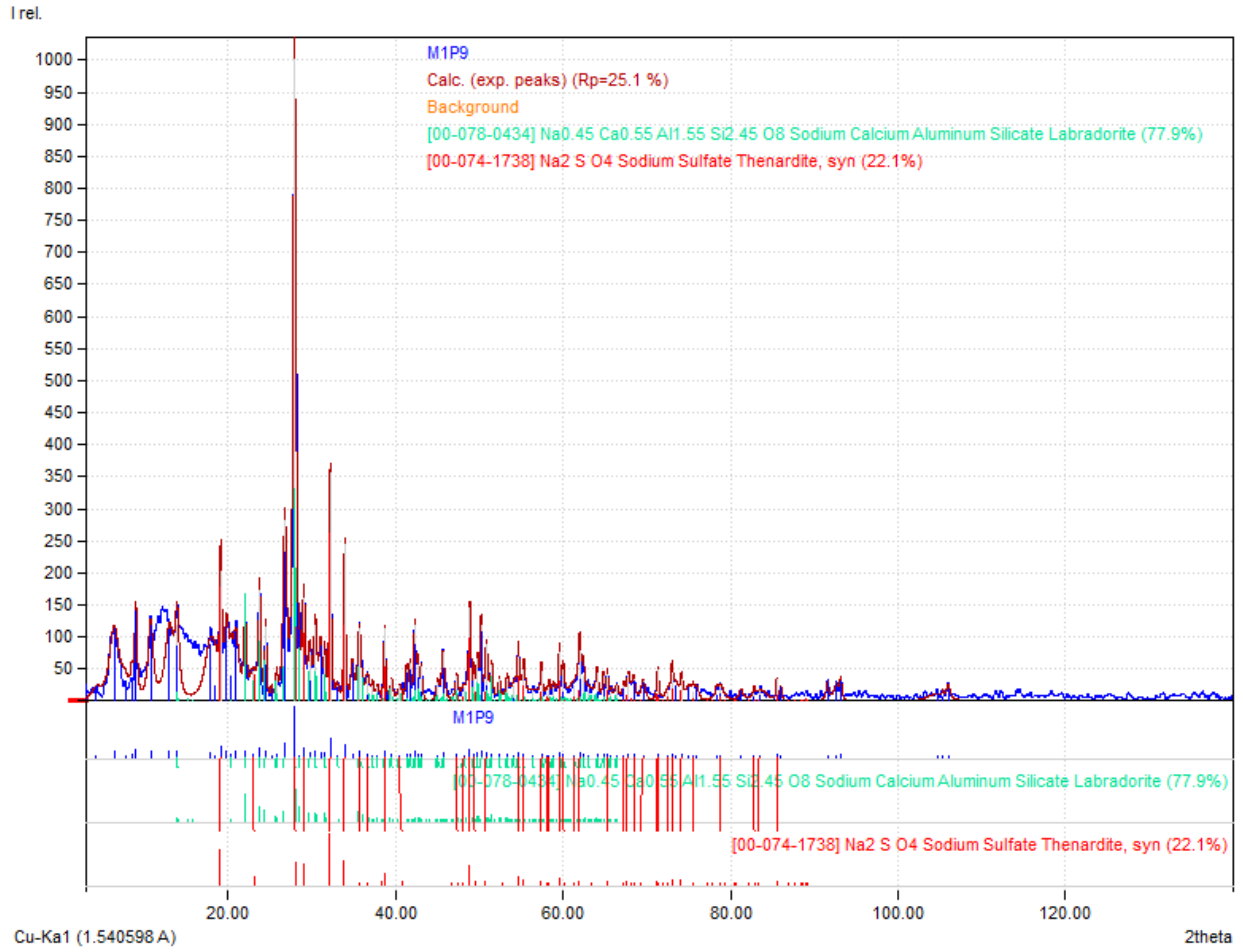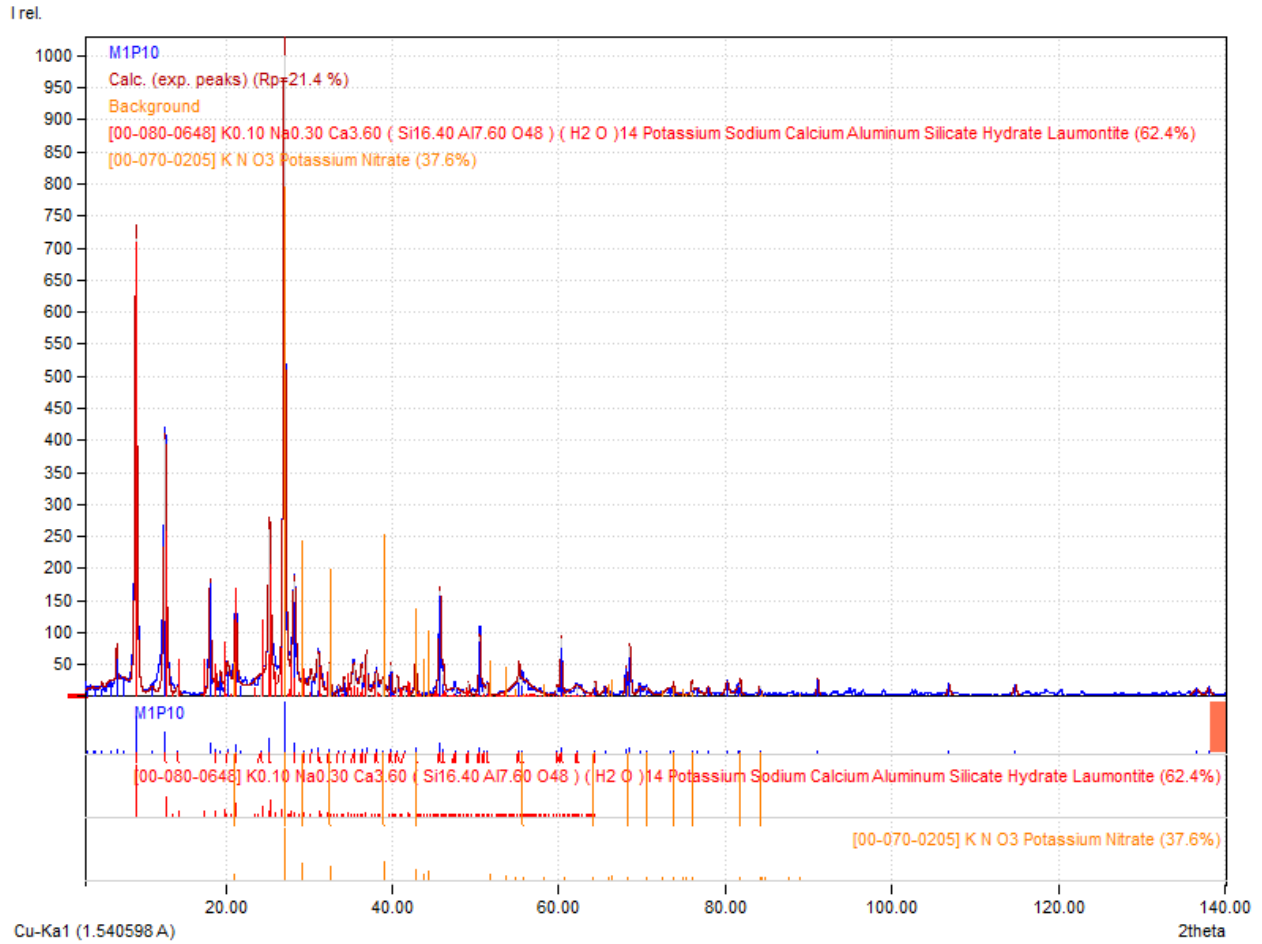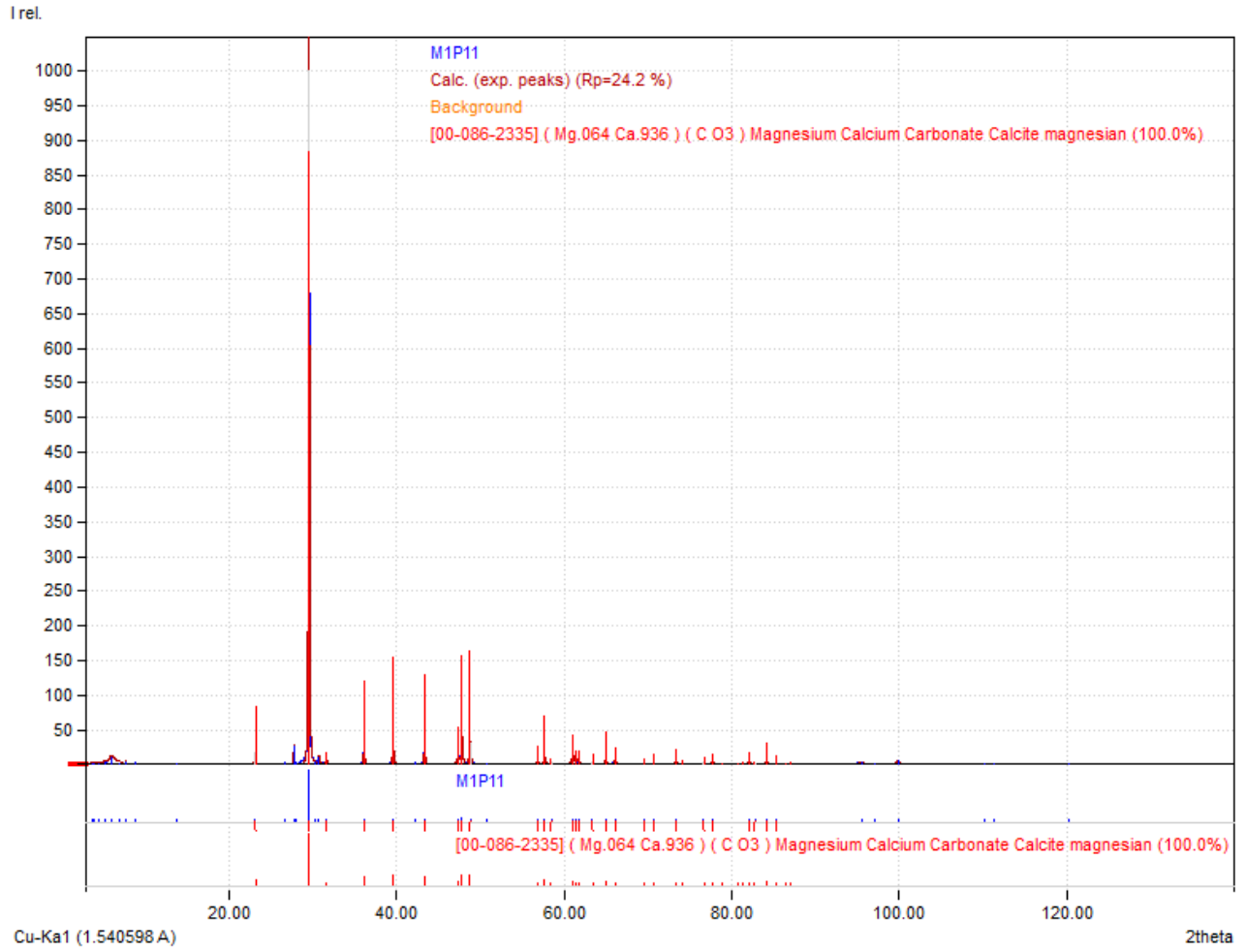
5. X-ray diffraction pattern of sample M1P10
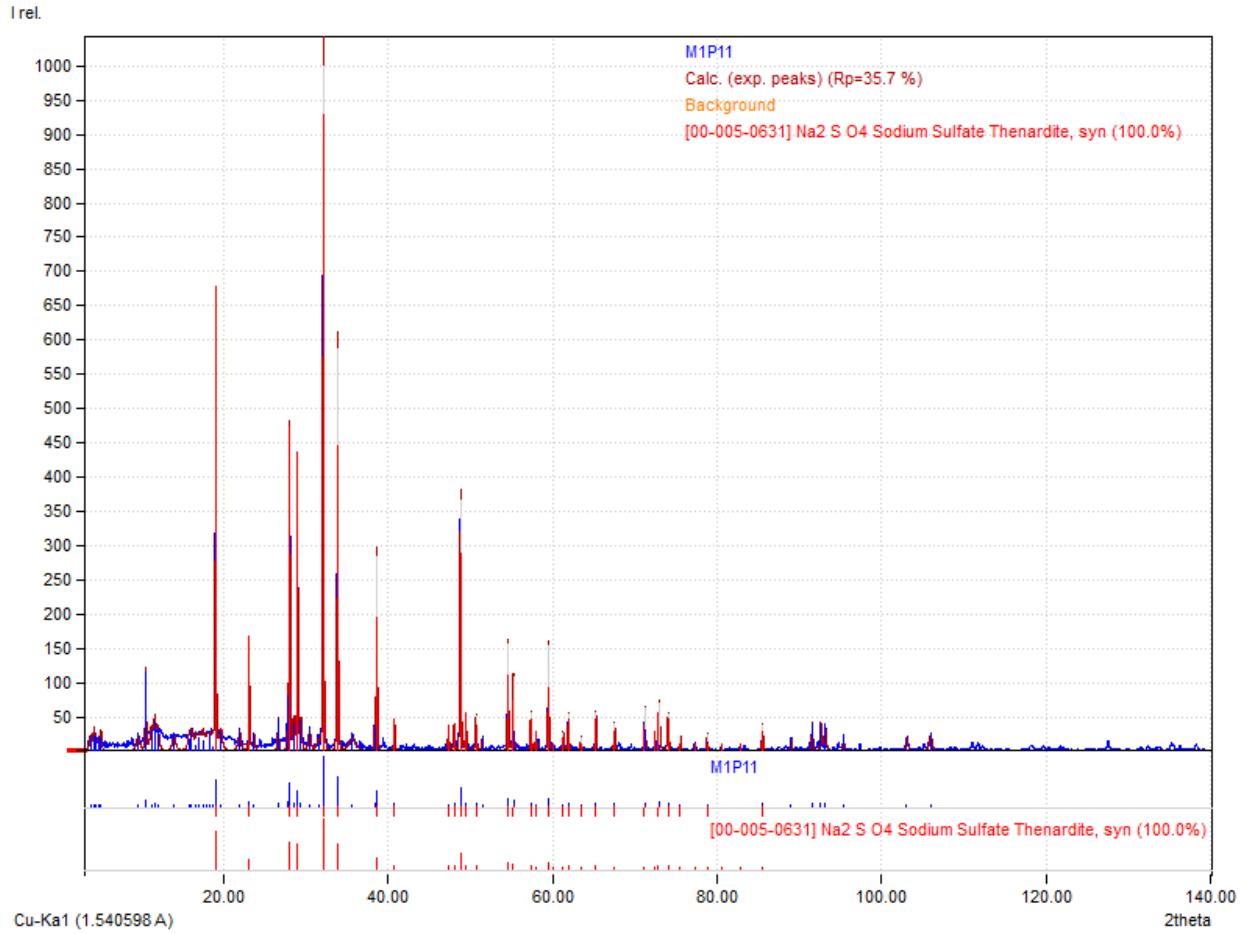
6. X-ray diffraction pattern of sample M1P11
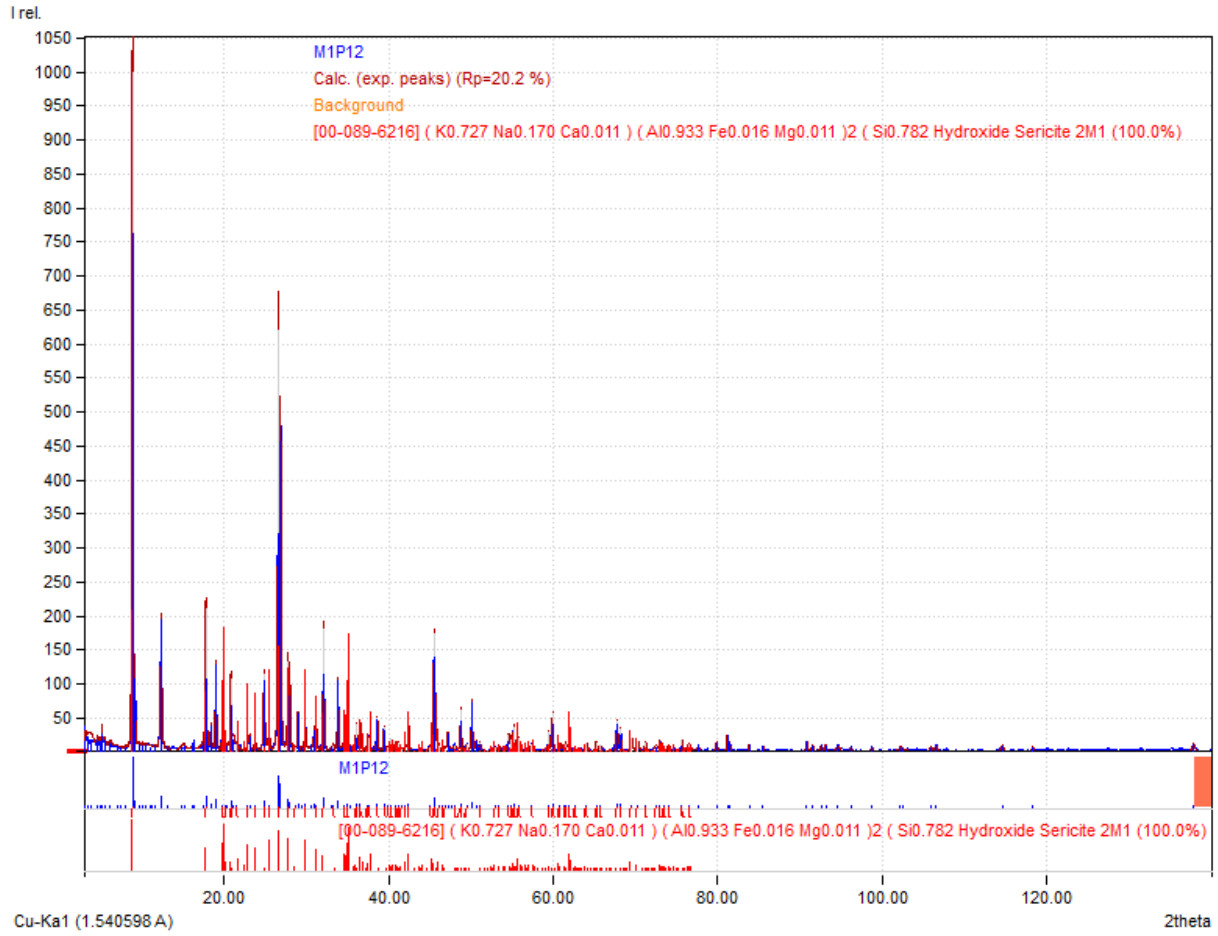
7. X-ray diffraction pattern of sample M1P12
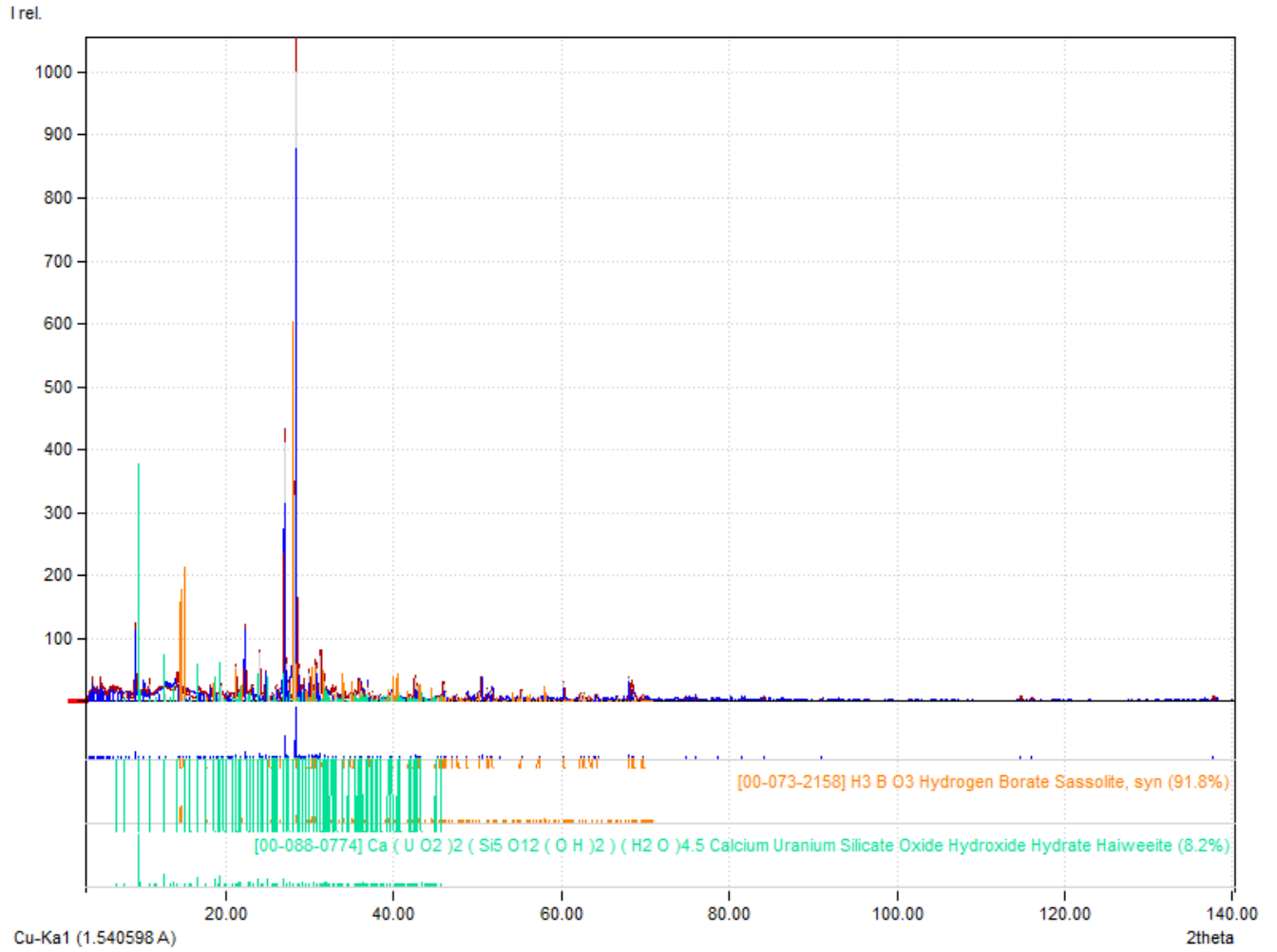
8. X-ray diffraction pattern of sample M1P13

UNIVERSIDAD
YACHAY
TECH

SCHOOL OF
EARTH SCIENCES,
ENERGY AND ENVIRONMENT
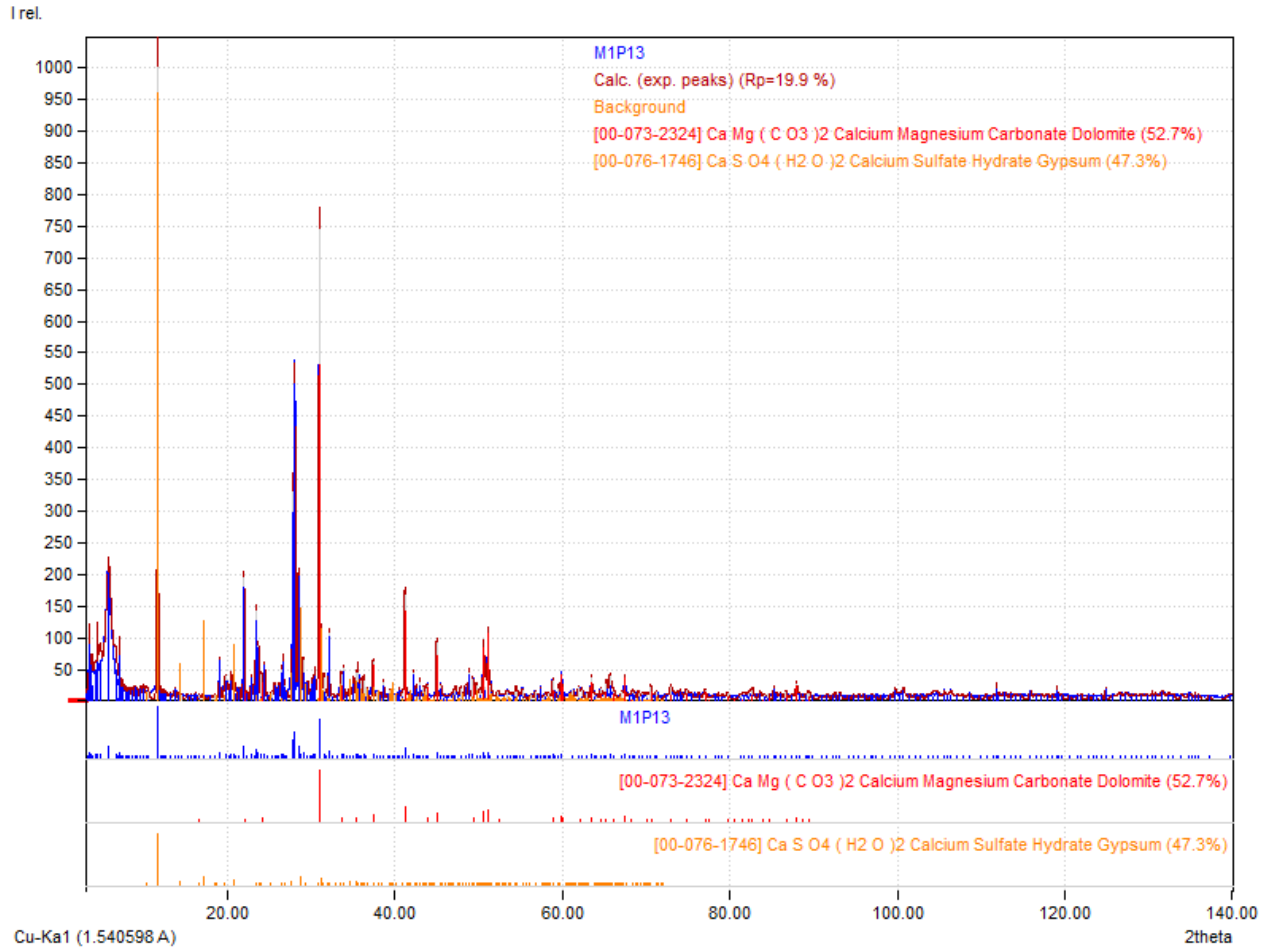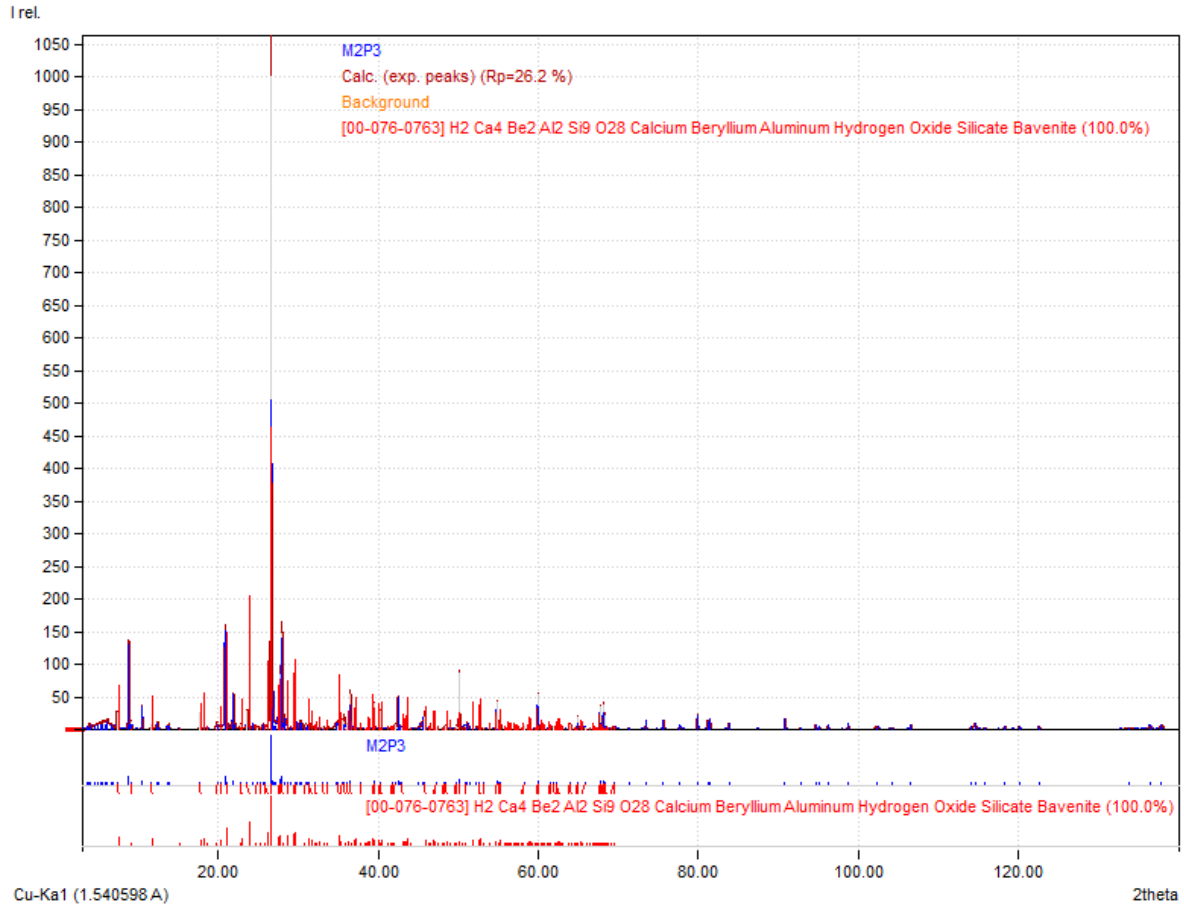
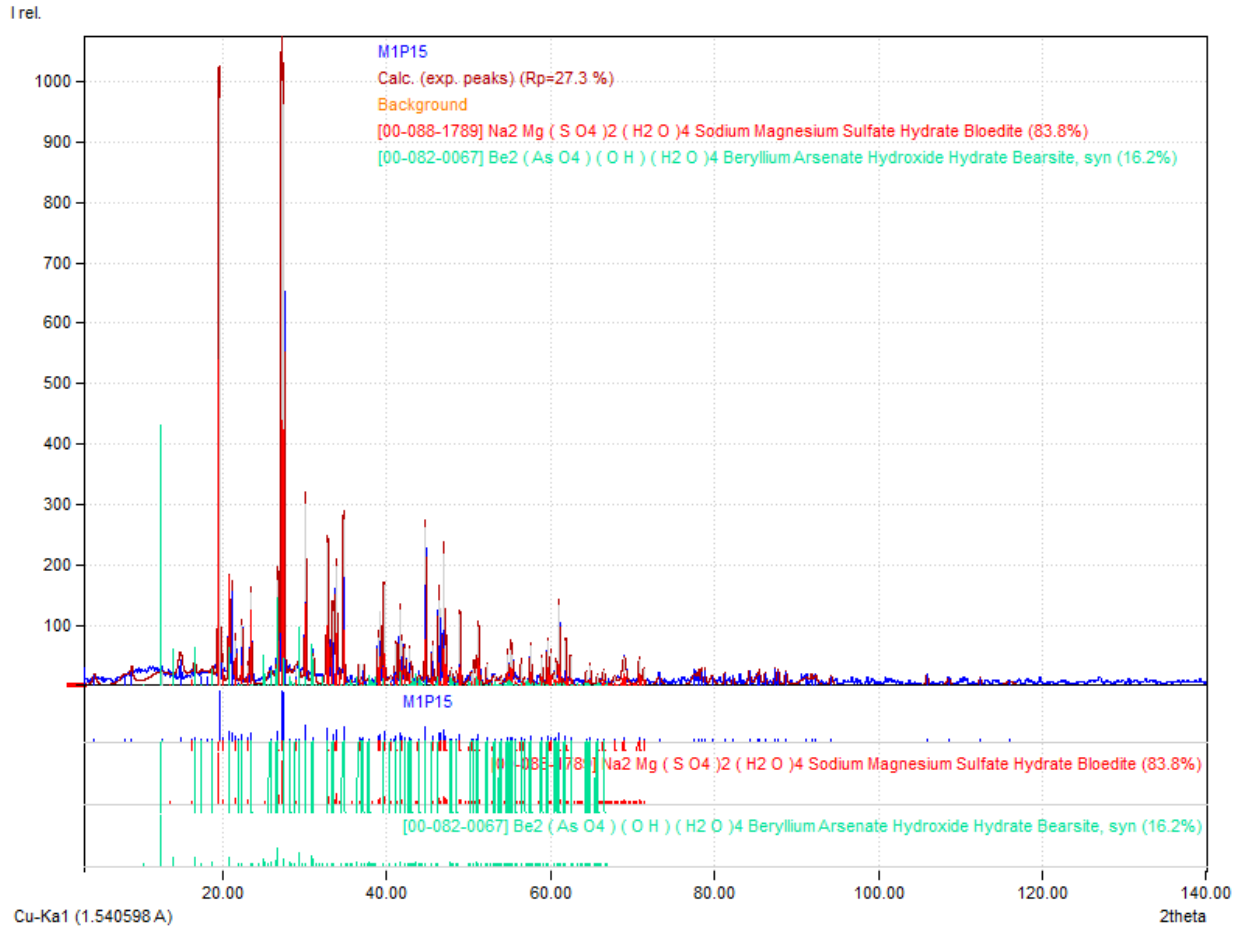*9. X-ray diffraction pattern of sample M2P3*
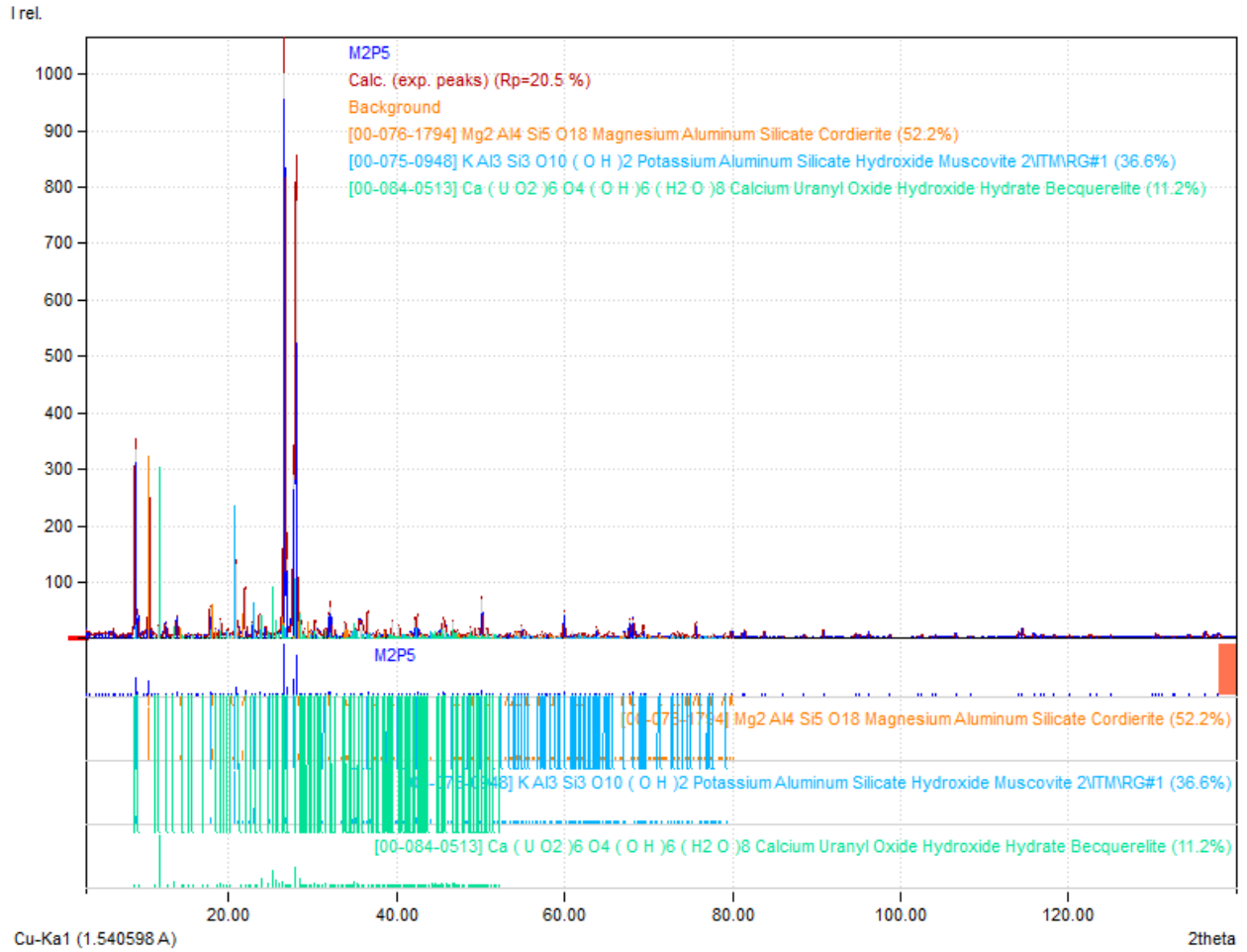
10. X-ray diffraction pattern of sample M2P5
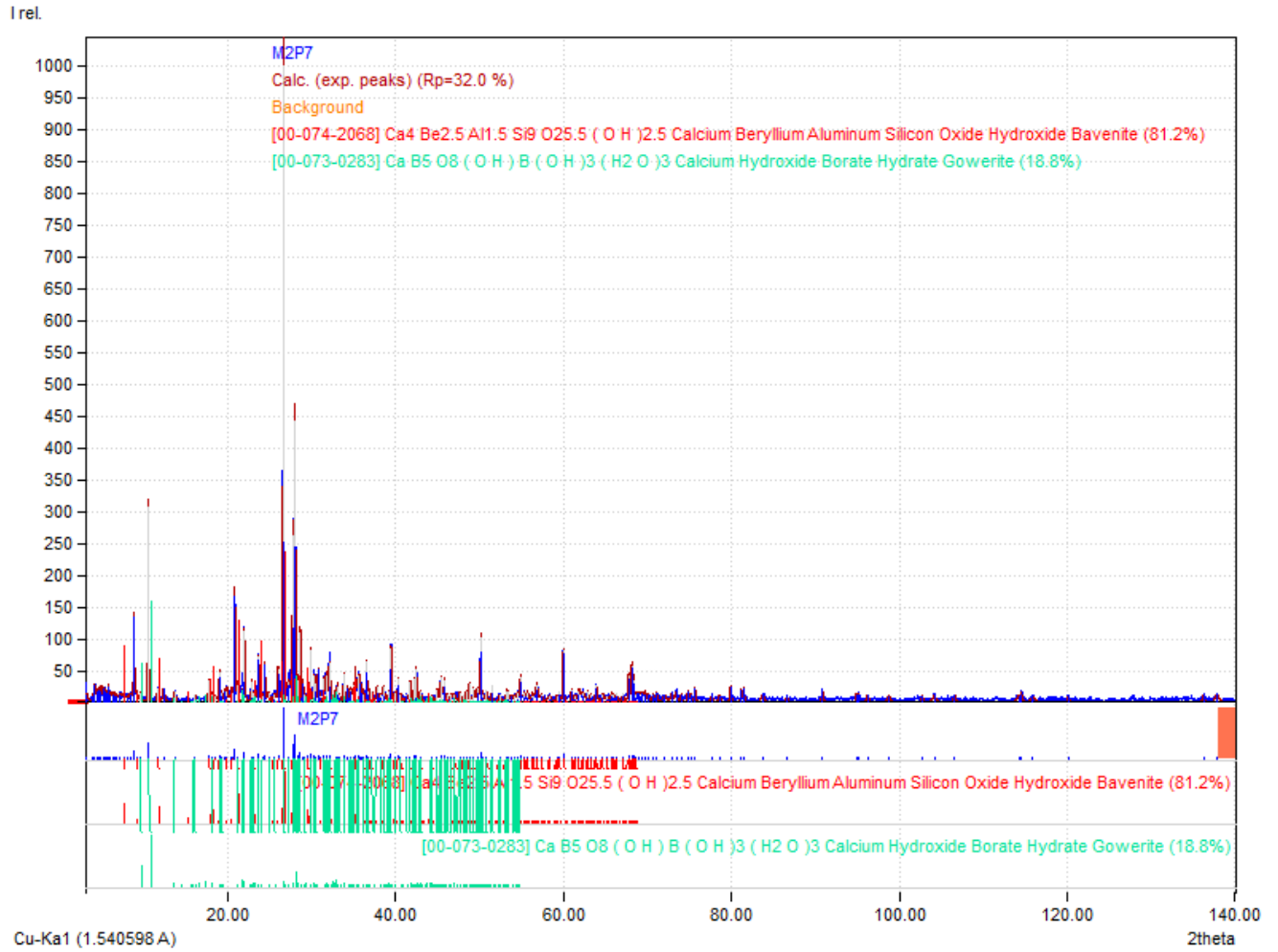
11. X-ray diffraction pattern of sample M2P7
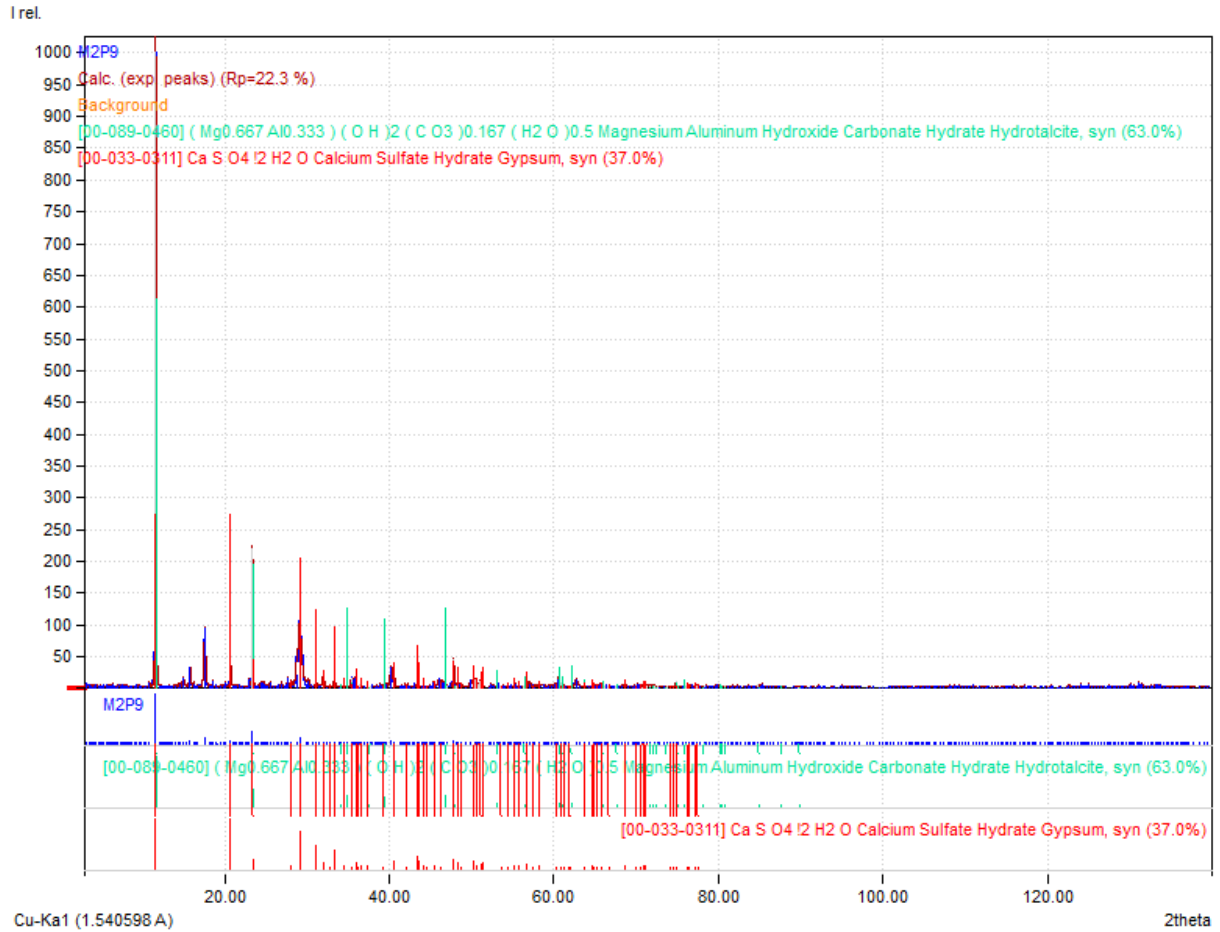
12. X-ray diffraction pattern of sample M2P9
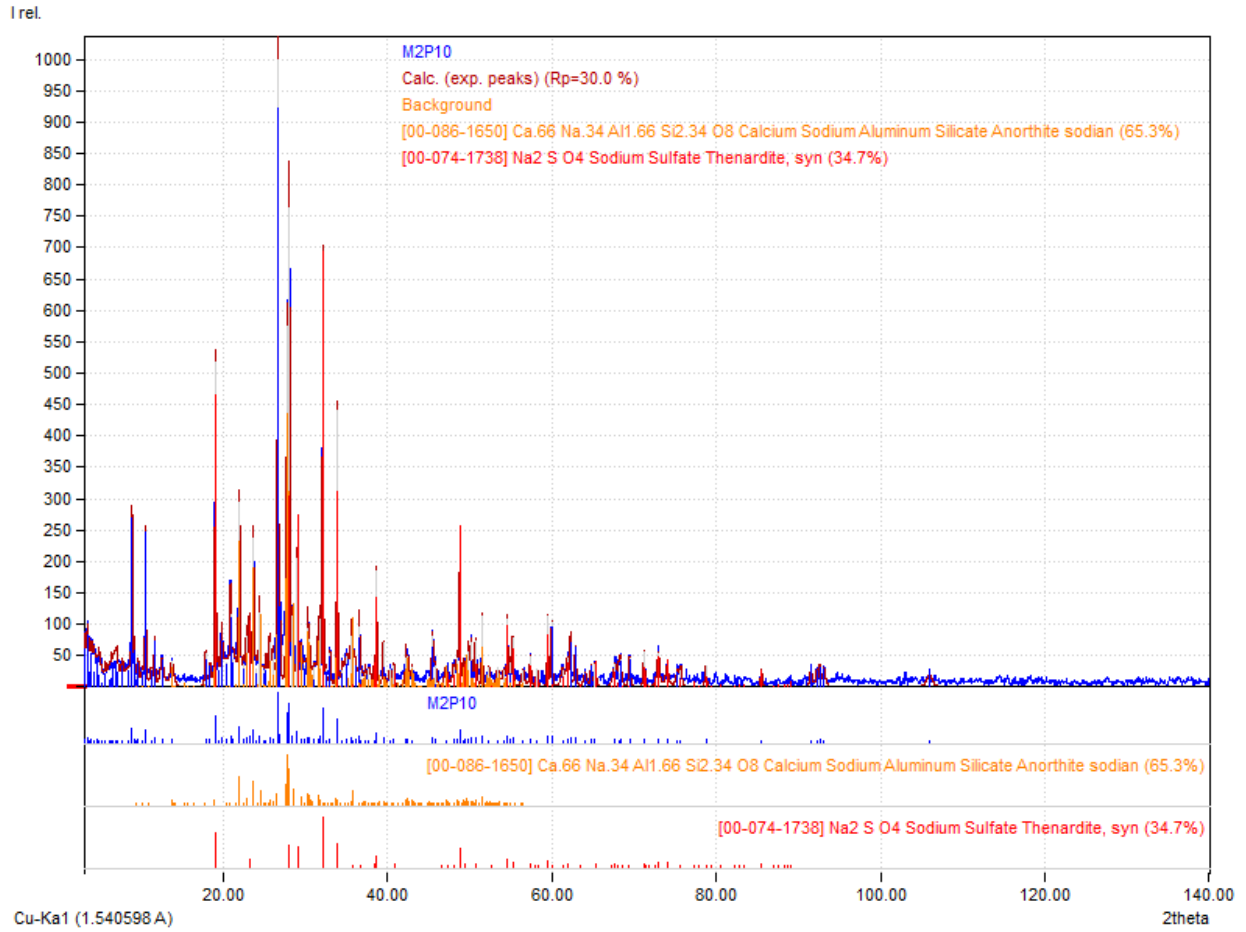
13. X-ray diffraction pattern of sample M2P10

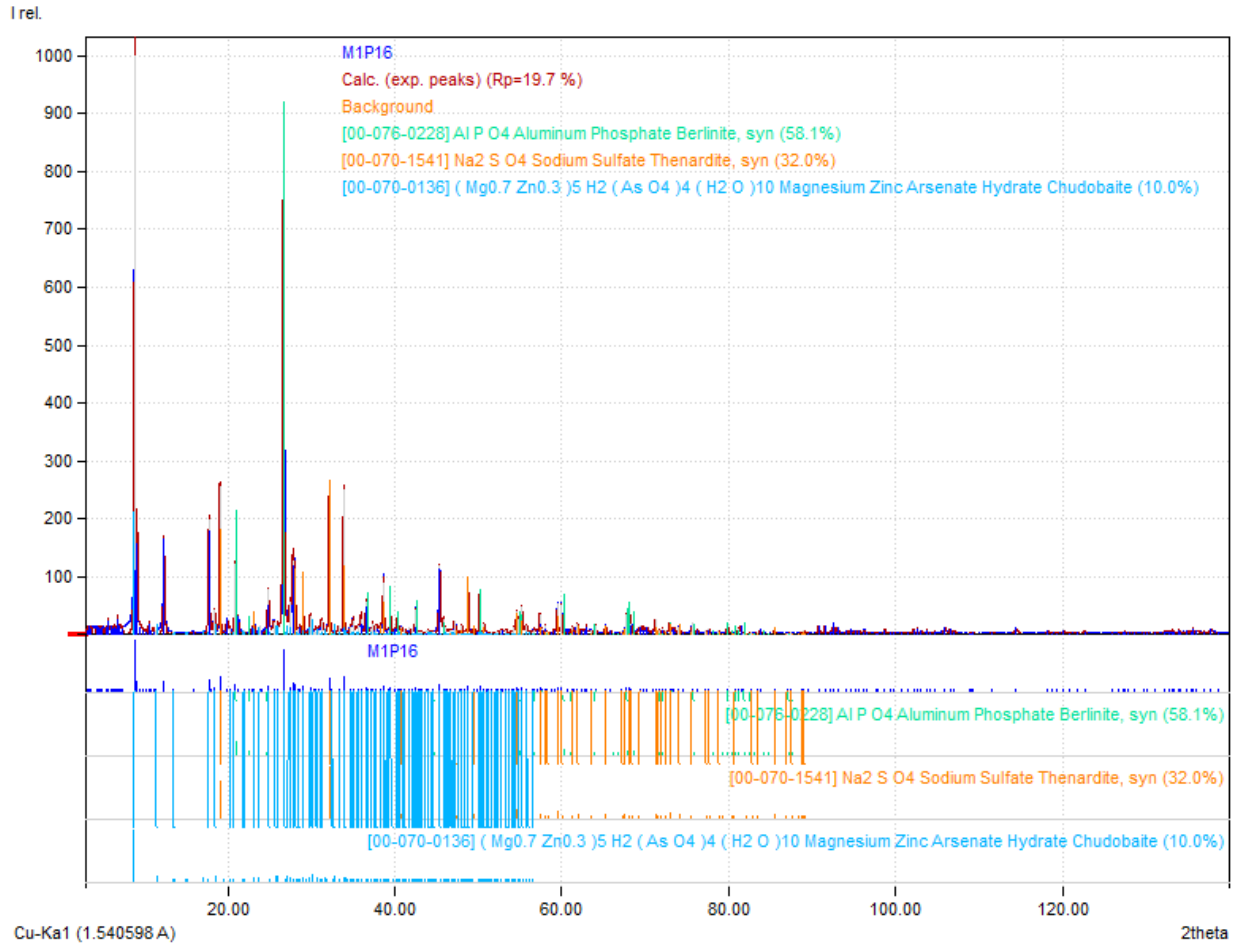*14. X-ray diffraction pattern of sample M2P17*

15. X-ray diffraction pattern of sample M3P16

16. X-ray diffraction pattern of sample M1P1

17. X-ray diffraction pattern of sample M1P2

18. X-ray diffraction pattern of sample M1P3

19. X-ray diffraction pattern of sample M1P9

20. X-ray diffraction pattern of sample M1P10

21. X-ray diffraction pattern of sample M1P11

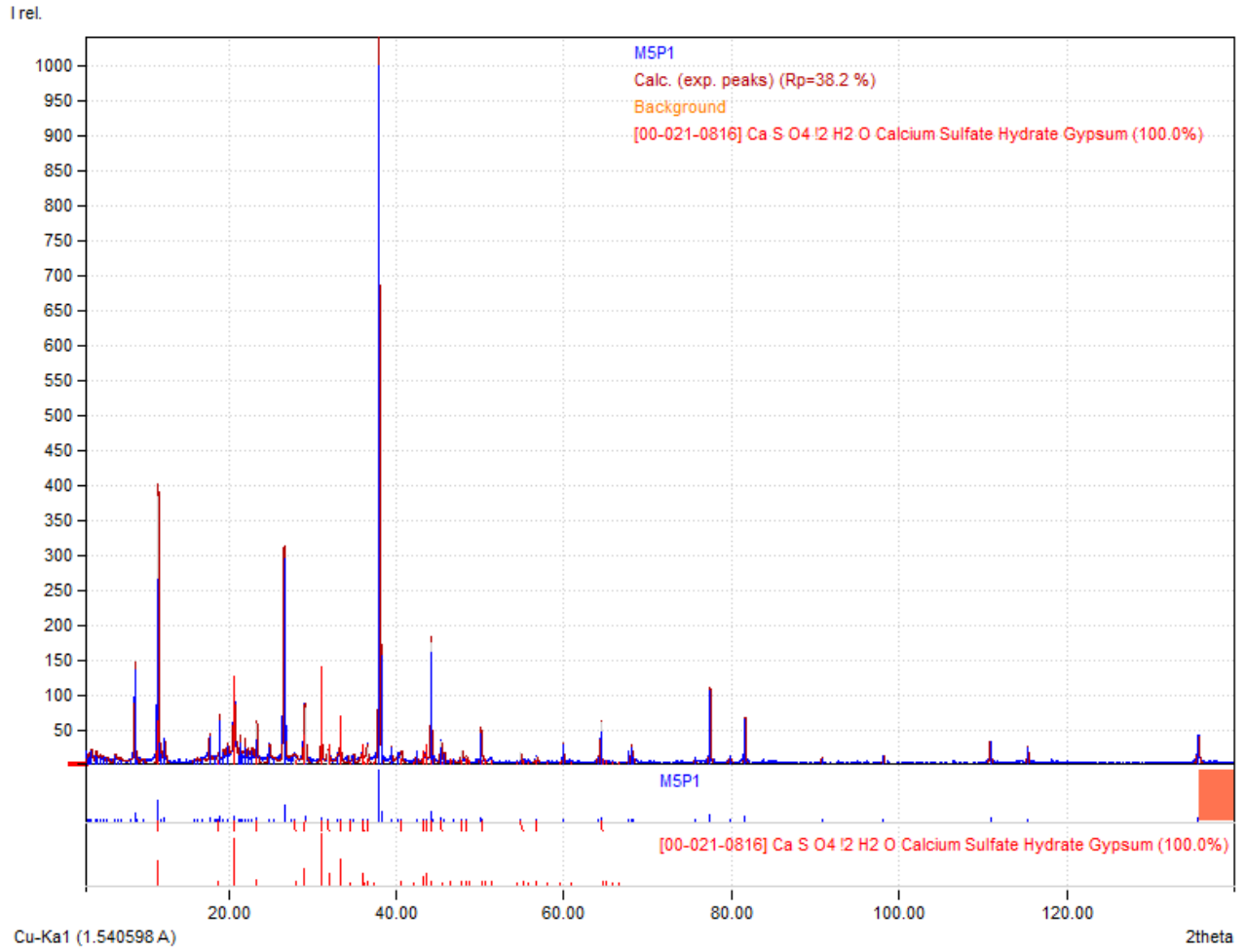*22. X-ray diffraction pattern of sample M1P14*

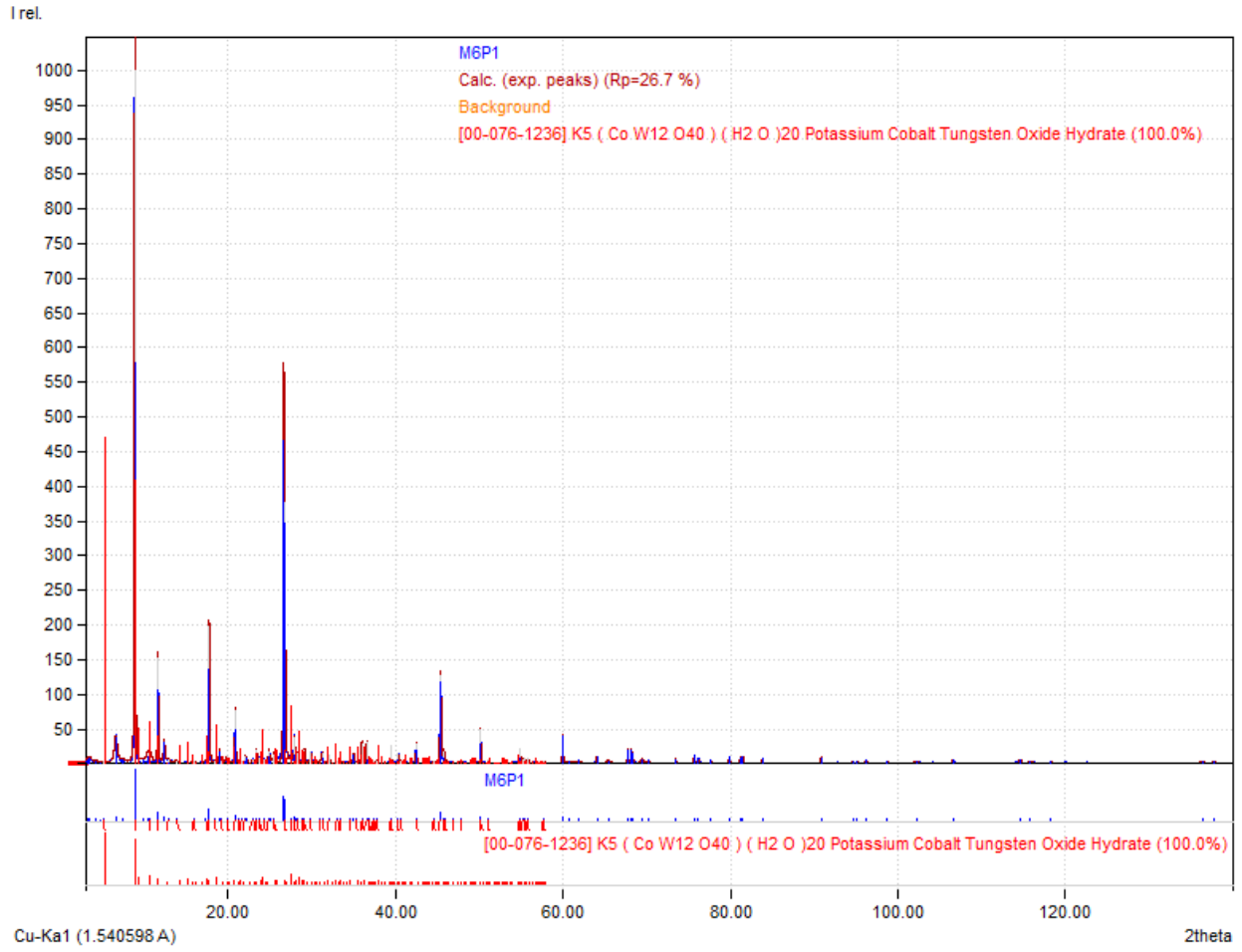*23. X-ray diffraction pattern of sample M1P15*

24. X-ray diffraction pattern of sample M1P16

25. X-ray diffraction pattern of sample M5P1

26. X-ray diffraction pattern of sample M6P1